



Small-Molecule Suppressors of Cytokine-Induced Beta-Cell Apoptosis

Citation

Chou, Danny Hung-Chieh. 2011. Small-Molecule Suppressors of Cytokine-Induced Beta-Cell Apoptosis. Doctoral dissertation, Harvard University.

Permanent link

<http://nrs.harvard.edu/urn-3:HUL.InstRepos:10121978>

Terms of Use

This article was downloaded from Harvard University's DASH repository, and is made available under the terms and conditions applicable to Other Posted Material, as set forth at <http://nrs.harvard.edu/urn-3:HUL.InstRepos:dash.current.terms-of-use#LAA>

Share Your Story

The Harvard community has made this article openly available.
Please share how this access benefits you. [Submit a story](#).

[Accessibility](#)

© 2011- Hung-Chieh Chou

All rights reserved.

Small-molecule suppressors of cytokine-induced beta-cell apoptosis

Abstract

Type-1 diabetes is caused by the autoimmune destruction of insulin-producing beta cells in the pancreas. Beta-cell apoptosis involves a complex set of signaling cascades initiated by interleukin-1 β (IL-1 β), interferon- γ (IFN- γ), and tumor necrosis factor- α (TNF- α). IL-1 β and TNF- α induce NF κ B expression, while IFN- γ induces STAT1 activation. These cytokines lead to a decrease of beta-cell function. The goal of this thesis is to identify small-molecule suppressors of cytokine-induced beta-cell apoptosis using high-throughput screening approach. Using the rat INS-1E beta-cell line, I developed an assay to measure cellular viability after 48 hours of cytokine treatment. I screened 29,760 compounds for their ability to suppress the negative effects of the cytokines. I identified several compounds to be suppressors of beta-cell apoptosis. These efforts led to the discovery of GSK-3 β and HDAC3 as novel targets for suppressing beta-cell apoptosis.

I also followed up on BRD0608, a novel suppressor that increased ATP levels and decreased caspase activity in the presence of cytokines. To follow up this compound, 35 analogs related to BRD0476 were synthesized using solid-phase synthesis and tested for their protective effects in the presence of cytokines. A structurally related analog,

BRD0476, was found to be more potent and active in human islets, decreasing caspase activation and increasing insulin secretion after a 6-day treatment.

I performed gene-expression profiling of INS-1E cells treated with the cytokine cocktail in the absence or presence of 10 μ M BRD0476. Gene-set enrichment analysis revealed that the gene sets most significantly changed by BRD0476 involved cellular responses to IFN- γ . I therefore assessed the effects of BRD0476 on STAT1 transcriptional activity. Cytokine treatment increased the reporter-gene luciferase activity, while co-treatment with BRD0476 reduced this activity significantly.

To identify the intracellular target(s) of BRD0476, I collaborated with the Proteomics Platform in Broad Institute using SILAC (stable isotope labeling by amino acids in cell culture). SILAC is a mass spectrometry-based method to identify proteins that bind a small molecule attached to a bead. Deubiquitinase USP9X was pulled down by BRD0476. Knock-down of USP9X by siRNA phenocopied the protective effects of BRD0476. Binding assays were performed to identify interactions between BRD0476 and USP9X.

Table of contents

Abstract	iii
Table of contents	v
Acknowledgements	ix
Thesis roadmap	xi
Chapter 1: Introduction	
1.1 Type-1 diabetes overview	1
1.2 Introduction of beta-cell apoptosis	3
1.3 Cytokine signaling pathways in pancreatic beta cells	6
1.4 Genetic approaches to suppress cytokine-induced beta-cell apoptosis in literature	9
1.5 Small-molecule precedents to suppress cytokine-induced beta-cell apoptosis	10
1.6 Small-molecule screening in beta-cell biology	12
1.7 Concluding remarks	13
1.8 Reference	14
Chapter 2: Development of assays to screen for suppressors of cytokine-induced beta-cell apoptosis	
2.1 Introduction	18
2.2 Development of four assays in measuring different aspects of beta-cell biology in rat INS-1E cell line	19

2.3 Pilot screen: results of a 2240-compound library	25
2.4 Follow-up studies of GSK-3 β inhibitors, glucocorticoids, and pyrazoles in suppressing beta-cell apoptosis	29
2.5 Discussion and conclusion	34
2.6 Methods and materials	36
2.7 Reference	40
Chapter 3: Identification of HDAC3 as a target for suppressing of cytokine-induced beta-cell apoptosis	
3.1 Introduction	44
3.2 MS-275 and CI-994 are better suppressors than SAHA and TsA in suppressing beta-cell apoptosis	47
3.3 siRNA-based knock-down studies identified HDAC3 as a target for suppressing of cytokine-induced beta-cell apoptosis	52
3.4 Further evidence from small-molecule HDAC inhibitors (“Merck 60” and HDAC3-seletive inhibitors)	55
3.5 Conclusion	58
3.6 Methods and materials	59
3.7 Reference	64
Chapter 4: Identification of BRD0476 as a novel suppressor of cytokine-induced beta-cell apoptosis	
4.1 Introduction	68

4.2 Results of a 29,760-compound library screen	69
4.3 Identification of BRD0608 and structure-activity relationships	76
4.4 Synthesis of analogs and discovery of BRD0476	81
4.5 Conclusion	85
4.6 Methods and materials	85
4.7 Reference	92
Chapter 5: Mechanistic studies of BRD0476 in suppressing of cytokine-induced beta-cell apoptosis	
5.1 Introduction	96
5.2 Effects of BRD0476 in primary dissociated human islets	97
5.3 Genome-wide gene expression profile revealed the JAK-STAT pathway as a target for the effects of BRD0476	101
5.4 SILAC studies suggested USP9X as a possible primary target for BRD0476	110
5.5 Relationship between the JAK-STAT pathway and USP9X	121
5.6 Conclusion	124
5.7 Methods and materials	125
5.8 Reference	133
Appendix 1	
Complete EC ₅₀ values and maximum activity for all synthesized analogs	136

Appendix 2

Characterization of Active Compounds 140

Appendix 3

Kinase profiling result of BRD0476 145

Acknowledgements

I would like to thank my advisor, Dr. Stuart Schreiber, as well as my mentor Dr. Bridget Wagner for their guidance throughout my graduate school years. Stuart and Bridget have been teaching me all kinds of things and supporting me in various ways that give me a wonderful time in the past years. I am such a lucky person to be able to work with you and learn from you.

I want to thank my thesis advisory committee members, Drs. Matthew Shair and Alan Saghatelian, for monitoring my progress and providing helpful comments and suggestions. Thank you, all the members of the Schreiber lab and the Chemical Biology community at the Broad Institute for creating a wonderful environment that makes me enjoy my lab life so much. Thanks to all my collaborators throughout the Broad Institute for making my research possible. I am especially grateful to Drs. Jeremy Duvall and Patrick Faloon for helping me learn new skills and working with me to drive my research even further. Thanks to all my co-workers and friends in the lab, Dina Fomina-Yadlin, Josh Paulk, Alicia Tang, Yuan Yuan, Qiu Wang, Tuoping Luo, Mingji Dai, Tammy Gilbert, Deepika Walpita, Drew Adams, Sudeshna Fisch, Clem Feau and Melissa Kemp for helpful discussions during my time in the Schreiber lab. Special thanks to Yuan Yuan for teaching me basic lab techniques and skills when I was new to the lab.

Thanks to my previous advisor, Dr. David Evans for his supports when I thought about changing my research field. Thanks to all the members in the Evans lab for giving me an incredible first-year life especially when that was my first year to live in this country. I want to thank my fellow organic chemistry classmates. You guys are so kind and helpful in the discussions when we were fighting the problem sets and midterms. I would like to thank Dr. Dieter Seebach. The attitude and vision you shared in the Chem 206 lectures made you a role model for me during my graduate career. Special thanks to

my undergraduate advisor, Dr. Ken-Tsung Wong. Your continuous supports give me the courage to come to the United States to pursue and finish my Ph.D.

I am deeply grateful to my family back in Taiwan for their unconditional love and support during my Ph.D. career at Harvard and during my entire life so far. Finally, thanks to my dear wife for leaving Taiwan to live with me. Although I come to lab for work almost every day, you never complain about that. “You are the best thing that has ever been mine.”

Thesis roadmap

My thesis research entails (1) assay development toward screening for suppressors of cytokine-induced beta-cell apoptosis, (2) identification of HDAC3 as a target for suppressing cytokine-induced beta-cell apoptosis and (3) discovery and target identification of BRD0476 in suppressing cytokine-induced beta-cell apoptosis.

Chapter 1 begins with an introduction to type-1 diabetes overview, pancreatic beta-cell apoptosis and cytokine signaling pathways in beta cells. Subsequently, it introduces previous works using either genetic approaches or small molecules to suppress cytokine-induced beta-cell apoptosis. It ends with discussion of high-throughput screens performed in the context of beta cells.

Chapter 2 describes assay development and execution of a small-scale pilot screen. I worked closely with Nicole Bodycombe, Hyman Carrinski and Dr. Paul Clemons in the Chemical Biology Program at the Broad Institute. They were largely involved in the computational chemical biological part of this chapter. This part of study was published in *ACS Chemical Biology*.

Chapter 3 describes the effects of different HDAC inhibitors in cytokine-induced beta-cell apoptosis. Later, using siRNAs to knock down individual HDAC, HDAC3 was found to be a target for suppressing cytokine-induced beta-cell apoptosis. Most of the HDAC inhibitors used here were obtained from Drs. Tim Lewis, Ed Holson and Florence Wagner in Broad Institute. HDAC3-selective inhibitors were from Dr. Jacob Hooker in Massachusetts General Hospital. This part of study was submitted for publication in *Chemistry & Biology*.

Chapter 4 describes a 29,760-compound high-throughput screen. Dr. Patrick Faloon was a “chaperon” from Chemical Biology Platform at the Broad Institute to help me finish the screen and analyze the screening data. BRD0608, a novel suppressor that

increased ATP levels and decreased caspase activity in the presence of cytokines, was discussed. To follow up this compound, 35 analogs related to BRD0476 were synthesized using solid-phase synthesis. Dr. Jeremy Duvall from Chemical Biology Platform at the Broad Institute worked closely with me for this part. The synthesis part of this chapter was published in *ACS Medicinal Chemistry Letters*.

Chapter 5 describes the efforts to identify targets for BRD0476. Gene-expression profiles were performed as a service from Genome Analysis Platform in Broad Institute. Quantitative proteomics study is a collaboration with the Proteomics Platform at the Broad Institute. These two approaches led to the discovery of the JAK-STAT pathway and USP9X as putative targets for BRD0476.

Chapter 1 Introduction to type-1 diabetes, cytokine-induced beta-cell apoptosis and small-molecule screening

1.1 Type-1 diabetes overview

Type-1 diabetes is one of the most severe chronic autoimmune diseases with 30,000 new cases annually in the United States(1). It is caused by an immune destruction of the insulin-secreting beta cells in the islets of Langerhans within the pancreas. A number of effector molecules produced by immune cells that infiltrate pancreatic islets led to beta-cell death(2). Once beta cells are destroyed, type-1 diabetic patients lose blood glucose control, which can result in severe conditions including hyperglycemia, heart disease, blindness and kidney failure(3). Although type-1 diabetes is described as an autoimmune disease, the precise immunological, genetic and physiologic events that control the disease initiation and progression remain unclear. The current type-1 diabetes therapies are the insulin injection and islet transplantation(4-5). Injection of recombinant insulin is used for patients to control their own blood glucose levels. However, if patients cannot ensure optimal glycemic control, complications would ultimately develop. Islet transplantation, on the other hand, provides a better regulation of blood glucose levels. However, due to the limited amount of qualified donor islet cells, islet transplantation is not available to most type-1 diabetes patients. Moreover, one-time transplantation is not enough for life-long insulin independence.

Two key models of type-1 diabetes-the BioBreeding (BB) rat(6) and non-obese diabetic (NOD) mouse(2, 7)- have been widely used to study the pathophysiology of the spontaneous form of type-1 diabetes. The two models share many similarities in loci of genetic susceptibility and pathogenesis of the disease. Therefore, the current understanding about the disease initiation and progression is mostly from the rodent

models. The studies in rodent models have shown that a breakdown of immune regulation results in the expansion of autoreactive CD4⁺ and CD8⁺ T cells, autoantibody-producing B cells and activation of the innate immune system, which then collaborate to destroy the insulin-secreting beta cells(8-10). These results are consistent with human type-1 diabetes since 19 out of the 26 loci identified through genome-wide association study of human type-1 diabetes are associated with immune regulations(11-12). Observations in NOD mice have shown that the first immune cells to infiltrate the pancreatic islets are macrophages and dendritic cells(13). These cells probably migrate to the pancreatic lymph nodes to recruit CD4⁺ T cells(14). Consistent with this observation, removal of pancreatic lymph nodes at 3 weeks of age protects NOD mice against the development of insulinitis(14). Macrophages and dendritic cells become antigen-presenting cells (APCs) and activate the naive Th0 CD4⁺ T cells via presentation of beta-cell antigens on their MHC class II molecules, favoring the differentiation in Th1 cells(14). The Th1 CD4⁺ T cells then secrete interleukin-2 (IL-2) and interferon-gamma (IFN-gamma) which further stimulate APC to secrete other cytokines, such as IL-1beta and tumor necrosis factor-alpha (TNF-alpha) and nitric oxide (NO). These secreted cytokines activate the migration of CD8⁺ cytotoxic T cells into the islets and stimulate beta cells to release chemokines and IL-15 which further induce the activation of immune cells(15).

Usually, more than 70% of the beta-cell population is destroyed upon diagnosis of type-1 diabetes(16). Apoptosis is the main form of beta-cell death observed in rodent models and in human islets from T1D patients(17). The mechanisms of beta-cell destruction in T1D have not yet completely clarified, but pro-inflammatory cytokines, including IL-1beta, TNF-alpha and IFN-gamma, by the immune cells infiltrating the islet are main mediators for the destruction of beta cells(17). The aim of this thesis is to

discover novel suppressors of cytokine-induced beta-cell apoptosis as probes to study beta-cell biology.

1.2 Beta-cell apoptosis

Apoptosis, or programmed cell death, normally describes the regulated death of a cell. When cells sense the “apoptosis signal”, they shrink and undergo processes including chromatin condensation, DNA degradation, and protein cleavage. Eventually, apoptotic cells are cleared by neighboring cells by phagocytosis. Apoptosis is different from necrosis, which would lead to cell swelling and disruption of organelles. It has become increasingly evident that beta-cell apoptosis contributes to the development of both type-1 and type-2 diabetes(16). In the case of type-1 diabetes, the mechanisms by which pancreatic beta cells are selectively killed by the immune system have been thought to involve several pathways including 1) expression of Fas ligand (FasL) and its receptor Fas at the surface of the activated CD8⁺ T-cells and pancreatic beta cells respectively; 2) secretion of perforin and granzyme B by activated CD8⁺ T-cells; 3) secretion of pro-inflammatory cytokines, including IL-1beta, IFN-gamma and TNF-alpha by the diverse immune cells infiltrating the islet (Figure 1-1) (17). Fas and FasL were expressed at the surface of beta cells and infiltrating T cells, respectively(18). Although the expression of Fas in beta cells is low, it was shown that Fas expression can be induced in rodent beta cells by IL-1beta and IFN-gamma(18). Activation of Fas by FasL converts pro-caspase-8 to active caspase-8. Caspase-8 then acts via the pro-apoptotic BH3-only Bcl family member Bid to induce permeabilization of the mitochondrial outer membrane and release of cytochrome c(19). Bid interacts directly with the pro-apoptotic effector Bcl protein Bax and activates its channel-forming functions in the outer

mitochondrial membrane. One study specifically overexpressed a dominant negative form of Fas in beta cells of the NOD mice and observed a delay of the onset of diabetes(20). This suggests a role of Fas in beta-cell apoptosis. Another pathway of beta-cell apoptosis in type-1 diabetes involves perforin and granzyme B, They are both cytotoxic components secreted by CD8⁺ T cells. Perforin is involved in pore formation across the plasma membranes of beta cells. This pore enables the entry of the serine protease granzyme B inside the cell. Granzyme B cleaves multiple substrates in beta cells, causing the cleavage and activation of several targets, such as effector caspases

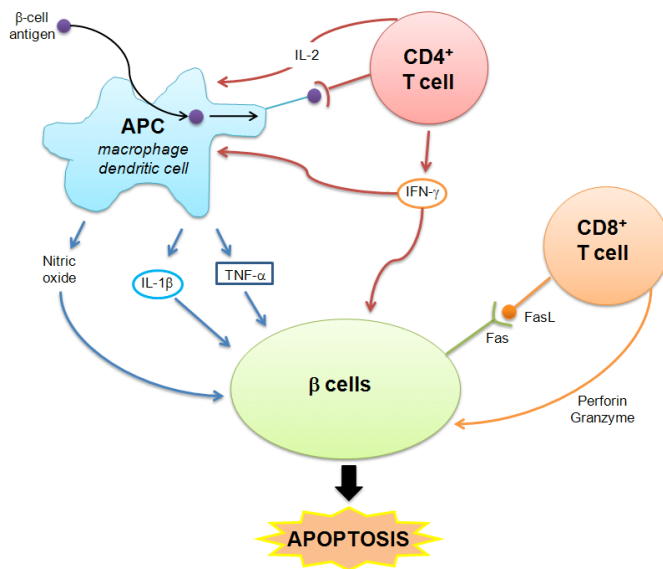


Figure 1-1. Effector molecules contributed to beta-cell apoptosis in type-1 diabetes

and the BH3 only protein Bid. NOD mice without perforin have reduced diabetes incidence compared with normal NOD controls; however, they still developed severe insulinitis(21). Pro-inflammatory cytokines are detectable during early stage of diabetes onset in both NOD mice and BB rats. Moreover, *in vitro* exposure of beta cells to IL-1β plus IFN-γ causes functional impairment similar to those observed in pre-diabetic animal models and human patients(22). Prolonged exposure of pro-

inflammatory cytokine cocktails, but not each cytokine alone, converts the functional impairment to beta-cell death. The detailed effects of each cytokine in beta cells will be described in next section.

Glucose toxicity, lipotoxicity, and ER stress are also some other mediators resulting in beta-cell apoptosis; however, they are more relevant in the situation of type-2 diabetes(16, 23). Beta cells are very sensitive to glucose concentration because they need to regulate the blood glucose level by secreting insulin. In order to release insulin, glucose enters beta cells, undergoes glycolysis and the respiratory cycle and results in the generation of ATP inside the cell. High ATP levels can close the ATP-dependent potassium channels, and the cell membrane depolarizes. On depolarization, voltage-controlled calcium channels open, calcium flows into the cells and beta cells release insulin. Constant high glucose levels can induce beta-cell apoptosis in several ways. First, reactive oxygen species (ROS) are generated by hyperactive mitochondria and ROS are toxic to beta cells(24). Constant high calcium ion levels are also toxic to the overworked beta cells(25). Moreover, prolonged hyperglycemia may induce Fas-mediated beta-cell apoptosis. Although the importance of glucose toxicity in the development of diabetes is still debated, glucose toxicity is definitely one of the factors contributing to beta-cell death. Lipotoxicity is more or less thought to be related to type-2 diabetes since obesity is thought to trigger the disease by causing hyperlipidemia and insulin resistance(23). Elevated fatty acids, such as palmitate and oleate, have direct toxic effects on beta cells, For example, palmitate activates caspase-3 dependent apoptosis pathway in beta cells(26). In another study, palmitate reduces the expression of Bcl-2, an antiapoptotic protein(27). Moreover, lipotoxicity is also thought to be synergistic with the detrimental effects of glucose toxicity(28). Fatty acids-induce beta-cell death also occurs at the ER level, where fatty acid esterification happens(29). A high

fatty acid load would exceed the capacity of beta cell's esterification capacity, impair ER function and lead to ER stress. When the ER cannot function well, lots of unfolded proteins are generated, which results in the unfolded protein response. Three ER-signaling molecules, PERK, ATF6, and IRE1, trigger cellular responses and lead to beta-cell apoptosis if the ER stress is not alleviated(29). ER stress has been proposed as the molecular mechanism linking obesity with insulin resistance but it is still debated(29).

1.3 Cytokine signaling pathways in pancreatic beta cells

Pro-inflammatory cytokines are thought to be the main mediators of beta-cell apoptosis, especially in the early stage of the disease. They induce stress-response genes that are either protective or deleterious for beta-cell survival. Gene-expression profile experiments revealed about 700 genes that are regulated after 1–24 hour of exposure to IL-1beta and IFN-gamma in rat beta cells(30). Among them, Nuclear Factor kappa B (NFkB) and STAT1 are the main regulators of the pathways triggered by these pro-inflammatory cytokines. Here, the pathways controlled by IL-1beta, IFN-gamma and TNF-alpha will be discussed (Figure 1-2).

IL-1beta binding to its receptor (IL-1R) induces the formation of a multi-protein complex and activates TNF-receptor associated factor-6 (TRAF-6) by phosphorylation. TRAF-6 then activates the NFkB and the mitogen activated protein (MAPK) pathways. TRAF-6 activates the I kappa B kinase (IKK) complex, which then phosphorylates the inhibitors of NFkB, I kBs, causing their degradation. This event releases NFkB and initiates its translocation into the nucleus, where it regulates the transcription of target genes. Activation of the NFkB pathway causes apoptosis in pancreatic beta cells. Overexpression of an NFkB super-repressor protects rodent pancreatic beta cells

against cytokine-induced apoptosis(16). IL-1R deficient NOD mice present a delayed onset of diabetes, which further proves the role of IL-1beta in *in vivo* beta-cell

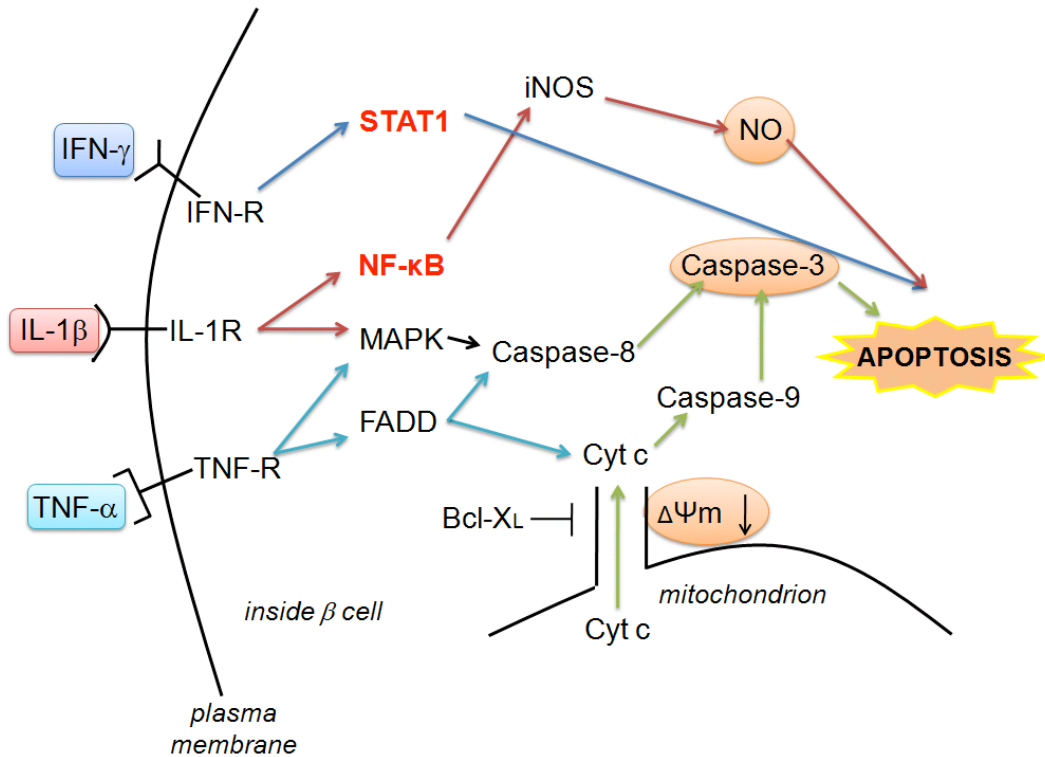


Figure1-2. Cytokine signaling pathways in beta cells

apoptosis(31). Moreover, blocking IL-1 signaling with an IL-1 receptor antagonist delays the onset of diabetes in NOD mice(31). IL-1beta also affects beta-cell function. For example, IL-1beta alone presents a progressive inhibition of glucose-stimulated insulin secretion (GSIS) in rodent beta cells(32). In human beta cells, IL-1beta, in combination with IFN-gamma, impairs conversion of pro-insulin into mature insulin and triggers beta-cell apoptosis after 7 days(22).

IFN-gamma binding to its receptor, IFN-R, induces the recruitment of two members of the Janus kinase (JAK) family, JAK1 and JAK2. Once activated by phosphorylation, JAK1 and 2 recruit STAT1 and trigger its activation by phosphorylation. STAT1 then

homodimerizes and migrates to the nucleus where it regulates the expression of genes containing gamma-activated sequence (GAS) elements in their promoter. The JAKs also activate the extracellular signal-regulated kinase (ERK) in beta cells. Experiments using IFN-R deficient NOD mice has provided inconsistent results, with one study showing a marked inhibition of insulinitis while the other has no changes in the prevalence of insulinitis(33-34). However, inhibition of STAT1, the main signaling pathway of IFN-gamma, by siRNA prevents cytokine-induced apoptosis in the rat beta-cell line INS-1 (35).

TNF-alpha binding to the TNF receptor 1 (TNF-R1) leads to its trimerization and recruitment of the adaptor protein TNF receptor-associated death domain protein (TRADD). TRADD then recruits TRAF-2 and the serine-threonine kinase Rip. TRAF-2 collaborates with Rip to induce NFκB via activation of the IKK complex. Besides TRAF-2-mediated events, TNF-R1 recruits FADD which in turn leads to pro-caspase-8 recruitment and activation of effector caspases such as caspase-3. TNF-R1 deficient NOD mice fail to develop spontaneous diabetes, which indicates the role of TNF-alpha in beta-cell death(13). Consistent with this finding, anti-TNF-alpha antibodies block the development of diabetes in NOD mice(36).

Although each cytokine triggers different pathways inside beta cells, their downstream effectors “crosstalk” with each other. Several studies observed synergistic effects of cytokines in causing beta-cell apoptosis *in vitro*(37). The resulting gene networks triggered by the cytokine cocktail are too complicated to select a single target for suppressing this cell death with small molecules. The next two sections will review up-to-date efforts in suppressing cytokine-induced beta-cell apoptosis using various approaches.

1.4 Genetic approaches to suppress cytokine-induced beta-cell apoptosis

Because of the important roles of cytokines in causing beta-cell apoptosis, various genetic approaches have been used to suppress beta-cell death. As mentioned earlier, removal of cytokine receptors could either prevent or delay the onset of diabetes in NOD mice. However, since individual cytokine receptors are conserved in different cell types, universal blockage of cytokine receptors would affect the functions of these cytokines in other physiological events. The NF κ B pathway is a key pro-apoptotic pathway induced by IL-1 β and TNF- α . Numerous studies investigated the potential of blocking NF κ B pathway to suppress cytokine-induced beta-cell death. Among them, one study generated a transgenic mouse line expressing a degradation-resistant NF κ B protein inhibitor (Δ N κ B α), acting specifically in beta cells, in an inducible and reversible manner(38). *In vitro*, islets expressing the Δ N κ B α protein were resistant to the deleterious effects of IL-1 β and IFN- γ , as assessed by reduced NO production and beta-cell apoptosis. This study indicated the whole NF κ B pathway as a possible target for suppressing beta-cell death induced by cytokines. Like the NF κ B pathway, the JAK-STAT pathway is activated by IFN- γ and would also lead to cell death eventually. When activated, STAT1 is a master transcription factor and regulates genes that have gamma-activating sequences (GAS) in their promoter regions. Therefore, a study used siRNA specific for STAT1 to transfect rat INS-1E cells to investigate the protective role of STAT1 knockdown for beta cells(35). siRNA-mediated STAT1 knockdown protects INS-1E and primary rat beta cells against cytokine-induced apoptosis. This study suggested STAT1 as a target for suppressing beta-cell death induced by cytokines. Although STAT1 is an important protein in beta-cell biology and other human diseases, there is still no direct small-molecule inhibitor or binder in the

literature to block the function of STAT1. Nevertheless, upstream proteins that regulate STAT1 activity such as JAKs were used to modulate STAT1 activities.

In addition to targeting pathways or proteins that are directly activated by individual cytokines, other pathways related to apoptosis were also investigated in order to suppress beta-cell apoptosis. One study used adenovirus-mediated overexpression of the anti-apoptotic protein, Bcl-X_L, to suppress apoptosis of rat RIN beta cells induced by cytokines(37). Considering these anti-apoptotic proteins are potential oncogenes, overexpression of these proteins does not seem to be a good approach in suppressing beta-cell death. One interesting study investigated the role of SIRT1, a class III histone deacetylase, in protecting beta cells(39). SIRT1 is known to interfere with the NFκB pathway and thereby thought to have an anti-inflammatory function. Adenovirus-mediated overexpression of SIRT1 in RIN cells was able to suppress apoptosis induced by cytokines. Furthermore, resveratrol, a SIRT1 activator, could suppress beta-cell apoptosis in either RIN cells or isolated rat islets in this case. Follow-up experiments demonstrated that the mechanism under this protection was by suppressing the NFκB pathway probably through deacetylation of p65 by SIRT1.

1.5 Small-molecule precedents to suppress cytokine-induced beta-cell apoptosis

Because of the important roles of cytokines in mediating beta-cell death, researchers have been searching for small molecules that could suppress the effects of cytokines. Among these studies, most of them use natural products or plant extracts to suppress cytokine-induced beta-cell apoptosis. For example, extracts of *Artemisia capillaries*(40), *St John's wort*(41), *Radix asari*(42), and natural products such as flavonoids were all reported to have protective effects in beta cells(43). The common

feature is that these compounds or extracts were demonstrated previously to be antioxidants or have anti-inflammatory effects in other cell types. Therefore, these are not designed specifically for pancreatic beta cells and would not have selective protection towards beta cells. Furthermore, the mechanisms of actions were not fully studied. Most of them were annotated in the paper as blockers of the NF κ B-iNOS pathway. One particular polyphenolic flavonoid, silymarin, is a special example in this type of compounds(44). Silymarin has a strong antioxidant activity and exhibits anticarcinogenic, antiinflammatory, and cytoprotective effects. Matsuda *et al.* therefore studied the effect of silymarin on IL-1 β and IFN- γ -induced beta-cell damage using RINm5F cells and human islets(44). Silymarin dose-dependently inhibited both cytokine-induced NO production and cell death in RINm5F cells. Furthermore, silymarin prevented cytokine-induced NO production and impairment of glucose-stimulated insulin secretion in human islets. These protective effects of silymarin were thought to be mediated through the suppression of JNK and JAK/STAT pathways.

The most interesting findings so far in the literature of small-molecule suppressors of cytokine-induced beta-cell apoptosis are the histone deacetylase (HDAC) inhibitors, suberoylanilide hydroxamic acid (SAHA) and trichostatin A (TSA)(45). In 2007, Larsen *et al.* reported that in both INS-1 cells and primary rat islets, SAHA or TSA could prevent cytokine-induced beta-cell toxicity(45). This finding seems counterintuitive, because HDAC inhibitors were thought to induce apoptosis in different cell types. Moreover, SAHA was actually approved by the U.S. Food and Drug Administration (FDA) in October 2006 for the treatment of cutaneous T cell lymphoma (CTCL). However, in cytokine-treated beta cells, SAHA and TSA reduced the amount of apoptotic cells. The expression of iNOS was also reduced by the treatment, which led to lower production of nitric oxide. On the other hand, SAHA and TSA failed to restore glucose-simulated

insulin secretion, although they could restore the accumulation of insulin over a 24-hr period. A follow-up study in the literature demonstrated that another HDAC inhibitor, ITF2357, could normalize streptozocin (STZ)-induced hyperglycemia in mice at the clinically relevant doses of 1.25-2.5 mg/kg(46). *In vitro*, at 25 and 250 nmol/L, ITF2357 increased islet cell viability, enhanced insulin secretion, reduced nitric oxide production, and decreased apoptotic cells. iNOS levels decreased in association with reduced islet-derived nitrite levels. These results point to HDACs as potential targets for suppressing beta-cell apoptosis. The mechanism of its protective effect was considered to be down-regulation of the NFκB pathway. Although similar positive effects of TSA or SAHA in cytokine-exposed cells were observed, minor toxicity on insulin secretion and apoptotic rate was observed in beta cell lines, especially with TSA. This may be due to the nonselective manner of these HDAC inhibitors. In summary, a number of efforts had been put in searching for small-molecule inhibitors of beta-cell apoptosis; however, there is still no systematic or large-scale approach to look for such inhibitors.

1.6 Small-molecule screening in beta-cell biology

Small-molecule high-throughput screening (HTS) is a method used for probe or drug discovery in both academia and pharmaceutical industry. This allows researchers to perform thousands to millions of chemical or biological tests in a relatively short time frame. The “hits” generated from HTS can be used as probes to study certain biological pathways or as drugs to cure certain diseases.

Because of the power of HTS, several studies used this approach to generate probes for beta-cell biology. In 2009, Wang *et al.* screened ~850,000 compounds to identify small-molecule inducers of pancreatic beta-cell expansion(47). They found a group of dihydropyridine derivatives that was shown to reversibly induce beta-cell

replication in a mouse R7T1 beta-cell line by activating L-type calcium channels. Later, Chen *et al.* discovered a small molecule, (-)-indolactam V, capable of converting a heterogeneous population of embryonic stem cells (HUES 9 cells) towards a pancreatic cell fate by inducing Pdx1 expression(48). In 2010, Fomina-Yadlin *et al.* screened a 30,710-compound library to identify BRD7389, a compound capable of inducing insulin mRNA and protein expression in the alphaTC1 cell line(49). Additionally, Kiselyuk *et al.* screened a library of 1,040 known drugs for modulators of human insulin promoter activity in the human fetal islet-derived T6PNE cell line, and found a class of phenothiazines that was able to activate the insulin promoter(50). However, no systematic screen for suppressors of cytokine-induced beta-cell apoptosis has been performed to date.

1.7 Concluding remarks

Beta-cell death, and the concomitant deficiency in insulin secretion, is a key feature of type-1 diabetes. For decades, the standard of care for this disease has been insulin therapy via intramuscular injection. Current approaches to develop new treatments have focused on islet transplantation and directed stem-cell differentiation, while many technological advances have focused on glucose detection and insulin delivery. Autoimmune-induced death of beta cells involves a complex set of signaling cascades initiated by IL-1beta, IFN-gamma and TNF-alpha. IL-1beta induces NFkB expression, while downstream activation of gene expression is thought to occur through nitric oxide signaling, which both increases the endoplasmic reticulum stress-response pathway and decreases beta-cell-specific functions; this pathway works together with IFN-gamma-induced STAT-1 signaling to effect beta-cell death. Small molecules that increase beta-cell survival will be beneficial to early-stage type-1 diabetic patients since there are still a

number of beta cells inside the pancreas and beta cells can be protected by preventing the attack from cytokines. Thus, the goal of my doctoral research is to develop a set of cell-based assays to identify small molecules capable of suppressing cytokine-mediated beta-cell death, and potentially of improving glycemic control in the context of the development of type-1 diabetes. This study is also one of the first large-scale efforts to screen for compounds with an impact on beta-cell biology.

1.8 References

1. Kaufman, D. B., and Lowe, W. L., Jr. (2003) Clinical islet transplantation, *Curr Diab Rep* 3, 344-350.
2. Anderson, M. S., and Bluestone, J. A. (2005) The NOD mouse: a model of immune dysregulation, *Annu Rev Immunol* 23, 447-485.
3. Vauzelle-Kervroedan, F., Delcourt, C., Forhan, A., Jouglu, E., Hatton, F., and Papoz, L. (1999) Analysis of mortality in French diabetic patients from death certificates: a comparative study, *Diabetes Metab* 25, 404-411.
4. Hirsch, I. B., Farkas-Hirsch, R., and Skyler, J. S. (1990) Intensive insulin therapy for treatment of type I diabetes, *Diabetes Care* 13, 1265-1283.
5. Rajab, A. (2010) Islet transplantation: alternative sites, *Curr Diab Rep* 10, 332-337.
6. Mordes, J. P., Bortell, R., Doukas, J., Rigby, M., Whalen, B., Zipris, D., Greiner, D. L., and Rossini, A. A. (1996) The BB/Wor rat and the balance hypothesis of autoimmunity, *Diabetes Metab Rev* 12, 103-109.
7. Makino, S., Kunitomo, K., Muraoka, Y., Mizushima, Y., Katagiri, K., and Tochino, Y. (1980) Breeding of a non-obese, diabetic strain of mice, *Jikken Dobutsu* 29, 1-13.
8. DiLorenzo, T. P., and Serreze, D. V. (2005) The good turned ugly: immunopathogenic basis for diabetogenic CD8+ T cells in NOD mice, *Immunol Rev* 204, 250-263.
9. Burton, A. R., Vincent, E., Arnold, P. Y., Lennon, G. P., Smeltzer, M., Li, C. S., Haskins, K., Hutton, J., Tisch, R. M., Sercarz, E. E., Santamaria, P., Workman, C. J., and Vignali, D. A. (2008) On the pathogenicity of autoantigen-specific T-cell receptors, *Diabetes* 57, 1321-1330.
10. Serreze, D. V., Fleming, S. A., Chapman, H. D., Richard, S. D., Leiter, E. H., and Tisch, R. M. (1998) B lymphocytes are critical antigen-presenting cells for the initiation of T cell-mediated autoimmune diabetes in nonobese diabetic mice, *J Immunol* 161, 3912-3918.
11. Concannon, P., Rich, S. S., and Nepom, G. T. (2009) Genetics of type 1A diabetes, *N Engl J Med* 360, 1646-1654.
12. Bluestone, J. A., Herold, K., and Eisenbarth, G. (2010) Genetics, pathogenesis and clinical interventions in type 1 diabetes, *Nature* 464, 1293-1300.

13. Yoon, J. W., and Jun, H. S. (2005) Autoimmune destruction of pancreatic beta cells, *Am J Ther* 12, 580-591.
14. Pearl-Yafe, M., Kaminitz, A., Yolcu, E. S., Yaniv, I., Stein, J., and Askenasy, N. (2007) Pancreatic islets under attack: cellular and molecular effectors, *Curr Pharm Des* 13, 749-760.
15. Cardozo, A. K., Proost, P., Gysemans, C., Chen, M. C., Mathieu, C., and Eizirik, D. L. (2003) IL-1beta and IFN-gamma induce the expression of diverse chemokines and IL-15 in human and rat pancreatic islet cells, and in islets from pre-diabetic NOD mice, *Diabetologia* 46, 255-266.
16. Cnop, M., Welsh, N., Jonas, J. C., Jorns, A., Lenzen, S., and Eizirik, D. L. (2005) Mechanisms of pancreatic beta-cell death in type 1 and type 2 diabetes: many differences, few similarities, *Diabetes* 54 Suppl 2, S97-107.
17. Eizirik, D. L., and Mandrup-Poulsen, T. (2001) A choice of death--the signal-transduction of immune-mediated beta-cell apoptosis, *Diabetologia* 44, 2115-2133.
18. Kawasaki, E., Abiru, N., and Eguchi, K. (2004) Prevention of type 1 diabetes: from the view point of beta cell damage, *Diabetes Res Clin Pract* 66 Suppl 1, S27-32.
19. McKenzie, M. D., Carrington, E. M., Kaufmann, T., Strasser, A., Huang, D. C., Kay, T. W., Allison, J., and Thomas, H. E. (2008) Proapoptotic BH3-only protein Bid is essential for death receptor-induced apoptosis of pancreatic beta-cells, *Diabetes* 57, 1284-1292.
20. Allison, J., Thomas, H. E., Catterall, T., Kay, T. W., and Strasser, A. (2005) Transgenic expression of dominant-negative Fas-associated death domain protein in beta cells protects against Fas ligand-induced apoptosis and reduces spontaneous diabetes in nonobese diabetic mice, *J Immunol* 175, 293-301.
21. Thomas, H. E., McKenzie, M. D., Angstedra, E., Campbell, P. D., and Kay, T. W. (2009) Beta cell apoptosis in diabetes, *Apoptosis* 14, 1389-1404.
22. Hostens, K., Pavlovic, D., Zambre, Y., Ling, Z., Van Schravendijk, C., Eizirik, D. L., and Pipeleers, D. G. (1999) Exposure of human islets to cytokines can result in disproportionately elevated proinsulin release, *J Clin Invest* 104, 67-72.
23. Robertson, R. P., Harmon, J., Tran, P. O., and Poitout, V. (2004) Beta-cell glucose toxicity, lipotoxicity, and chronic oxidative stress in type 2 diabetes, *Diabetes* 53 Suppl 1, S119-124.
24. Federici, M., Hribal, M., Perego, L., Ranalli, M., Caradonna, Z., Perego, C., Usellini, L., Nano, R., Bonini, P., Bertuzzi, F., Marlier, L. N., Davalli, A. M., Carandente, O., Pontiroli, A. E., Melino, G., Marchetti, P., Lauro, R., Sesti, G., and Folli, F. (2001) High glucose causes apoptosis in cultured human pancreatic islets of Langerhans: a potential role for regulation of specific Bcl family genes toward an apoptotic cell death program, *Diabetes* 50, 1290-1301.
25. Maedler, K., Storling, J., Sturis, J., Zuellig, R. A., Spinas, G. A., Arkhammar, P. O., Mandrup-Poulsen, T., and Donath, M. Y. (2004) Glucose- and interleukin-1beta-induced beta-cell apoptosis requires Ca²⁺ influx and extracellular signal-regulated kinase (ERK) 1/2 activation and is prevented by a sulfonylurea receptor 1/inwardly rectifying K⁺ channel 6.2 (SUR/Kir6.2) selective potassium channel opener in human islets, *Diabetes* 53, 1706-1713.
26. Jeffrey, K. D., Alejandro, E. U., Luciani, D. S., Kalynyak, T. B., Hu, X., Li, H., Lin, Y., Townsend, R. R., Polonsky, K. S., and Johnson, J. D. (2008) Carboxypeptidase E mediates palmitate-induced beta-cell ER stress and apoptosis, *Proc Natl Acad Sci U S A* 105, 8452-8457.

27. Lupi, R., Dotta, F., Marselli, L., Del Guerra, S., Masini, M., Santangelo, C., Patane, G., Boggi, U., Piro, S., Anello, M., Bergamini, E., Mosca, F., Di Mario, U., Del Prato, S., and Marchetti, P. (2002) Prolonged exposure to free fatty acids has cytostatic and pro-apoptotic effects on human pancreatic islets: evidence that beta-cell death is caspase mediated, partially dependent on ceramide pathway, and Bcl-2 regulated, *Diabetes* 51, 1437-1442.
28. El-Assaad, W., Buteau, J., Peyot, M. L., Nolan, C., Roduit, R., Hardy, S., Joly, E., Dbaibo, G., Rosenberg, L., and Prentki, M. (2003) Saturated fatty acids synergize with elevated glucose to cause pancreatic beta-cell death, *Endocrinology* 144, 4154-4163.
29. Eizirik, D. L., Cardozo, A. K., and Cnop, M. (2008) The role for endoplasmic reticulum stress in diabetes mellitus, *Endocr Rev* 29, 42-61.
30. Cardozo, A. K., Kruhoffer, M., Leeman, R., Orntoft, T., and Eizirik, D. L. (2001) Identification of novel cytokine-induced genes in pancreatic beta-cells by high-density oligonucleotide arrays, *Diabetes* 50, 909-920.
31. Thomas, H. E., Irawaty, W., Darwiche, R., Brodnicki, T. C., Santamaria, P., Allison, J., and Kay, T. W. (2004) IL-1 receptor deficiency slows progression to diabetes in the NOD mouse, *Diabetes* 53, 113-121.
32. Sandler, S., Eizirik, D. L., Svensson, C., Strandell, E., Welsh, M., and Welsh, N. (1991) Biochemical and molecular actions of interleukin-1 on pancreatic beta-cells, *Autoimmunity* 10, 241-253.
33. Wang, B., Andre, I., Gonzalez, A., Katz, J. D., Aguet, M., Benoist, C., and Mathis, D. (1997) Interferon-gamma impacts at multiple points during the progression of autoimmune diabetes, *Proc Natl Acad Sci U S A* 94, 13844-13849.
34. Thomas, H. E., Parker, J. L., Schreiber, R. D., and Kay, T. W. (1998) IFN-gamma action on pancreatic beta cells causes class I MHC upregulation but not diabetes, *J Clin Invest* 102, 1249-1257.
35. Moore, F., Naamane, N., Colli, M. L., Bouckenooghe, T., Ortis, F., Gurzov, E. N., Igoillo-Esteve, M., Mathieu, C., Bontempi, G., Thykjaer, T., Orntoft, T. F., and Eizirik, D. L. (2011) STAT1 is a master regulator of pancreatic {beta}-cell apoptosis and islet inflammation, *J Biol Chem* 286, 929-941.
36. Suk, K., Kim, S., Kim, Y. H., Kim, K. A., Chang, I., Yagita, H., Shong, M., and Lee, M. S. (2001) IFN-gamma/TNF-alpha synergism as the final effector in autoimmune diabetes: a key role for STAT1/IFN regulatory factor-1 pathway in pancreatic beta cell death, *J Immunol* 166, 4481-4489.
37. Holohan, C., Szegezdi, E., Ritter, T., O'Brien, T., and Samali, A. (2008) Cytokine-induced beta-cell apoptosis is NO-dependent, mitochondria-mediated and inhibited by BCL-XL, *J Cell Mol Med* 12, 591-606.
38. Eldor, R., Yeffet, A., Baum, K., Doviner, V., Amar, D., Ben-Neriah, Y., Christofori, G., Peled, A., Carel, J. C., Boitard, C., Klein, T., Serup, P., Eizirik, D. L., and Melloul, D. (2006) Conditional and specific NF-kappaB blockade protects pancreatic beta cells from diabetogenic agents, *Proc Natl Acad Sci U S A* 103, 5072-5077.
39. Lee, J. H., Song, M. Y., Song, E. K., Kim, E. K., Moon, W. S., Han, M. K., Park, J. W., Kwon, K. B., and Park, B. H. (2009) Overexpression of SIRT1 protects pancreatic beta-cells against cytokine toxicity by suppressing the nuclear factor-kappaB signaling pathway, *Diabetes* 58, 344-351.
40. Kim, E. K., Kwon, K. B., Han, M. J., Song, M. Y., Lee, J. H., Lv, N., Choi, K. B., Ryu, D. G., Kim, K. S., Park, J. W., and Park, B. H. (2007) Inhibitory effect of Artemisia capillaris extract on cytokine-induced nitric oxide formation and cytotoxicity of RINm5F cells, *Int J Mol Med* 19, 535-540.

41. Menegazzi, M., Novelli, M., Befly, P., D'Aleo, V., Tedeschi, E., Lupi, R., Zoratti, E., Marchetti, P., Suzuki, H., and Masiello, P. (2008) Protective effects of St. John's wort extract and its component hyperforin against cytokine-induced cytotoxicity in a pancreatic beta-cell line, *Int J Biochem Cell Biol* 40, 1509-1521.
42. Song, M. Y., Kim, K. A., Lee, S. Y., Kim, E. K., Lv, N., Lee, J. H., Park, J. W., Ryu, D. G., Kwon, K. B., and Park, B. H. (2007) Radix asari extract protects pancreatic beta cells against cytokine-induced toxicity: implication of the NF-kappaB-iNOS signaling cascade, *Int J Mol Med* 20, 769-775.
43. Kim, E. K., Kwon, K. B., Song, M. Y., Han, M. J., Lee, J. H., Lee, Y. R., Ryu, D. G., Park, B. H., and Park, J. W. (2007) Flavonoids protect against cytokine-induced pancreatic beta-cell damage through suppression of nuclear factor kappaB activation, *Pancreas* 35, e1-9.
44. Matsuda, T., Ferreri, K., Todorov, I., Kuroda, Y., Smith, C. V., Kandeel, F., and Mullen, Y. (2005) Silymarin protects pancreatic beta-cells against cytokine-mediated toxicity: implication of c-Jun NH2-terminal kinase and janus kinase/signal transducer and activator of transcription pathways, *Endocrinology* 146, 175-185.
45. Larsen, L., Tonnesen, M., Ronn, S. G., Storling, J., Jorgensen, S., Mascagni, P., Dinarello, C. A., Billestrup, N., and Mandrup-Poulsen, T. (2007) Inhibition of histone deacetylases prevents cytokine-induced toxicity in beta cells, *Diabetologia* 50, 779-789.
46. Lewis, E. C., Blaabjerg, L., Storling, J., Ronn, S. G., Mascagni, P., Dinarello, C. A., and Mandrup-Poulsen, T. (2011) The oral histone deacetylase inhibitor ITF2357 reduces cytokines and protects islet beta cells in vivo and in vitro, *Mol Med* 17, 369-377.
47. Wang, W., Walker, J. R., Wang, X., Tremblay, M. S., Lee, J. W., Wu, X., and Schultz, P. G. (2009) Identification of small-molecule inducers of pancreatic beta-cell expansion, *Proc Natl Acad Sci U S A* 106, 1427-1432.
48. Chen, S., Borowiak, M., Fox, J. L., Maehr, R., Osafune, K., Davidow, L., Lam, K., Peng, L. F., Schreiber, S. L., Rubin, L. L., and Melton, D. (2009) A small molecule that directs differentiation of human ESCs into the pancreatic lineage, *Nat Chem Biol* 5, 258-265.
49. Fomina-Yadlin, D., Kubicek, S., Walpita, D., Dancik, V., Hecksher-Sorensen, J., Bittker, J. A., Sharifnia, T., Shamji, A., Clemons, P. A., Wagner, B. K., and Schreiber, S. L. (2010) Small-molecule inducers of insulin expression in pancreatic alpha-cells, *Proc Natl Acad Sci U S A* 107, 15099-15104.
50. Kiselyuk, A., Farber-Katz, S., Cohen, T., Lee, S. H., Geron, I., Azimi, B., Heynen-Genel, S., Singer, O., Price, J., Mercola, M., Itkin-Ansari, P., and Levine, F. (2010) Phenothiazine neuroleptics signal to the human insulin promoter as revealed by a novel high-throughput screen, *J Biomol Screen* 15, 663-670.

Chapter 2: Assay development toward screening for suppressors of cytokine-induced beta-cell apoptosis

2.1 Introduction

As mentioned in Chapter 1, pro-inflammatory cytokines, IL-1beta, IFN-gamma and TNF-alpha, are main mediators in pancreatic beta-cell death in type-1 diabetes. Suppressors of beta-cell death could be used as valuable chemical probes to study beta-cell biology, or as therapeutic agents for type-1 diabetics in the future. In order to identify novel suppressors of cytokine-induced beta-cell death, I planned to use high-throughput screening (HTS) to identify such small molecules. HTS is a powerful method used by both academic and industrial researchers to screen for small molecules with desired properties from libraries of 10,000-1,000,000 compounds. Therefore, HTS requires high-throughput and miniaturized primary assays to complete the whole campaign in a manageable time. For this reason, I developed a suite of cell-based assays to probe for different aspects of beta-cell biology. Moreover, HTS requires a huge amount of cells for the campaign. Therefore, it is not practical and feasible to use primary beta cells in the primary screen. The choice of the right cell line is then crucial for the screening outcome. In this chapter, I will describe my efforts in using rat insulinoma cells, INS-1E, to develop four different high-throughput cell-based assays. Using cellular ATP levels as the primary readout, I screened a

library containing 2,240 compounds and measured the effects of top positive compounds in follow-up assays. These efforts led to the discovery of several previously unknown suppressors of cytokine-induced beta-cell apoptosis(1).

2.2 Development of four assays in measuring different aspects of beta-cell biology in rat INS-1E cell line

I sought to find a suitable cell line to mimic the physiologically relevant condition of the development of type-1 diabetes. Previous studies in the literature had used a few beta-cell lines in a two-day cytokine cocktail treatment to mimic physiological conditions(2-4). Therefore, I tested different cocktails of cytokines suggested in the literature in six different beta-cell lines. These are two rat insulinoma cells, INS-1E and RIN-m5f, three mouse insulinoma cells, MIN6, betaTC-6 and NIT-1, and one hamster insulinoma cell, HIT-T15. The first three cytokine cocktails tested were 10ng/mL IL-1beta + 10ng/mL IFN-gamma, 2ng/mL IL-1beta + 50ng/mL IFN-gamma and 5ng/mL IL-1beta + 50ng/mL IFN-gamma (Figure 2-1). INS-1E and HIT-T15 are the best two cell lines in sensing cytokine cocktail, since the cellular ATP levels of treated cells were reduced to ~70% of the control cells (no cytokine treatment). Here, cellular ATP levels are measured using the commercial reagent CellTiter-Glo from

Promega. CellTiter-Glo contains luciferase and luciferin. When ATP is present, luciferase can convert luciferin to oxyluciferin and generate luminescence. The luminescence can be detected here to indicate the amount of ATP inside cells.

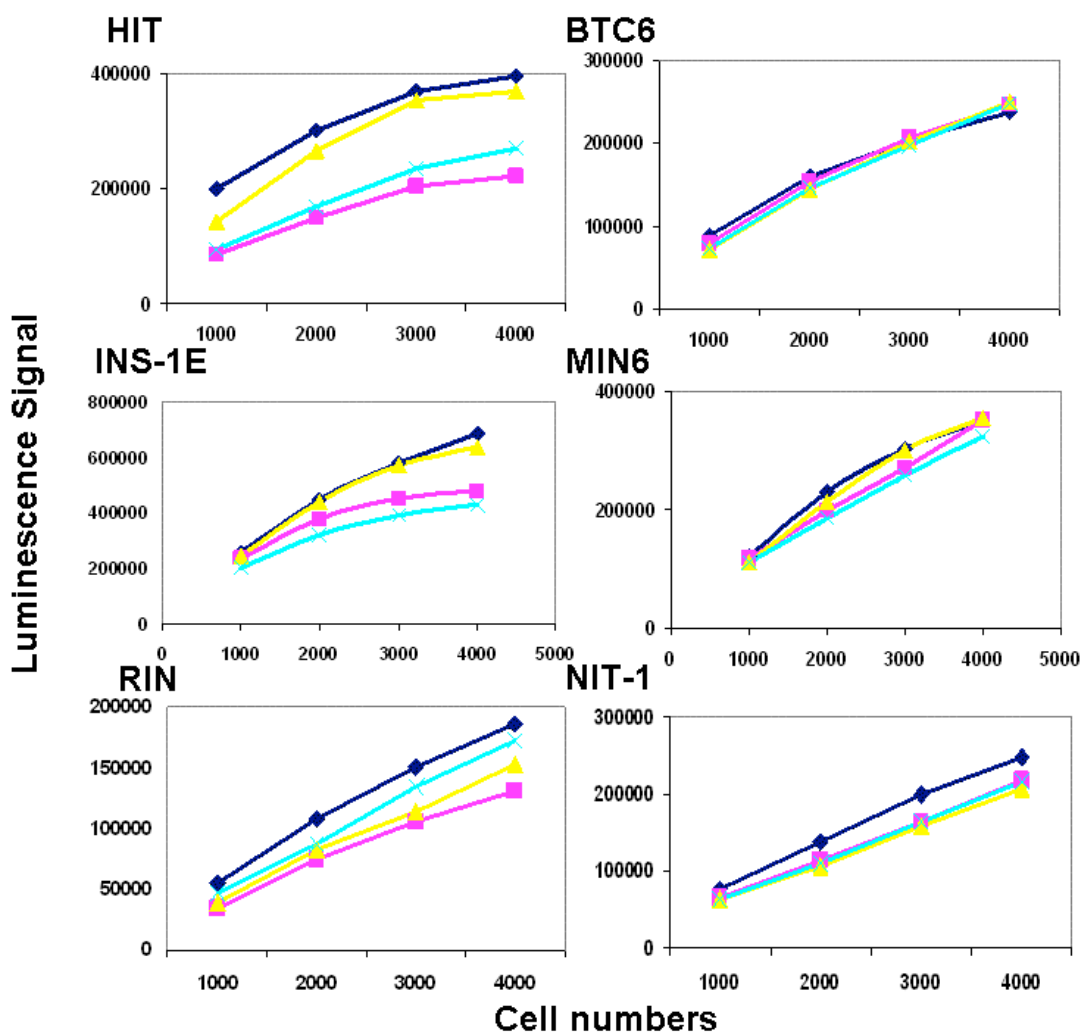


Figure 2-1. Cell viability assay for six different beta-cell lines. CellTiter-Glo is a luciferase-based assay for cellular ATP levels, which can be used as a surrogate of cell viability. Higher luminescence signal corresponds to higher cell viability. Blue: no cytokine treatment; Pink: 10ng/mL IL-1beta and 10ng/mL IFN-gamma; Yellow: 2ng/mL IL-1beta and 50ng/mL IFN-gamma; Cyan: 5ng/mL IL-1beta and 50ng/mL IFN-gamma. Concentrations are chosen from literature precedents.

I decided to use INS-1E cells in future experiments for two main reasons. First,

INS-1E cells and their parental cell line, INS-1, were well-studied in the literature, giving us the opportunity to compare our finding with others in the literature in the same cell line. Second, INS-1E is a good cell line for measuring glucose-stimulated insulin secretion (GSIS)(5). When beta cells are in a low glucose condition (the fasting state), they only secrete a basal level of insulin. When the glucose level rises (after meal), beta cells secrete more insulin to reduce the blood glucose levels. The ratio of secreted insulin levels is called the stimulation index. In INS-1E cells, GSIS results in a stimulation index of greater than 3, which is more similar to primary beta cells compared to other beta-cell lines. Several groups have shown in the literature that INS-1E cells become apoptotic after 2-day cytokine treatments and their ability to secrete insulin in response of high glucose concentration is also impaired due to cytokine treatments(6-7). Therefore, the model using INS-1E cells to mimic the physiologically relevant condition of the development of type-1 diabetes is well-established in literature.

Next, I wanted to decide the optimal concentration of each cytokine in the cocktail. I first did a titration experiment to decide the optimal combination for IL-1beta (0 to 20 ng/mL) and IFN-gamma (0 to 100 ng/mL). IL-1beta or IFN-gamma alone did not reduce the viability of INS-1E cells (Figure 2-2). This observation is consistent with previous studies showing that each individual cytokine does not induce apoptosis in

pancreatic beta cells, but rather they act synergistically to induce beta-cell apoptosis(8). The combination of both cytokines reduced the viability of INS-1E cells ranging from 65% to 85% of the untreated control.

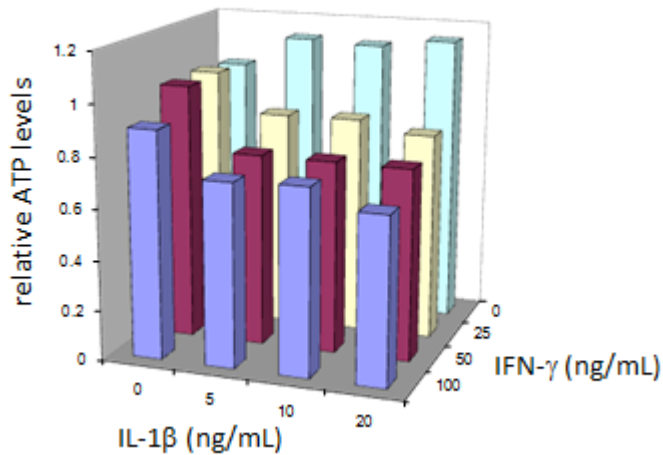


Figure 2-2. Titration experiment for IL-1beta and IFN-gamma. A titration experiment was performed using cellular ATP levels as a surrogate of viability. The relative ATP levels are normalized to untreated controls. Data are represented as the mean of 12 independent wells.

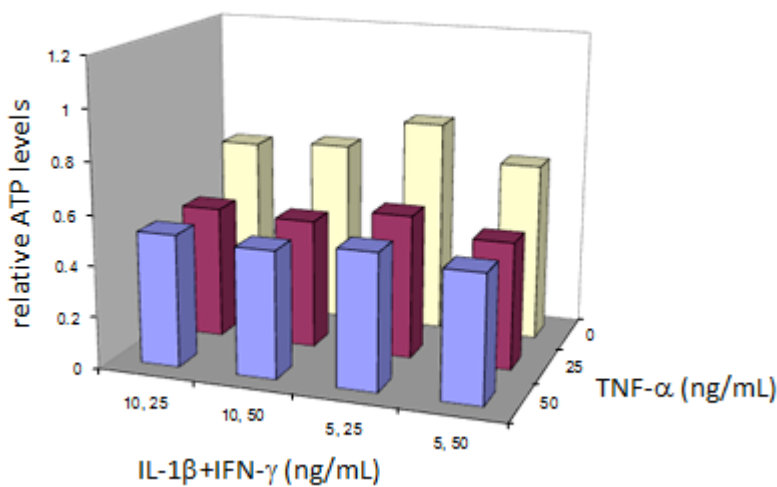


Figure 2-3. Titration experiment for IL-1beta, IFN-gamma and TNF-alpha. A titration experiment was performed using cellular ATP levels as a surrogate of viability. The relative ATP levels are normalized to untreated controls. Data are represented as the mean of 12 independent wells.

I decided to add the third pro-inflammatory cytokine, TNF-alpha, because these three cytokines are all detected in the pancreas during the development of type-1 diabetes and are proven to cause beta-cell apoptosis. I then performed another titration to decide the optimal condition (Figure 2-3). The addition of TNF-alpha (25

ng/mL) further reduced the viability of INS-1E cells to 20% of the control. A higher dose TNF-alpha (50 ng/mL) does not lead to lower cell viability. It turns out that 10ng/mL IL-1beta + 50ng/mL IFN-gamma + 25ng/mL TNF-alpha is the optimal cocktail for this readout. This cocktail reduces the cellular ATP levels by 2-fold after two-day treatment, while even higher concentrations of cytokines do not further reduce cellular ATP levels.

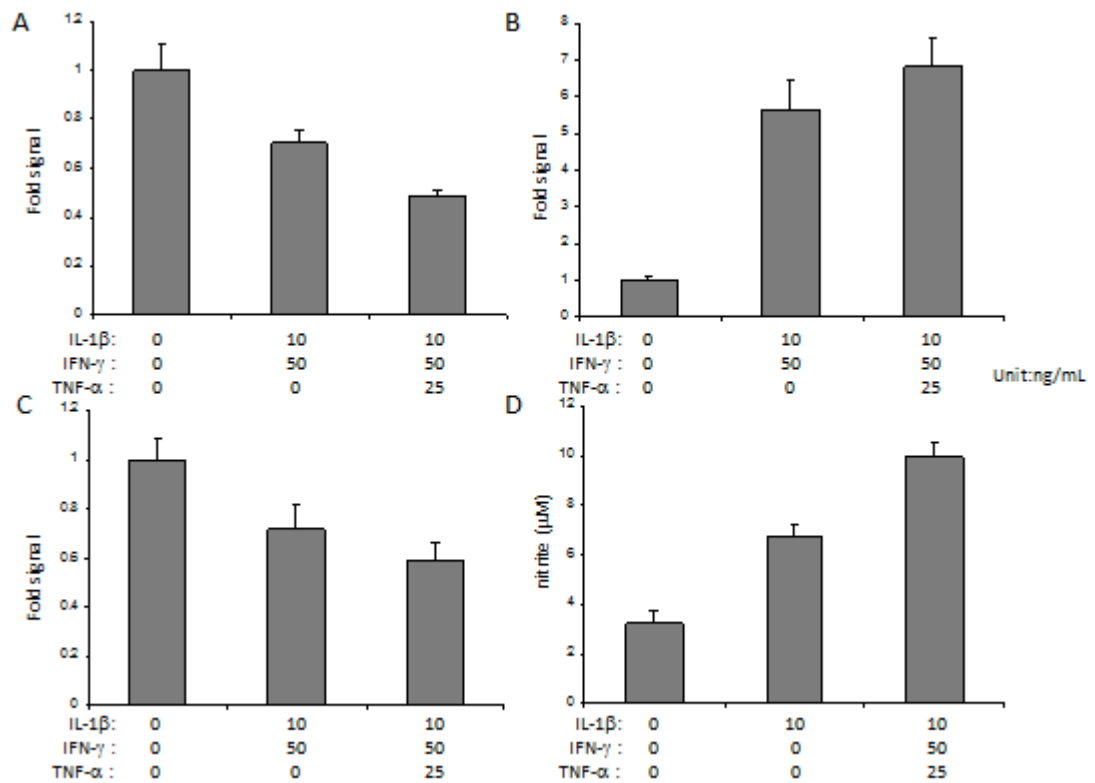


Figure 2-4. Effects of cytokines in four different aspects of beta-cell biology. A) Cell viability assay; B) Caspase-3 assay; C) Mitochondrial membrane potential; D) Nitrite assay. Data are represented as the mean + standard deviation of 24 independent wells.

This specific set of conditions was then used as a standard condition in future experiments. As a result, I was able to develop a high-throughput assay to measure

cellular ATP levels in 384-well plates (Figure 2-4 A). Other than the cellular ATP assay, I also developed three different high-throughput assays to measure caspase-3 activity, mitochondrial membrane potential, and nitrite production. Caspase-3 is a downstream effector of the apoptotic pathway, and its activity is increased by a two-day exposure of INS-1E cells to the cytokine cocktail. Caspase-3 activity is measured by means of the luminometric Caspase Glo3/7 assay. After a two-day treatment of cytokine cocktail, caspase-3 activity is elevated by 6-fold compared to the no treatment condition (Figure 2-4 B). Cytokine-mediated beta-cell apoptosis has been reported to involve mitochondria, specifically through the loss of the mitochondrial membrane potential ($\Delta\Psi_m$). JC-1, a dye for the measurement of $\Delta\Psi_m$, is initially green but forms red fluorescent aggregates in response to hyperpolarization, enabling a ratiometric calculation upon compound treatment(9). After a two-day treatment of cytokine cocktail, mitochondrial membrane potential is reduced by 40% compared to the no treatment condition (Figure 2-4 C). Nitric oxide will be measured colorimetrically by the nitrite accumulated in the cell-culture media, using the Griess reagent (a combination of naphthylethylenediamine dihydrochloride and sulphanilamide). IL-1beta is known to induce expression of the gene encoding iNOS, an effect that is potentiated by IFN-gamma. The subsequent formation of NO drives cell death by both necrosis and apoptosis. After a two-day treatment of cytokine cocktail, nitrite

production is elevated by 4-fold compared to the no-treatment condition (Figure 2-4 D).

Among the four assays developed to probe beta-cell biology, the ATP assay was chosen as the primary assay for HTS due to its robustness. A standard used to judge the robustness of a high-throughput assay is Z' factor. The assay Z' factor was calculated on the basis of the means and standard deviations of untreated and cytokine-treated wells (Equation 2-1) (10). An assay Z' factor between 0.5 and 1 means an excellent assay for HTS. The Z' factor of the high-throughput assay to measure cellular ATP levels in INS-1E cells in 384-well plates is 0.5, which means the assay is ready for HTS. All three other assays are used as secondary assays to further characterize the performance of top positives in protecting beta cells from apoptosis.

$$Z'\text{-factor} = 1 - \frac{3(\sigma_p + \sigma_n)}{|\mu_p - \mu_n|}$$

Equation 2-1. The equation for calculation Z' factor.

σ_p and σ_n are standard deviations for positive and negative control. μ_p and μ_n are means for positive and negative control.

2.3 Pilot screen: results of a 2240-compound library

I performed a pilot screen of 2,240 compounds to identify small-molecule suppressors of the cytokine cocktail on cellular ATP levels in INS-1E cells. These

seven 384-well plates included compounds from diverse sources such as known bioactives, natural products, commercial “drug-like” compounds, etc. and were screened in duplicate. The high reproducibility of both replicates further demonstrated the robustness of using this assay as the primary readout in the following HTS (Figure 2-5). Compounds were considered “hits” if they increased ATP levels by 3 standard deviations relative to the mock-treatment (DMSO) distribution (Figure 2-6). Using this criterion, I identified 49 “hits”, including 21 bioactives, 9 compounds synthesized by diversity-oriented synthesis(11), 5 natural products, and 14 compounds from commercial vendors. Chemical similarity analysis of the 49 “hits” was performed in collaboration with Paul Clemons at the Broad Institute, and revealed four clusters containing similar compounds by inspection (Figure 2-7A). These clusters included two virtually identical compounds (alsterpaullone and kenpaullone), several pyrazole derivatives from commercial vendor libraries, nine compounds from diversity-oriented synthesis, and eight glucocorticoid derivatives (Figure 2-7).

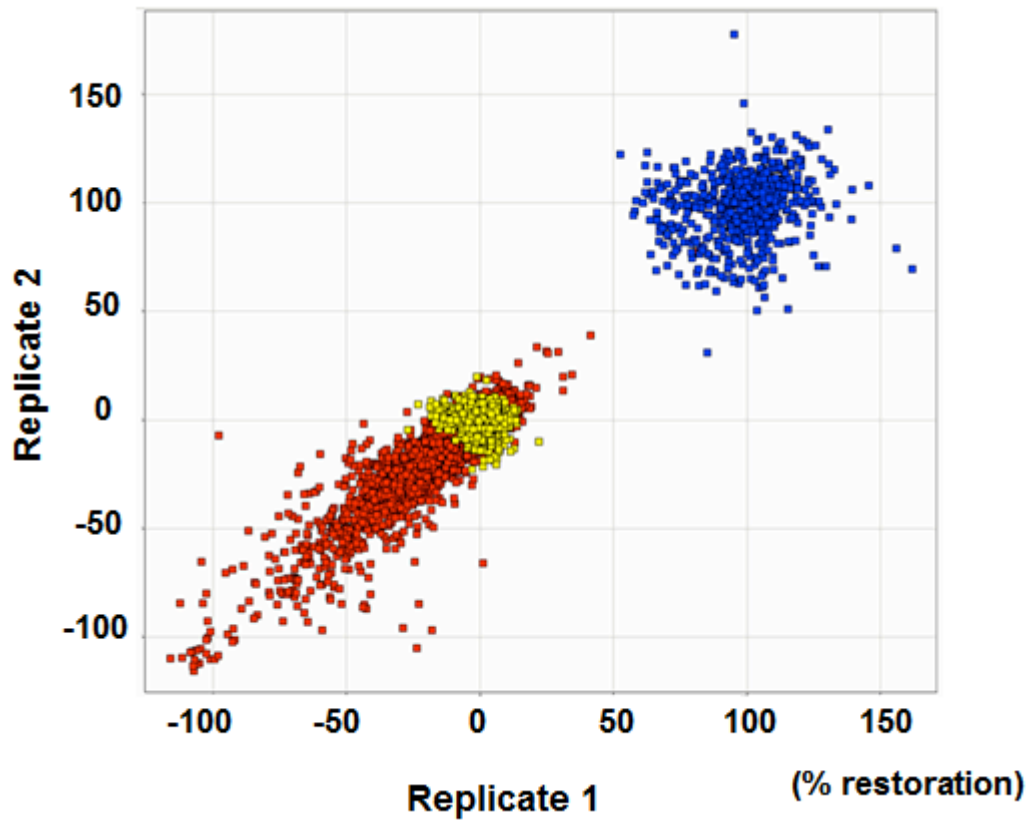


Figure 2-5. Scatter-plot results of the pilot screen. Each plate had been screened twice. Yellow dots are mock controls- wells treated with cytokine cocktails and DMSO. Blue dots are positive controls- wells treated with DMSO but without cytokine cocktails. Red dots represent different compounds. Axis is normalized to the average of positive controls (100% restoration) and mock controls (0% restoration).

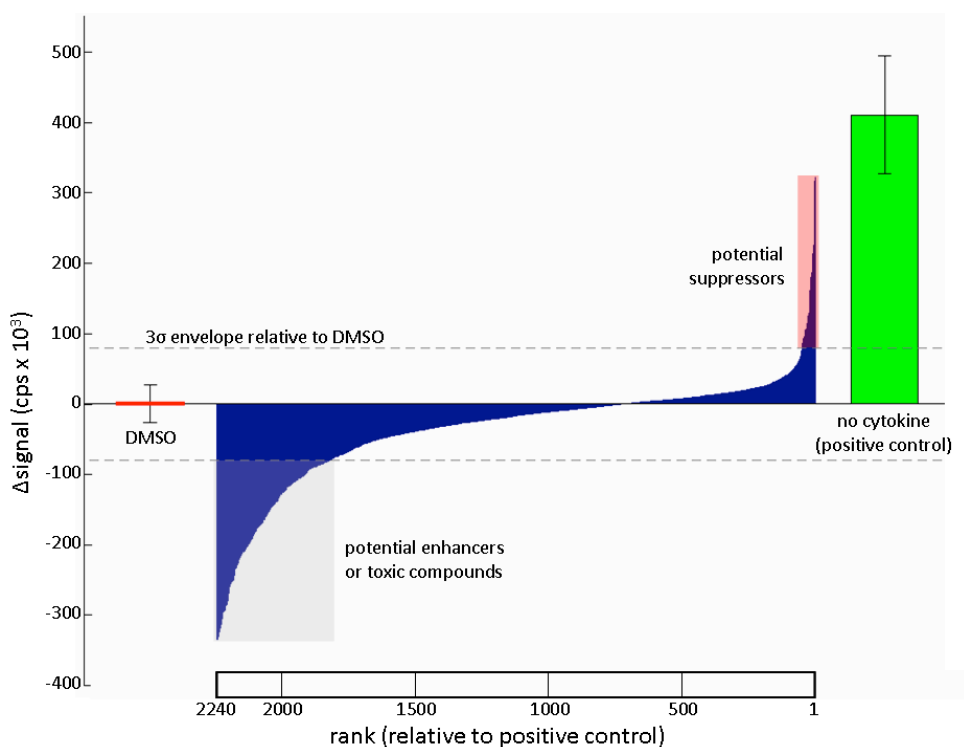


Figure 2-6. Evaluation of the screening results. Cellular ATP levels were assessed after treatment with each of 2,240 compounds. The signal change induced by compound treatment (“ Δ signal”) represents the value for each compound normalized to mock-treated wells. The means and standard deviations of mock-treated (DMSO) wells and positive-control (no cytokine) wells are shown. Potential suppressors (shaded pink) were identified as those resulting in Δ signal three standard deviations above the DMSO distribution.

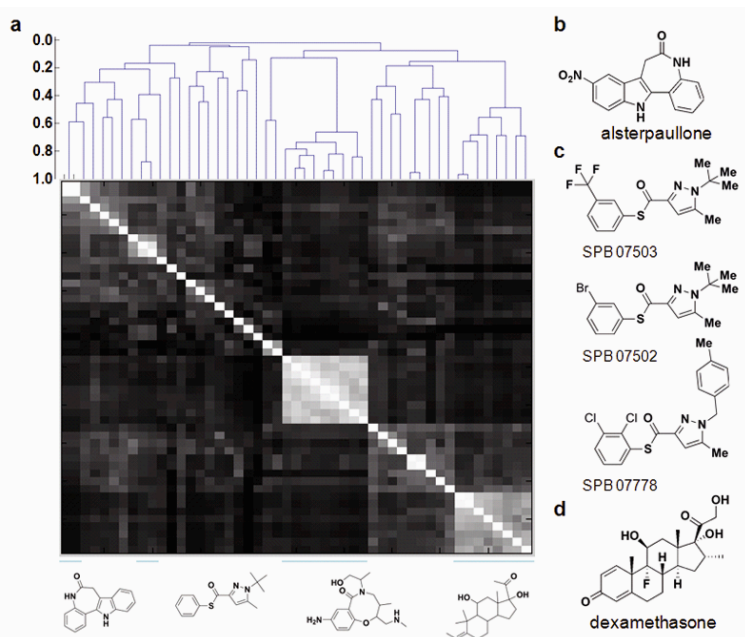


Figure 2-7. Chemical similarity among screening ‘hits’. A) Forty-nine compounds

Fig. 2-7 (Continued)

exceeding the “hit” threshold (*c.f.*, Figure 2-6) were selected for cluster analysis (see Methods). Pairwise Tanimoto (T) similarity scores were computed among all compounds (heat map; T=0, black; T=1, white; linear grayscale), after which “hits” were clustered hierarchically (dendrogram). For groups with visually apparent similarities (four white/light blocks in heat map; blue bars at bottom), the maximum common substructure for each group is depicted. Structures of the compounds tested in this study: B) alsterpaullone, C) pyrazole derivatives, D) dexamethasone.

2.4 Follow-up studies of GSK-3 β inhibitors, glucocorticoids, and pyrazoles in suppressing beta-cell apoptosis

I decided to focus initially on a set of commercially available compounds. Alsterpaullone (12) (Figure 2-7 B), annotated as an inhibitor of both glycogen synthase kinase-3 β (GSK-3 β) and cyclin-dependent kinase 2/5 (CDK2/5), completely restored beta-cell ATP levels in a dose-dependent manner (Figure 2-8 A). Similarly, three pyrazole derivatives (Figure 2-7 C) increased ATP levels to >90% of untreated controls (Figure 2-8 B). Dexamethasone (Figure 2-7D), chosen as a representative glucocorticoid, was slightly less potent in enhancing ATP levels, to approximately 80% of untreated levels (Figure 2-8 C). Caspase-3 is a downstream effector of the apoptotic pathway, and its activity is increased by a two-day exposure of INS-1E cells to the cytokine cocktail. This increase in activity was suppressed more than 50% by 1 μ M alsterpaullone (Figure 2-8 D). The pyrazole derivatives also reduced caspase-3 activity in a dose-dependent manner (Figure 2-8 E), but dexamethasone was only

partially effective at reducing this activity. (Figure 2-8 F) These results indicate that screening for an increase in ATP levels can identify small molecules capable of halting the apoptotic process in the presence of inflammatory cytokines. However, secondary assays are still required to eliminate false positives.

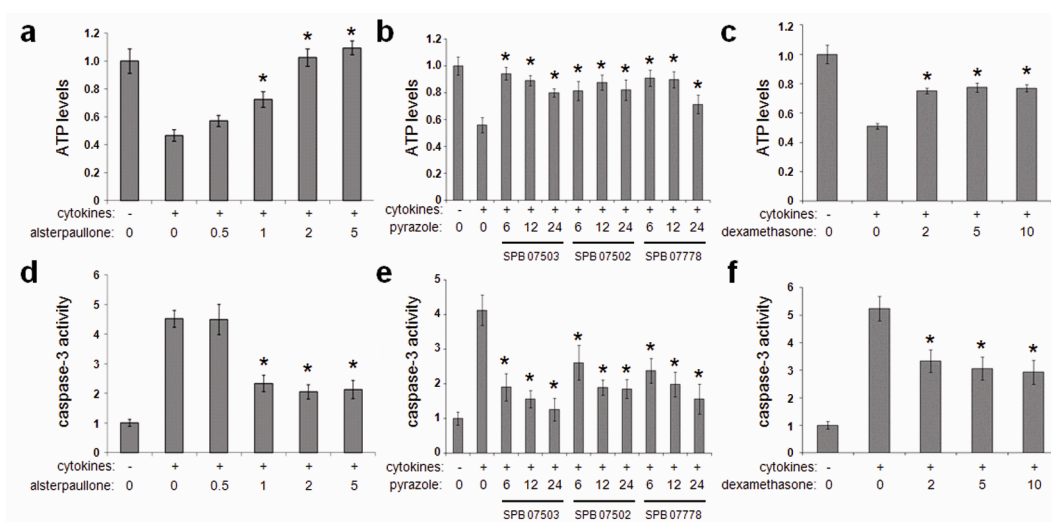


Figure 2-8. Suppression of cytokine-induced beta-cell damage. INS-1E cells were treated with cytokine cocktail in the presence of increasing concentrations of alsterpauillone (A,D), pyrazole derivatives (B, E), or dexamethasone (C, F), all expressed as micromolar concentrations. Cellular ATP levels (A, B, C) and caspase-3 activities (D, E, F) were measured and normalized to untreated controls. Data are represented as the mean \pm standard deviation of 24 independent wells. *, $p < 0.01$ relative to cytokine-treated cells.

IL-1 β induces expression of inducible nitric oxide synthase (iNOS), an effect potentiated by IFN- γ and TNF- α (13); the subsequent formation of NO drives β -cell death. Cellular production of nitrite, a stable oxidized product of NO used as a surrogate for NO levels, increased 3.5-fold after cytokine treatment and was completely inhibited by 2 μ M alsterpauillone (Figure 2-9 A). The pyrazole derivatives were also effective in reducing nitrite production, though less so than alsterpauillone

(Figure 2-9 B). Interestingly, dexamethasone had no effect on cytokine-induced nitrite production (Figure 2-9 C). Finally, I examined the effects of these compounds on GSIS in INS-1E cells. Under normal conditions, stimulation with 15 mM glucose leads to a 3.6-fold increase in insulin secretion relative to low-glucose (2 mM) conditions (Figure 2-9 D). Cytokine treatment reduced GSIS to 1.4-fold. This loss of response was largely suppressed by the addition of 4 μM alsterpaullone to the cytokine cocktail, with stimulation elevated to 3.2-fold. Treatment with the pyrazole derivative SPB07503 resulted in 50% enhancement of GSIS, while dexamethasone had no effect. Together, these results suggest that cellular nitrite levels are correlated with GSIS in INS-1E cells; compounds that are capable of reducing nitrite production in the face of cytokine treatment also restore GSIS.

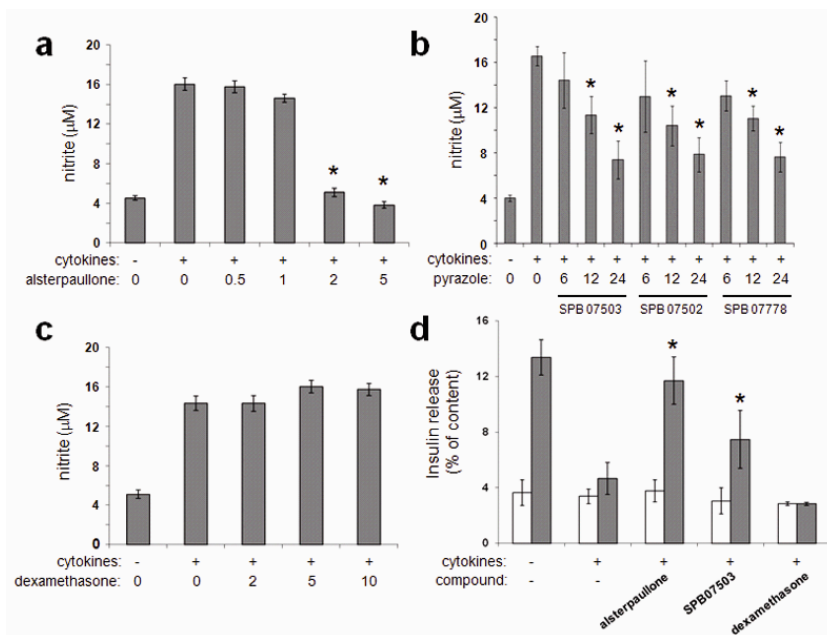


Figure 2-9. Reduction of nitrite production correlates with restoration of

Fig. 2-9 (Continued)

glucose-stimulated insulin secretion. Cellular nitrite production was measured after treatment with cytokine cocktail and increasing concentrations of A) alsterpaullone, B) pyrazole derivatives, or C) dexamethasone. Data represent the mean \pm standard deviation of 24 independent wells. D) Glucose-stimulated insulin secretion was measured in the presence of 2 mM glucose (white bars) and 15 mM glucose (gray bars) in the absence or presence of cytokines and alsterpaullone (4 μ M), the pyrazole derivative SPB07503 (12 μ M), or dexamethasone (10 μ M). Data are represented as the mean \pm standard deviation of 8 independent wells. *, $p < 0.01$ relative to cytokine-treated cells.

Another GSK-3 β inhibitor, Ro 31-8220, was, like alsterpaullone, among the top-scoring compounds. Although these kinase inhibitors likely interact with several targets, I reasoned that GSK-3 β could be a relevant target accounting for the protective effect on β cells. Ro 31-8220 increased ATP levels, decreased caspase-3 activity, and reduced cellular nitrite production (Figure 2-10 A,B,C). Similarly, the selective GSK-3 β inhibitors lithium chloride(14) and CHIR99021(15) increased ATP levels in the presence of cytokines (Figure 2-10 D,G). However, lithium chloride completely abolished nitrite production, while CHIR99021 only decreased nitrite by 20% (Figure 2-10 E,H). On the other hand, lithium cannot reduce caspase-3 activity but CHIR-99021 was able to decrease caspase-3 activity dose-dependently (Figure 2-10 F,I).

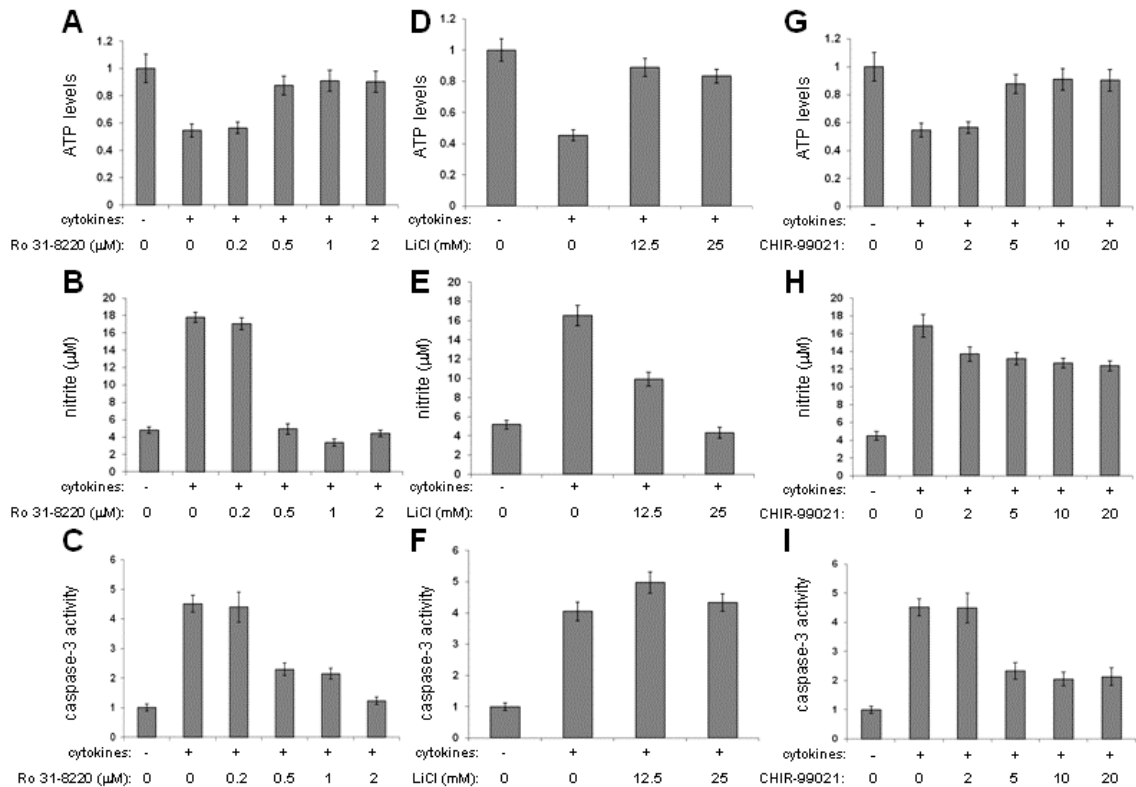


Figure 2-10. Suppression of cytokine-induced beta-cell damage by GSK-3 β kinase inhibitors. INS-1E cells were treated with cytokine cocktail in the presence of increasing concentrations of Ro 31-8220 (**A, B, C**), lithium chloride (**D, E, F**), or CHIR-99021 (**G, H, I**). Cellular ATP levels were assessed by luciferase-based luminescence (**A, D, G**) and normalized to untreated controls. Cellular nitrite production was determined using the Griess reagent (**B, E, H**) and represented as micromolar concentrations of nitrite. Caspase-3 activity was measured with a commercial kit (**C, F, I**) and normalized to the untreated controls. Data are represented as the mean \pm standard deviation of 24 independent wells.

To evaluate the specificity of these responses, I knocked down GSK-3 β in INS-1E cells with small-interfering RNA (siRNA) constructs. Knock-down of *GSK3B* resulted in ATP levels that were 75% that of the mock-transfected control (Figure 2-11 A), in a complete reduction of caspase-3 activity, and in a 20% reduction in nitrite production (Figure 2-11 C). These results were similar to those achieved by

CHIR99021 and suggest that selective inhibition of GSK-3 β is only partially protective of cytokine-treated INS-1E beta cells.

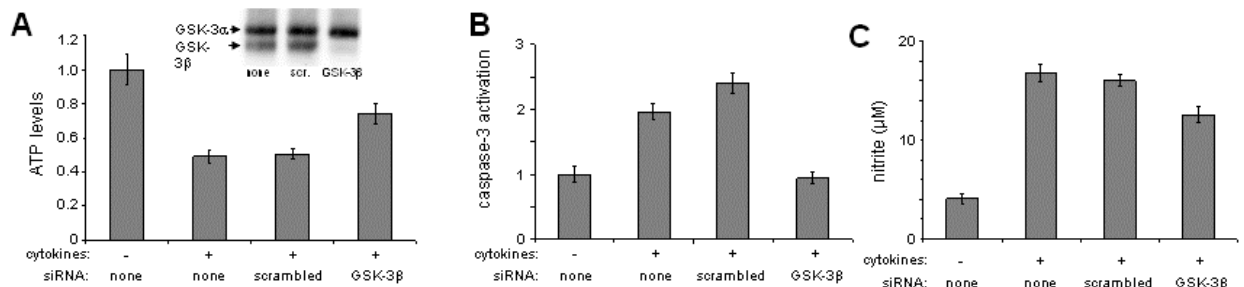


Figure 2-11. Effects of genetic silencing of GSK-3 β on beta-cell viability. (A) Cellular ATP levels were determined in INS-1E treated with cytokine cocktail in the presence of mock transfection, scrambled siRNA, and GSK-3 β -specific siRNA. Decreases in GSK-3 β protein levels after siRNA transfection are shown by Western blot. (B) Caspase-3 activity and (C) cellular nitrite production under the same gene-silencing conditions. Data are represented as the mean \pm standard deviation of 24 independent wells.

2.5 Discussion and conclusion

Inhibition of GSK-3 β has been reported to protect beta cells against glucolipototoxicity and endoplasmic reticulum stress-induced β -cell death(16-17). There are key differences between these mechanisms and cytokine-induced apoptosis, so the fact that GSK-3 β inhibitors could also suppress cytokine-induced β -cell apoptosis is not intuitively obvious. For example, the expression of iNOS and I κ B α is upregulated by cytokines but not by high glucose concentrations(18-19). Further, fatty acids such as oleate and palmitate do not activate the NF κ B pathway in either INS-1E or rat islets, and fatty acid-induced beta-cell death is independent of iNOS or nitrite

production(20). Because I observed a correlation between cellular nitrite production and GSIS, it is likely that inhibition of GSK-3 β alone is insufficient to enhance beta-cell function lost due to inflammatory cytokines. These results suggest that alsterpaullone acts through multiple mechanisms, including GSK-3 β inhibition, to protect beta cells from cytokine-induced apoptosis.

Glucocorticoids are a class of steroid hormones that bind to nuclear hormone receptors, which in turn translocate to the nucleus and upregulate the expression of anti-inflammatory proteins(21). Although glucocorticoids are generally detrimental to β -cell development and insulin secretion(22), a recent study showed that high doses of dexamethasone increase beta-cell proliferation in rat islets(23). Here, I demonstrate that low-micromolar concentrations of dexamethasone increased cellular ATP levels and reduced caspase-3 activity in the presence of cytokines. However, dexamethasone neither reduced cytokine-induced nitrite production nor restored GSIS. These results indicate that glucocorticoids can only partially increase β -cell viability in this system.

The novel pyrazole derivatives were obtained from commercially available libraries. I observed that these compounds protected cells against the detrimental effects of cytokines in all assays tested. To my knowledge, there have been no previous reports of the biological activities of these or related structures. These data

suggest that the pyrazole derivatives in this study could protect beta cells by an as-yet unknown mechanism.

Because of the importance of pro-inflammatory cytokines to the beta cell, many efforts have been made to identify genetic or small-molecule approaches to protect beta cells from cytokine-induced death(3-4, 24-26). I have demonstrated the feasibility of cell-based screening to identify small molecules that prevent loss of β -cell viability in the presence of cytokines. I also find that reduction of cytokine-induced caspase activity and nitrite production appear to be prerequisites for enhancing physiological beta-cell function. The cytokines used here have numerous effects on beta cells, but I believe the use of this cocktail is a relatively fair model of the development of type-1 diabetes. The suppressors identified here could be used as chemical probes to study beta-cell biology in the future.

2.6 Methods and Materials

Cell culture and reagents. INS-1E cells (generously provided by C. Wollheim and P. Maechler, University of Geneva) were maintained in RPMI 1640 containing 11 mM glucose, 10% fetal bovine serum, 10 mM HEPES, 50 μ M 2-mercaptoethanol, 1 mM sodium pyruvate, cultivated at 37C with 5% CO₂ in a humidified atmosphere, and split

every week. Recombinant rat IL-1 β and recombinant mouse TNF- α were purchased from R&D Systems. Recombinant mouse IFN- γ , Griess reagent, and dexamethasone were purchased from Sigma. CellTiter-Glo and Caspase-Glo 3/7 reagents were purchased from Promega. Alsterpaullone and Ro 31-8220 were purchased from EMD Biosciences. The pyrazole derivatives were purchased from Maybridge. CHIR99021 was synthesized as described (27) by Dr. Tim Lewis in Broad Institute.

High-throughput screening for compounds affecting cellular ATP levels. INS-1E

cells were seeded at 10,000 cells/well using a Multidrop Combi (Thermo LabSystems) in white optical 384-well plates (Corning Life Sciences). After overnight incubation, medium was removed and 50 μ L RPMI containing 1% FBS and a combination of cytokines (10 ng mL⁻¹ IL-1 β , 50 ng mL⁻¹ IFN- γ , 25 ng mL⁻¹ TNF- α) was added to every well. Using libraries of compounds dissolved in DMSO and a CyBi-Well pin-transfer robot (CyBio Corp.), 0.1 μ L of each compound was added. After 48 hr, medium was removed and 20 μ L CellTiter-Glo reagent was added. Luminescence was measured after 10-min incubation using an EnVision plate reader (PerkinElmer).

Screening data analysis. Instrument output files were processed using Pipeline Pilot (Accelrys) and input to MATLAB (The MathWorks) for data normalization. Compound

performance scores relative to a distribution of mock-treated (DMSO) wells were calculated using a revised version of the scoring system underlying *ChemBank* (28). The role of replicate treatments was further developed as follows: first, mock-treatment distributions were modeled using all mock-treated wells measured on a single day, regardless of their nominal replicate; second, per-compound scores weighted each in-plate background-subtracted measurement by the uncertainty in that measurement, using the method of maximum likelihood (29). The uncertainty in a single background-subtracted measurement was estimated using the number of mock-treated wells on the plate and, as a measure of the assay noise, the standard deviation of the per-day mock-treatment distribution. The signal, a weighted average of differences, was scaled by the noise, the standard deviation of the mock-treatment distribution.

Chemical similarity analysis. Cluster analysis was performed using Pipeline Pilot extended connectivity fingerprints (unfolded ECFP_4s). Bits representing substructures present in more than 10%, and less than 90%, of the 49 compounds were selected to generate 96-bit representations for each structure. Pairwise Tanimoto (T) similarity scores were computed among all compounds, after which “hits” were clustered hierarchically (complete linkage), both using MATLAB. Maximum

common substructures for each group with similarities apparent by inspection were determined using Pipeline Pilot.

Measurement of cellular nitrite production. INS-1E cells were seeded and treated as described for high-throughput screening. After treatment with cytokine and compounds for 48 hr, 10 μ L modified Griess reagent (1:1 mixture of 1% sulfanilamide in 30% acetic acid and 0.1% *N*-(1-naphthyl) ethylenediamine dihydrochloride in 60% acetic acid) was added to each well. After 5-min incubation at room temperature, the absorbance at 540 nm was measured using an Envision plate reader.

Caspase-3 activity assay. INS-1E cells were seeded at 5,000 cells/well in white optical 384-well plates and treated as described for high-throughput screening. After treatment with cytokines and compounds for 48 hr, medium was removed and 20 μ L Caspase-Glo 3/7 reagent was added. Luminescence was measured after 2-hr incubation using an Envision plate reader.

RNA interference and Western blotting. Small-interfering RNA against *Gsk3b* was obtained from Dharmacon. siRNAs (100 nM) were transfected into INS-1E cells (5,000 cells/well in a 384-well plate) using DharmaFECT reagent. Transfected cells

were cultured for 72hr, then collected for Western blot analysis and cell-based assays.

For Western blotting, cells were lysed in RIPA buffer. Total protein was separated by 4-12% SDS-PAGE and transferred to a PVDF membrane. Blots were developed using the chemiluminescence detection system SuperSignal (Thermo Fisher Scientific) and light emission was captured using an Imaging Station 4000MM (Carestream).

Glucose-stimulated insulin secretion. INS1-E cells were seeded in 96-well plates at 20,000 cells/well and incubated for 48 hr in 100 μ L fresh RPMI containing 1% FBS and the cytokine cocktail, in the presence or absence of compounds. Cells were washed and incubated for 2 hr in KRBH (135 mM NaCl, 3.6 mM KCl, 5 mM NaHCO₃, 0.5 mM NaH₂PO₄, 0.5 mM MgCl₂, 1.5 mM CaCl₂, 10 mM HEPES, pH 7.4, 0.1% BSA) buffer without glucose. Cells were subsequently incubated with KRBH buffer containing 2 mM or 15 mM glucose for 1 hr. The supernatant was taken for measurement of released insulin, and 100 μ L acidified ethanol added to each well for extraction and measurement of cellular insulin content. Insulin was measured with a rat insulin ELISA kit (Alpco).

2.7 References

1. Chou, D. H., Bodycombe, N. E., Carrinski, H. A., Lewis, T. A., Clemons, P. A., Schreiber, S. L., and Wagner, B. K. (2010) Small-Molecule Suppressors of Cytokine-Induced beta-Cell Apoptosis, *ACS Chem Biol* 5, 729-734.
2. Holohan, C., Szegezdi, E., Ritter, T., O'Brien, T., and Samali, A. (2008) Cytokine-induced beta-cell apoptosis is NO-dependent, mitochondria-mediated and inhibited by BCL-XL, *J Cell Mol Med* 12, 591-606.
3. Larsen, L., Tonnesen, M., Ronn, S. G., Storling, J., Jorgensen, S., Mascagni, P., Dinarello, C. A., Billestrup, N., and Mandrup-Poulsen, T. (2007) Inhibition of histone deacetylases prevents cytokine-induced toxicity in beta cells, *Diabetologia* 50, 779-789.
4. Lee, J. H., Song, M. Y., Song, E. K., Kim, E. K., Moon, W. S., Han, M. K., Park, J. W., Kwon, K. B., and Park, B. H. (2009) Overexpression of SIRT1 protects pancreatic beta-cells against cytokine toxicity by suppressing the nuclear factor-kappaB signaling pathway, *Diabetes* 58, 344-351.
5. Merglen, A., Theander, S., Rubi, B., Chaffard, G., Wollheim, C. B., and Maechler, P. (2004) Glucose sensitivity and metabolism-secretion coupling studied during two-year continuous culture in INS-1E insulinoma cells, *Endocrinology* 145, 667-678.
6. Kalis, M., Kumar, R., Janciauskiene, S., Salehi, A., and Cilio, C. M. (2010) alpha 1-antitrypsin enhances insulin secretion and prevents cytokine-mediated apoptosis in pancreatic beta-cells, *Islets* 2, 185-189.
7. Uhles, S., Wang, H., Benardeau, A., Prummer, M., Brecheisen, M., Sewing, S., Tobalina, L., Bosco, D., Wollheim, C. B., Migliorini, C., and Sebokova, E. (2011) Taspoglutide, a novel human once-weekly GLP-1 analogue, protects pancreatic beta-cells in vitro and preserves islet structure and function in the Zucker diabetic fatty rat in vivo, *Diabetes Obes Metab* 13, 326-336.
8. Eizirik, D. L., and Mandrup-Poulsen, T. (2001) A choice of death--the signal-transduction of immune-mediated beta-cell apoptosis, *Diabetologia* 44, 2115-2133.
9. Smiley, S. T., Reers, M., Mottola-Hartshorn, C., Lin, M., Chen, A., Smith, T. W., Steele, G. D., Jr., and Chen, L. B. (1991) Intracellular heterogeneity in mitochondrial membrane potentials revealed by a J-aggregate-forming lipophilic cation JC-1, *Proc Natl Acad Sci U S A* 88, 3671-3675.
10. Zhang, J. H., Chung, T. D., and Oldenburg, K. R. (1999) A Simple Statistical Parameter for Use in Evaluation and Validation of High Throughput Screening Assays, *J Biomol Screen* 4, 67-73.
11. Nielsen, T. E., and Schreiber, S. L. (2008) Towards the optimal screening collection: a synthesis strategy, *Angew Chem Int Ed Engl* 47, 48-56.

12. Leost, M., Schultz, C., Link, A., Wu, Y. Z., Biernat, J., Mandelkow, E. M., Bibb, J. A., Snyder, G. L., Greengard, P., Zaharevitz, D. W., Gussio, R., Senderowicz, A. M., Sausville, E. A., Kunick, C., and Meijer, L. (2000) Paullones are potent inhibitors of glycogen synthase kinase-3 β and cyclin-dependent kinase 5/p25, *Eur J Biochem* 267, 5983-5994.
13. Darville, M. I., and Eizirik, D. L. (1998) Regulation by cytokines of the inducible nitric oxide synthase promoter in insulin-producing cells, *Diabetologia* 41, 1101-1108.
14. Klein, P. S., and Melton, D. A. (1996) A molecular mechanism for the effect of lithium on development, *Proc Natl Acad Sci U S A* 93, 8455-8459.
15. Ring, D. B., Johnson, K. W., Henriksen, E. J., Nuss, J. M., Goff, D., Kinnick, T. R., Ma, S. T., Reeder, J. W., Samuels, I., Slabiak, T., Wagman, A. S., Hammond, M. E., and Harrison, S. D. (2003) Selective glycogen synthase kinase 3 inhibitors potentiate insulin activation of glucose transport and utilization in vitro and in vivo, *Diabetes* 52, 588-595.
16. Mussmann, R., Geese, M., Harder, F., Kegel, S., Andag, U., Lomow, A., Burk, U., Onichtchouk, D., Dohrmann, C., and Austen, M. (2007) Inhibition of GSK3 promotes replication and survival of pancreatic beta cells, *J Biol Chem* 282, 12030-12037.
17. Stukenbrock, H., Mussmann, R., Geese, M., Ferandin, Y., Lozach, O., Lemcke, T., Kegel, S., Lomow, A., Burk, U., Dohrmann, C., Meijer, L., Austen, M., and Kunick, C. (2008) 9-cyano-1-azapauellone (cazpaullone), a glycogen synthase kinase-3 (GSK-3) inhibitor activating pancreatic beta cell protection and replication, *J Med Chem* 51, 2196-2207.
18. Cardozo, A. K., Kruhoffer, M., Leeman, R., Orntoft, T., and Eizirik, D. L. (2001) Identification of novel cytokine-induced genes in pancreatic beta-cells by high-density oligonucleotide arrays, *Diabetes* 50, 909-920.
19. Eizirik, D. L., Kutlu, B., Rasschaert, J., Darville, M., and Cardozo, A. K. (2003) Use of microarray analysis to unveil transcription factor and gene networks contributing to Beta cell dysfunction and apoptosis, *Ann N Y Acad Sci* 1005, 55-74.
20. Kharroubi, I., Ladriere, L., Cardozo, A. K., Dogusan, Z., Cnop, M., and Eizirik, D. L. (2004) Free fatty acids and cytokines induce pancreatic beta-cell apoptosis by different mechanisms: role of nuclear factor-kappaB and endoplasmic reticulum stress, *Endocrinology* 145, 5087-5096.
21. Rhen, T., and Cidlowski, J. A. (2005) Antiinflammatory action of glucocorticoids--new mechanisms for old drugs, *N Engl J Med* 353, 1711-1723.

22. Lambillotte, C., Gilon, P., and Henquin, J. C. (1997) Direct glucocorticoid inhibition of insulin secretion. An in vitro study of dexamethasone effects in mouse islets, *J Clin Invest* 99, 414-423.
23. Rafacho, A., Cestari, T. M., Taboga, S. R., Boschero, A. C., and Bosqueiro, J. R. (2009) High doses of dexamethasone induce increased beta-cell proliferation in pancreatic rat islets, *Am J Physiol Endocrinol Metab* 296, E681-689.
24. Kim, E. K., Kwon, K. B., Song, M. Y., Han, M. J., Lee, J. H., Lee, Y. R., Ryu, D. G., Park, B. H., and Park, J. W. (2007) Flavonoids protect against cytokine-induced pancreatic beta-cell damage through suppression of nuclear factor kappaB activation, *Pancreas* 35, e1-9.
25. Matsuda, T., Ferreri, K., Todorov, I., Kuroda, Y., Smith, C. V., Kandeel, F., and Mullen, Y. (2005) Silymarin protects pancreatic beta-cells against cytokine-mediated toxicity: implication of c-Jun NH2-terminal kinase and janus kinase/signal transducer and activator of transcription pathways, *Endocrinology* 146, 175-185.
26. Eldor, R., Yeffet, A., Baum, K., Doviner, V., Amar, D., Ben-Neriah, Y., Christofori, G., Peled, A., Carel, J. C., Boitard, C., Klein, T., Serup, P., Eizirik, D. L., and Melloul, D. (2006) Conditional and specific NF-kappaB blockade protects pancreatic beta cells from diabetogenic agents, *Proc Natl Acad Sci U S A* 103, 5072-5077.
27. Nuss, J. M., Harrison, S. D., Ring, D. B., Boyce, R. S., Brown, S. P., Goff, D., Johnson, K., Pfister, K. B., Ramurthy, S., Renhowe, P. A., Seely, L., Subramanian, S., Wagman, A. S., and Zhou, X. A. (1999) A preparation of aminopyrimidines and -pyridines as glycogen synthase kinase 3 inhibitors, In *PCT Int. Appl.*, pp 115-116.
28. Seiler, K. P., George, G. A., Happ, M. P., Bodycombe, N. E., Carrinski, H. A., Norton, S., Brudz, S., Sullivan, J. P., Muhlich, J., Serrano, M., Ferraiolo, P., Tolliday, N. J., Schreiber, S. L., and Clemons, P. A. (2008) ChemBank: a small-molecule screening and cheminformatics resource database, *Nucleic Acids Res* 36, D351-359.
29. Bevington, P. R., and Robinson, D. K. (2003) Data Reduction and Error Analysis for the Physical Sciences, 3rd edition ed., pp 51-61, McGraw-Hill, Boston, MA.

Chapter 3: Identification of HDAC3 as a target for suppressing cytokine-induced beta-cell apoptosis

3.1 Introduction

Protein acetylation has emerged as an important post-translational modification that regulates multiple cellular functions, including chromatin remodeling and transcriptional regulation(1-2), microtubule dynamics and intracellular transport(3-4), metabolism, and ageing(5). Histone deacetylases (HDACs) and histone acetyltransferases (HATs) regulate these processes by modulating the lysine acetylation of proteins. Much research has focused on the acetylation of histones — major components of chromatin — owing to the important roles these proteins have in vital cellular functions and in disease(6-7). Levels of histone acetylation depend on the activities of HATs and HDACs, which add or remove acetyl groups from protein substrates, respectively. In general, an increase in histone acetylation causes remodeling of chromatin from a tightly packed configuration to a loosely packed configuration, which subsequently leads to transcriptional activation. Conversely, a decrease in histone acetylation may cause chromatin structure to condense and result in transcriptional silencing. Therefore, upregulation of transcription can be achieved in cells either by stimulation of HAT or by inhibition of HDAC activities

Traditionally, HDACs have been classified based on the molecular analysis of

protein structure and their homology to yeast enzymes(8). Class I (HDAC1, HDAC2, HDAC3 and HDAC8), class IIa (HDAC4, HDAC5, HDAC7 and HDAC9), class IIb (HDAC6 and HDAC10) and class IV (HDAC11) HDACs contain zinc-dependent deacetylase domains. The class III HDACs (sirtuins, SIRT1–SIRT7) belong to a distinct class of NAD⁺-dependent hydrolases. Class I and class II HDACs share significant structural homology, especially within the highly conserved catalytic domains. HDAC1 was the first HDAC to be identified and characterized. HDAC1 was isolated by affinity chromatography with a derivative of a natural product, trapoxin A, which was discovered in a phenotypic screen involving the change in the spindle-like morphology of v-sis-transformed NIH 3T3 cells to the flattened morphology of fibroblasts(9). Subsequently, trapoxin A was shown to inhibit the histone deacetylase activity(10-11). By affinity chromatography, trapoxin A was found to bind to a previously unidentified protein, HDAC1(12). This discovery of HDAC1 opened up many investigations of histone deacetylase function and quickly led to the observation that HDACs both deacetylate histones in vitro and silence gene expression in vivo(12-13).

In the past decade, a number of HDAC inhibitors were developed as tool compounds for studying chromatin biology and clinical candidates of cancer(14). Crystallographic study using HDAC inhibitors, trichostatin A (TsA) and

suberoylanilide hydroxamic acid (SAHA), indicates that these compounds inhibit HDAC activity by interacting with the catalytic site of HDACs(15). Recently, a study demonstrated that erstwhile pan-HDAC inhibitors possess different isoform selectivity based on their activities in biochemical assays(16). For example, suberoylanilide hydroxamic acid (SAHA) inhibits the activities of HDAC1, 2, 3, 6, and 8, while MS-275 only inhibits the activities of HDAC1, 2, and 3. Therefore, structurally diverse HDAC inhibitors may have different cellular effects because of different isoform selectivity. Intensive therapeutic development efforts have focused on small-molecule HDAC inhibitors. Initially, this interest was precipitated by the discovery of the anticancer potential of HDAC inhibitors(17). Subsequently, potential therapeutic applications were broadened to include other human illnesses, including CNS diseases(18) and cystic fibrosis(19). Therefore, although cancer remains a primary target for HDAC-based therapy, significant efforts have been made to develop compounds, especially isoform-selective inhibitors, for the treatment of numerous diseases.

Recently, an important role for histone deacetylases (HDACs) in suppressing beta-cell apoptosis was suggested, perhaps by decreasing NF κ B transactivation (reviewed in (20)). Larsen *et al.* demonstrated that the HDAC inhibitors SAHA and trichostatin A (TsA) partially prevented cytokine-induced beta-cell toxicity (21). However, neither SAHA nor TsA could restore GSIS. ITF2357, another

broad-spectrum HDAC inhibitor, had *in vivo* activity, protecting mouse islets from cytokines and preventing hyperglycemia in streptozocin-treated mice (22).

In this chapter, I investigated a structurally diverse panel of HDAC inhibitors for their cellular effects in cytokine-induced beta-cell apoptosis. I demonstrate that MS-275, an inhibitor specific for HDAC1, 2, and 3, prevents beta-cell apoptosis and restores GSIS to a greater extent than more promiscuous HDAC inhibitors, such as SAHA. I further show that specific inhibition of HDAC3 is responsible for the protective effects of MS-275.

3.2 MS-275 and CI-994 are better suppressors than SAHA and TsA in suppressing beta-cell apoptosis

Using cellular ATP levels as a surrogate for cell viability (23), I tested the effects of eleven structurally diverse HDAC inhibitors (Figure 3-1) in protecting the rat INS-1E insulinoma cell line (24) from cytokine-induced apoptosis. Most of these compounds restored ATP levels to varying degrees (Figure 3-2 A). However, we observed very different effects on caspase-3 activity after compound treatment. MS-275 and CI-994 were the only two compounds that reduced caspase-3 activity significantly, while other HDAC inhibitors either were inactive or, like PXD101 and SAHA, even increased caspase-3 activity (Figure 3-2 B). Most compounds decreased nitrite secretion, a

surrogate for nitric oxide production, but the effects were more moderate (Figure 3-2 C). When I performed hierarchical clustering (Figure 3-2 D), the compounds with the most beneficial effects on cytokine-treated beta cells clustered together, and in particular were those that selectively inhibited the activities of HDAC1, 2, and 3 (MS-275 and CI-994) (Figure 3-2 A,B). These results suggest that only certain HDAC isoforms are important to cytokine-induced beta-cell apoptosis, and that the selectivity of HDAC inhibitors is an important consideration in assessing this activity.

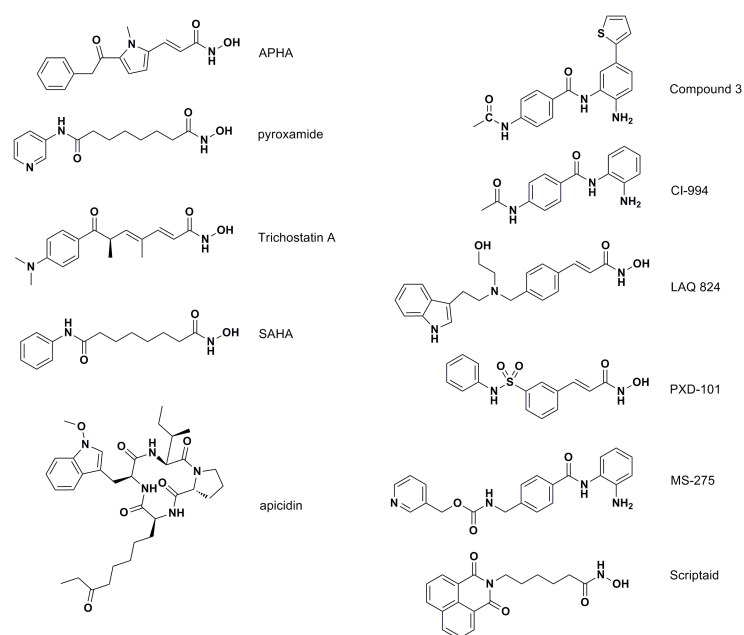


Figure 3- 1. Structures of HDAC inhibitors used in this study. Concentrations used were: APHA, 5 μ M; pyroxamide, 5 μ M; TsA, 0.05 μ M; SAHA, 1 μ M; apicidin, 0.05 μ M; **3**, 5 μ M; CI-994, 10 μ M; LAQ824, 1 μ M; PXD101, 0.2 μ M; MS-275, 5 μ M; Scriptaid, 1 μ M.

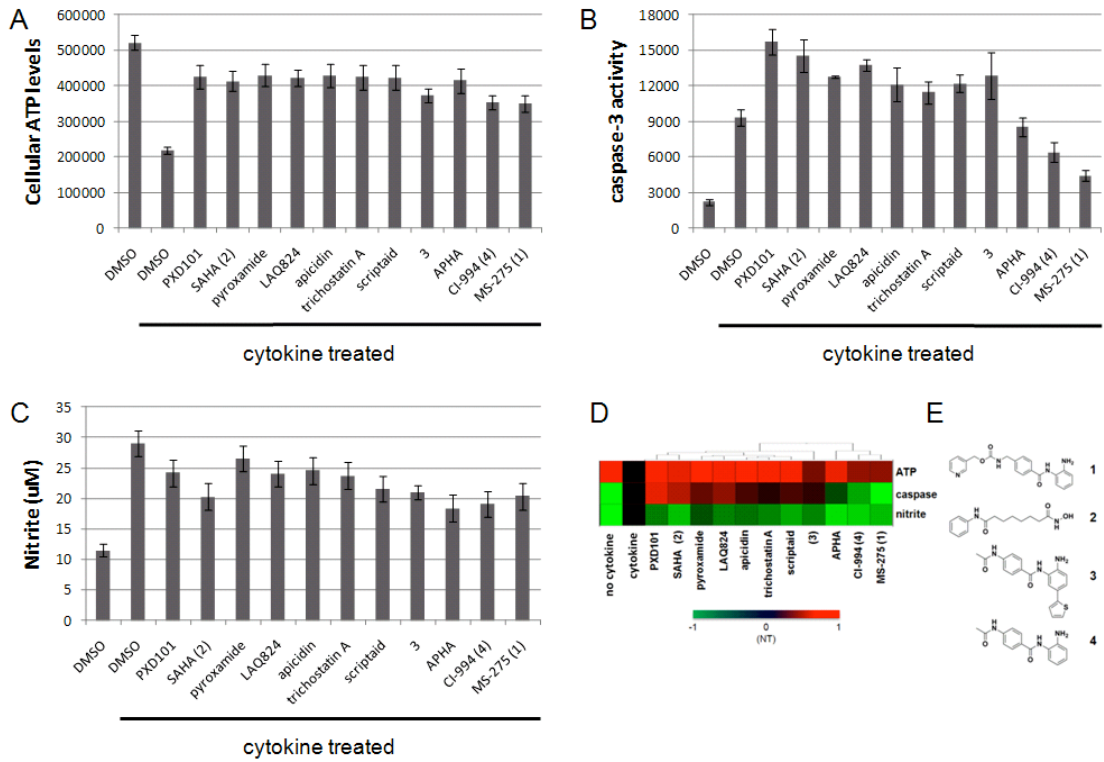


Figure 3-2. Phenotypic profiling of eleven HDAC inhibitors in beta cells. Eleven HDAC inhibitors were tested for activity in the presence of a cocktail of inflammatory cytokines in rat INS-1E cells for **(A)** cellular ATP levels, **(B)** caspase-3 activity and **(C)** nitrite production. **(D)** Results from (A), (B) and (C) was displayed into heat map. Activity was normalized to a range of -1 (green), decrease in signal relative to the untreated condition (“NT”), to 1 (red), increase in signal relative to the untreated condition. **(E)** The chemical structures of HDAC inhibitors studied in more detail: **1** (MS-275), **2** (SAHA), **3**, and **4** (CI-994).

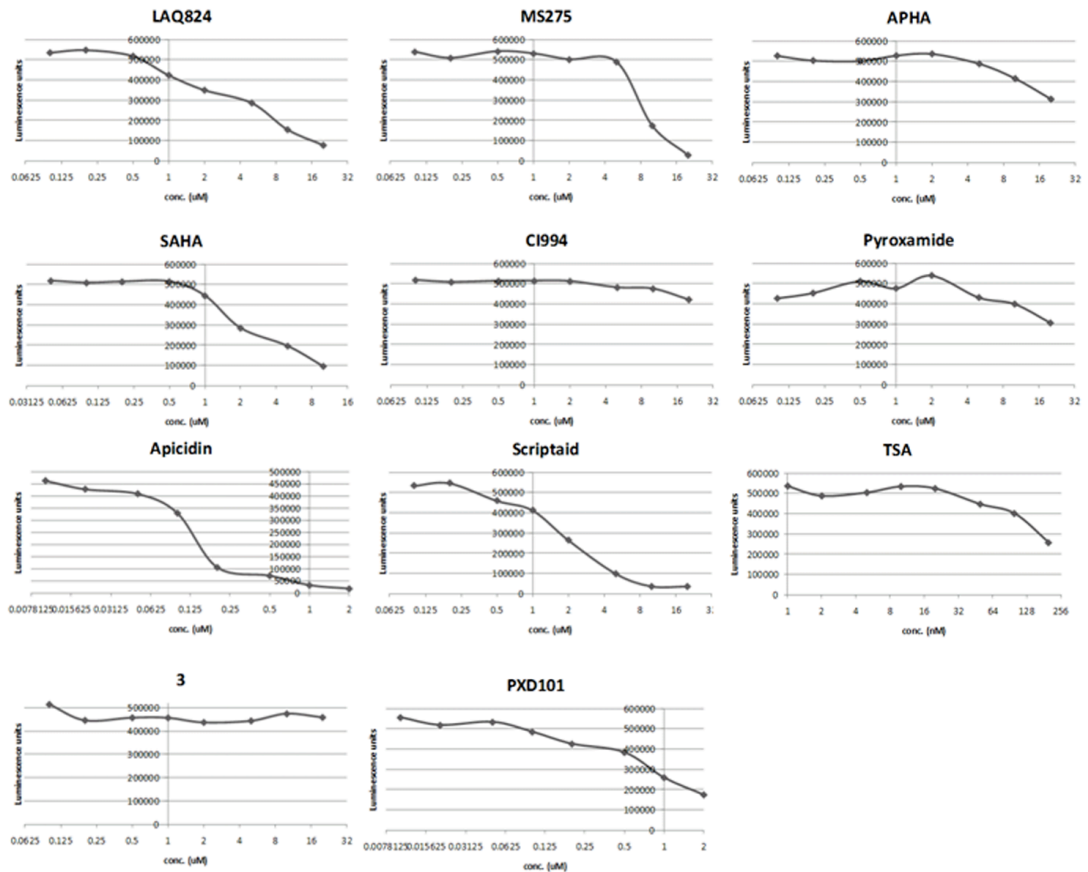


Figure 3-3. Cellular ATP levels of INS-1E cells treated with 11 different HDAC inhibitors in the absence of the cytokine cocktail were used to determine the maximum concentration of each compound used in the follow-up assays.

These measurements were made at a single compound concentration, the highest at which the cells remained viable (Figure 3-3). In order to determine concentration dependence, we tested MS-275 and SAHA as exemplars of class I (HDAC1, 2, 3) and broad-spectrum inhibition, respectively, over a 4- to 5-fold range of concentrations. Both MS-275 and SAHA restored ATP levels in INS-1E cells treated with cytokines, with SAHA resulting in a greater suppression (Figure 3-4 A). However, SAHA slightly increased caspase-3 activity, while MS-275 reduced caspase-3 activity

in the presence of cytokines by approximately 50% (Figure 3-4 B). MS-275 and SAHA resulted in comparable reduction of nitrite production in the presence of cytokines (Figure 3-4 C). Consistent with previous reports that SAHA could not restore the impairment in GSIS caused by treatment with cytokines (21), we confirmed that 1 μ M SAHA had no effect on GSIS, while 5 μ M MS-275 restored GSIS in the presence of cytokines (Figure 3-4 D). Moreover, MS-275 was also more effective in restoring mitochondrial membrane potential, another readout of apoptosis, than SAHA (Figure 3-5). These results suggest that MS-275 may be a superior suppressor of cytokine-induced beta-cell apoptosis than less selective HDAC inhibitors.

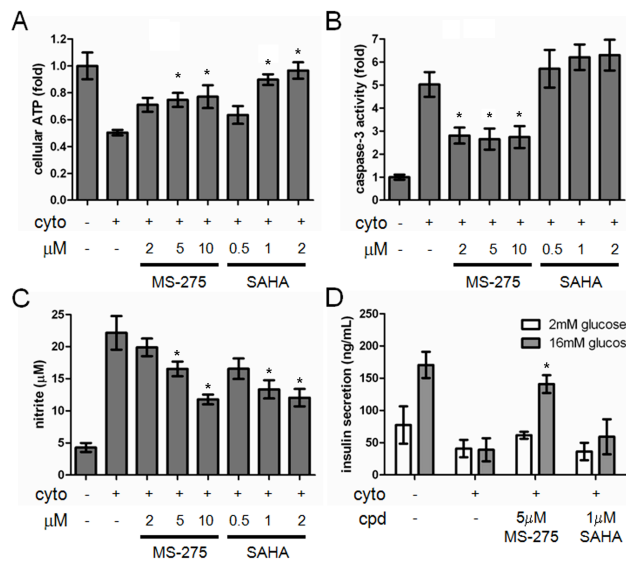


Figure 3-4. Cytokine-induced apoptosis is suppressed by MS-275 but not SAHA. (A) Effects of MS-275 and SAHA on cellular ATP levels in INS-1E cells after 48 hours in the presence of the cytokine cocktail. (B) Effects of MS-275 and SAHA on caspase-3 activity in the presence of the cytokine cocktail. (C) Effects of MS-275 and SAHA on nitrite production in the presence of the cytokine cocktail. (D) Effects of MS-275 and SAHA on insulin secretion in the presence of the cytokine cocktail.

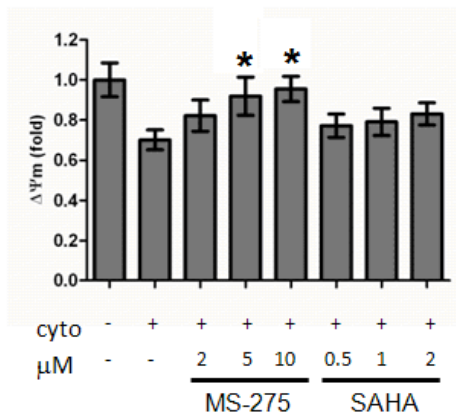
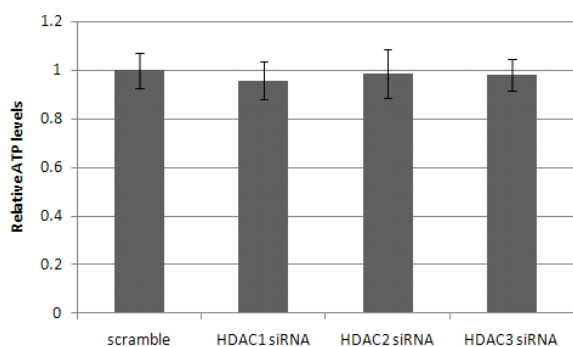
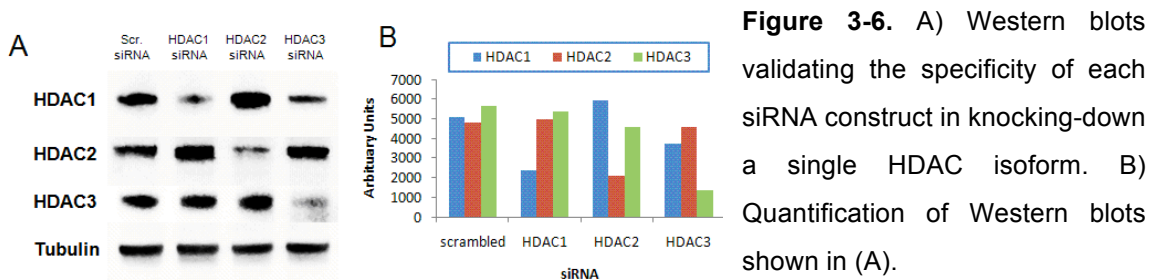


Figure 3-5. Effects of MS-275 and SAHA on restoring mitochondrial membrane potential ($\Delta\Psi_m$) in the presence of cytokines. Data represent the mean \pm standard deviation of 24 independent wells. * indicates $p < 0.05$.

3.3 siRNA-based knock-down studies identified HDAC3 as a target for suppressing of cytokine-induced beta-cell apoptosis

I then sought to determine the HDAC isoform(s) responsible for suppression of cytokine-induced beta-cell apoptosis. MS-275 is a selective inhibitor of HDAC1, 2, and 3, while SAHA additionally inhibits HDAC6 and 8(16). I reasoned that inhibition of HDAC1, 2, or 3 led to the protective effects of MS-275. To test this hypothesis, I performed gene-silencing experiments targeting these HDACs using small-interfering RNA (siRNA). siRNA duplexes specific for *Hdac1*, *Hdac2*, or *Hdac3* were transfected into INS-1E cells, leading to a selective decrease in protein expression of the appropriate HDAC (Figure 3-6). Each knock-down alone had no effect on viability (Figure 3-7).



Knock-down of *Hdac2* or *Hdac3* in the presence of cytokines each resulted in a 35% restoration of ATP levels, while knock-down of *Hdac1* had no effect (Figures 3-8 A). Only knock-down of *Hdac3* was sufficient to reduce caspase-3 activity (Figure 3-8 B). The protective effect of *Hdac3* knock-down is verified using two different siRNA constructs (Figure 3-9). Knock-down of either *Hdac2* or *Hdac3* resulted in slight but statistically significant reduction in nitrite production (Figure 3-8 C), while again knock-down of *Hdac1* had no effect. We observed similar effects of genetic knock-downs using a cell death ELISA readout measuring DNA-histone complexes (Figure 3-10). Importantly, knock-down of *Hdac3* alone led to restoration of GSIS (Figure 3-8 D), showing that the beta cells are fully functional. Moreover, knock-down of either *Hdac2* or *Hdac3* resulted in restoration in mitochondrial membrane potential (Figure 3-11). These results indicate that inhibition of HDAC3 is responsible for the

protective effects of MS-275 on beta cells in the presence of inflammatory cytokines.

Further, insulin secretion does not appear to be correlated with ATP levels alone, but

rather is more related to caspase activity.

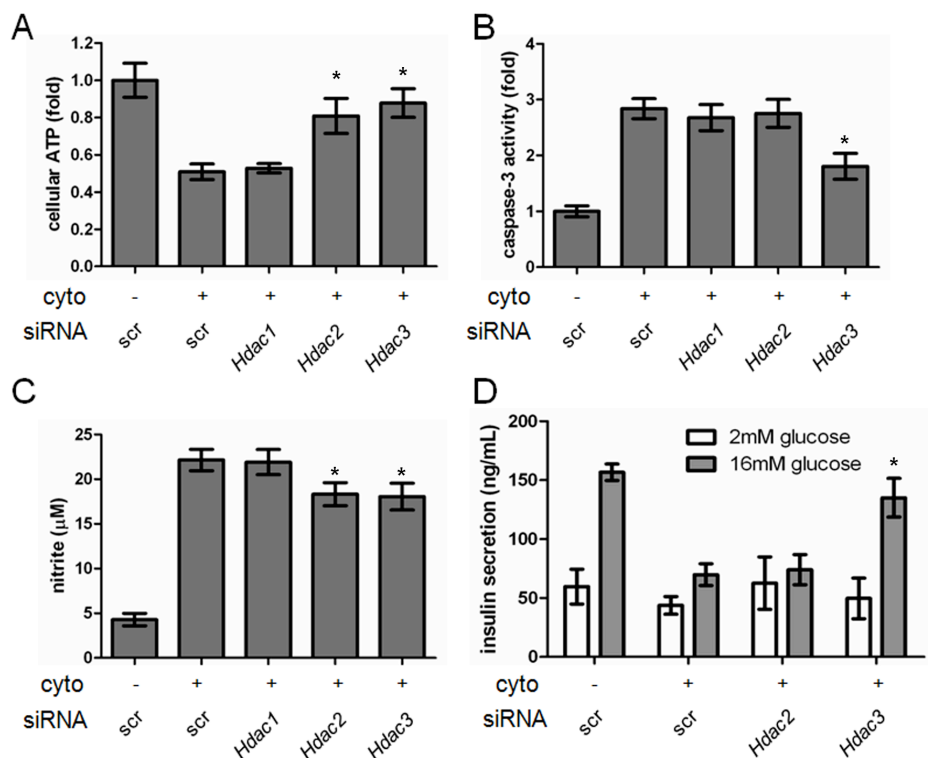


Figure 3-8. Genetic knock-down of *Hdac3* suppresses beta-cell apoptosis. The effects of knocking down *Hdac1*, 2, or 3 on (A) cellular ATP levels, (B) caspase-3 activity, (C) nitrite production, or (D) glucose-stimulated insulin secretion. Data represent the mean \pm standard deviation of 8 independent wells for insulin secretion and 24 independent wells for others. * indicates $p < 0.01$ as compared to the cytokine treatment alone.

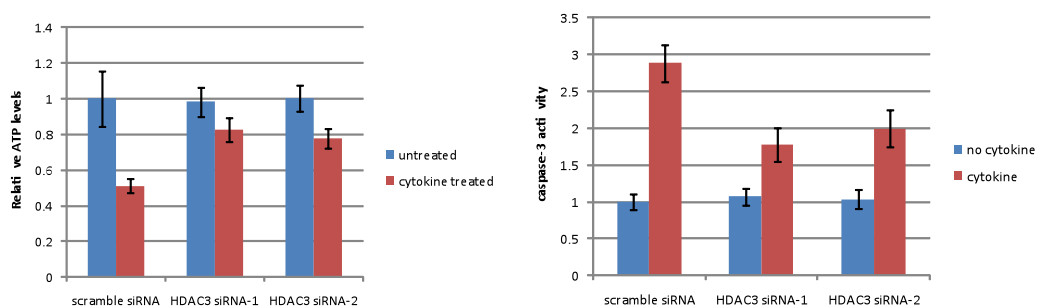


Figure 3-9. Two independent siRNA constructs of rat *Hdac3* restored cellular ATP levels and reduced caspase-3 activity in the presence of the cytokine cocktail. Data represent the mean \pm standard deviation of 24 independent wells.

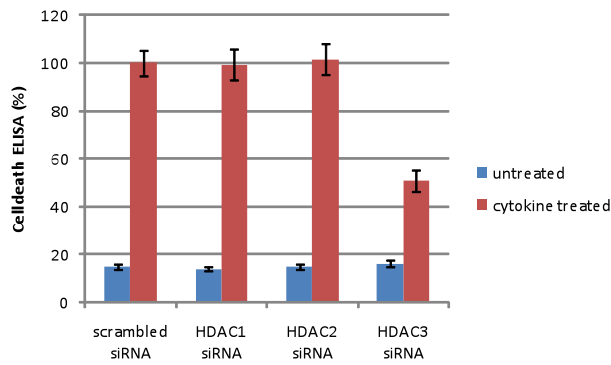


Figure 3-10. Effects of knocking down each HDAC isoform on reducing DNA-histone complexes released from the nucleus to the cytoplasm in the presence of cytokines. Data represent the mean \pm standard deviation of 4 independent wells. Data were normalized

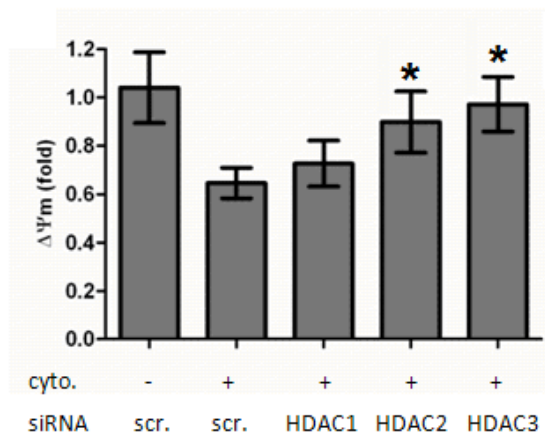


Figure 3-11. Effects of knocking down each HDAC isoform on restoring mitochondrial membrane potential ($\Delta\Psi_m$) in the presence of cytokines. Data represent the mean \pm standard deviation of 24 independent wells.

3.4 Further evidence from small-molecule HDAC inhibitors (“Merck 60” and HDAC3-selective inhibitors)

To further demonstrate the importance of HDAC3 in protecting insulin-secreting cells from cytokine-induced apoptosis, I used small-molecule inhibitors to chemically isolate HDAC3 activity. CI-994, an inhibitor selective for HDAC1, 2, and 3, restored ATP levels and reduced caspase-3 activity in INS-1E cells (Figure 3-12 A, B). A 2-thiophenyl analog of CI-994, **3** (Figure 3-2 E), exhibits inhibitory activity toward HDAC1 and 2 only (IC₅₀ 7 and 49 nM, respectively, vs. 10 μ M for HDAC3) (25). Thus, I could indirectly assess the effects of HDAC3 inhibition by comparing the activities of

3 and CI-994. Although **3** restored ATP levels (Figure 3-12 A), it did not reduce caspase-3 activity (Figure 3-12 B). Mitochondrial membrane potential was completely restored by CI-994, but not by **3** (Figure 3-13). These results further demonstrate the crucial role of HDAC3 in cytokine-induced beta-cell apoptosis.

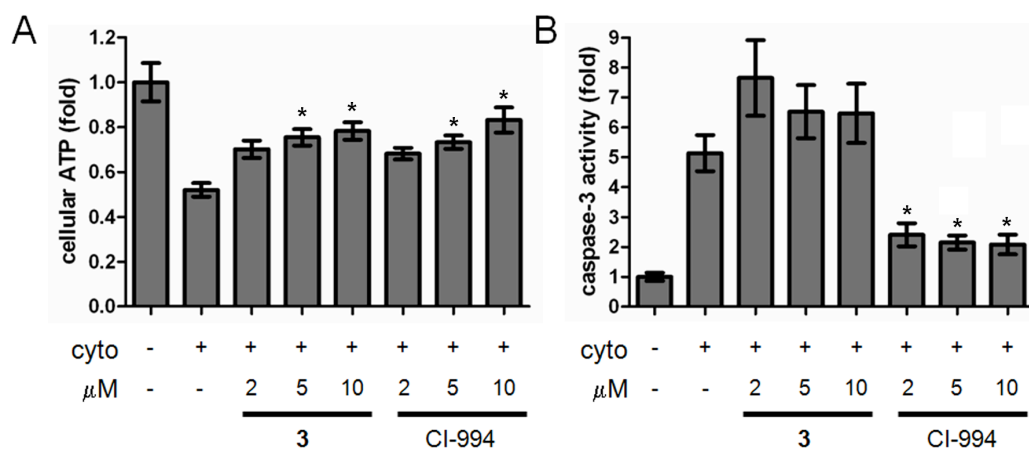


Figure 3-12. Analysis of chemical HDAC3 inhibition on beta-cell apoptosis. Effects of **3** and **4** (CI-994) on (A) cellular ATP levels and (B) caspase-3 activity in the presence of cytokines. Data represent the mean \pm standard deviation of 24 independent wells. * indicates $p < 0.01$ as compared to the cytokine treatment alone.

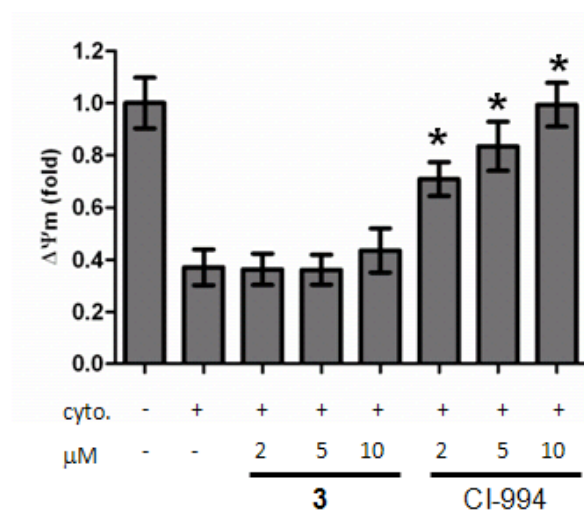


Figure 3-13. Effects of **3** and CI-994 on restoring mitochondrial membrane potential ($\Delta\Psi_m$) in the presence of cytokines. Data represent the mean \pm standard deviation of 24 independent wells. * indicates $p < 0.01$ as compared to the cytokine treatment alone.

I also tested some HDAC inhibitors that show selectivity toward HDAC3, but not HDAC1 and HDAC2. These compounds were synthesized by Professor Jacob

Hooker at Massachusetts General Hospital (Figure 3-14), originally as part of an effort to identify potential *in vivo* imaging agents for HDAC activity. Compound **5-9** are HDAC inhibitors that show selectivity toward HDAC3. However, compound **10**, like **3**, has an aromatic substituent in the biasing element and is selective toward HDAC1 and HDAC2.

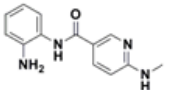
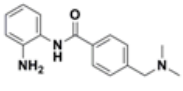
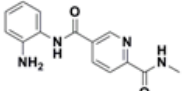
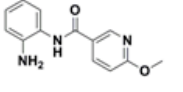
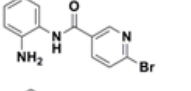
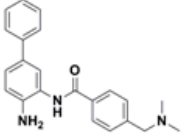
	HDAC1 (nM)	HDAC2 (nM)	HDAC3 (nM)	
	5	104	319	61
	6	226	444	112
	7	882	1080	126
	8	1140	421	227
	9	940	1060	178
	10	12	76	1750

Figure 3-14. HDAC inhibitors synthesized by Prof. Jacob Hooker, a collaborator at MGH. Biochemical assay was done using caliper assay (Caliper Life Sciences).

In measuring cellular ATP levels in the presence of cytokines, I found that all the compounds were able to restore cell viability in the presence of cytokines (Figure 3-15). This result is consistent with the result of CI-994 and compound **3**. However, only compounds **5-9** were able to reduce caspase-3 activity by 40% in the presence of cytokines (Figure 3-16). Compound **10** cannot reduce caspase-3 activity. Here, the

results from small-molecule HDAC3-selective inhibitors further show the important role of HDAC3 in cytokine-induced beta-cell apoptosis.

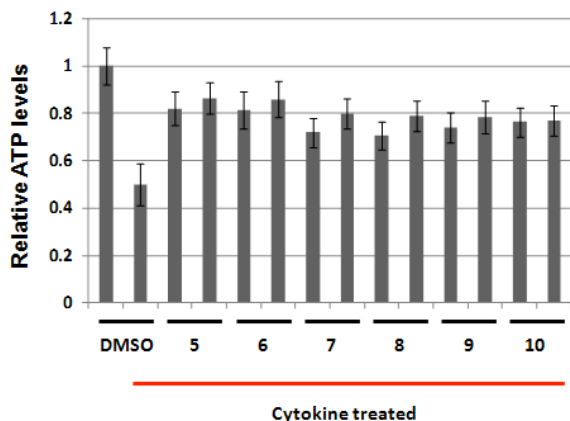


Figure 3-15. Analysis of small-molecule HDAC3 inhibition on beta-cell apoptosis.

Effects of **5** to **10** were tested in cellular ATP levels. Concentrations used were: **5**, 2.5 μM and 5 μM; **6**, 5 μM and 10 μM; **7**, 5 μM and 10 μM; **8**, 5 μM and 10 μM; **9**, 5 μM and 10 μM; **10**, 5 μM and 10 μM.

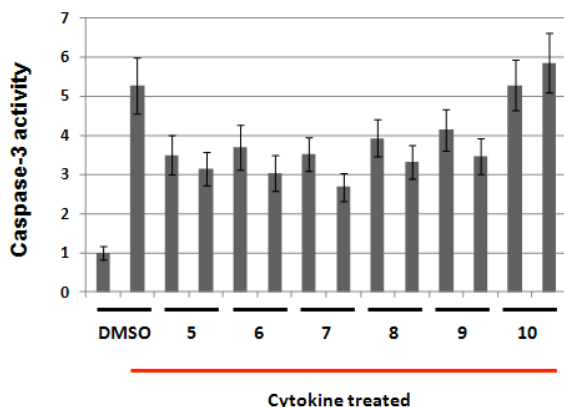


Figure 3-16. Analysis of small-molecule HDAC3 inhibition on beta-cell apoptosis.

Effects of **5** to **10** were tested in caspase-3 activity. Concentrations used were: **5**, 2.5 μM and 5 μM; **6**, 5 μM and 10 μM; **7**, 5 μM and 10 μM; **8**, 5 μM and 10 μM; **9**, 5 μM and 10 μM; **10**, 5 μM and 10 μM.

3.5 Conclusion

In conclusion, I evaluated a panel of eleven clinically advanced HDAC inhibitors and found that MS-275 and CI-994 suppress cytokine-induced beta-cell apoptosis, while the less selective inhibitors SAHA and TsA do not. By comparing these results to biochemical activities, I narrowed down the possible HDAC targets to a combination of HDAC1, 2, or 3. Using siRNA reagents and isoform-selective inhibitors, I observed that inhibition of HDAC3 appears to be critical for the protective effects of

HDAC inhibitors, while the inhibition of additional isoforms may be deleterious to beta-cell function. The lack of correlation between ATP levels and caspase activity after treatment with some of these compounds suggests that these assays are reading out different aspects of cell toxicity. This notion is consistent with a previous analysis of the lack of overlap between viability assay readouts in hepatoma cells (26). Larsen *et al.* demonstrated that inhibition of the NF κ B pathway is responsible for the protective effects of HDAC inhibitors. The p65 subunit of NF κ B is acetylated by both p300 and PCAF on lysines 122 and 123(27). Acetylated p65 is subsequently deacetylated through a specific interaction with HDAC3(28). Acetylation of p65 reduces its ability to bind κ B-DNA(27). Moreover, acetylation of p65 facilitated its removal from DNA and consequently its I κ B α -mediated export from the nucleus(27). Therefore, inhibition of HDAC3 could reduce the activity of NF κ B. This is totally consistent with my finding that selective inhibition of HDAC3 is responsible for preventing cytokine-induced beta-cell apoptosis. This study suggests the development of more selective HDAC3 inhibitors, and exploration of their potential uses in protecting pancreatic beta cells from inflammatory attack during the development of type-1 diabetes.

3.6 Methods and Materials

Cell culture and reagents. INS-1E cells (generously provided by Claes Wollheim and Pierre Maechler, University of Geneva, Switzerland) were maintained in culture medium (RPMI 1640 containing 11 mM glucose, 10% fetal bovine serum, 10 mM HEPES, 50 μ M 2-mercaptoethanol, 1 mM sodium pyruvate) and cultivated at 37C with 5% CO₂ in a humidified atmosphere. Recombinant rat IL-1 β and recombinant mouse TNF- α were purchased from R&D Systems. Recombinant mouse IFN- γ and Griess reagent were purchased from Sigma. CellTiter-Glo and Caspase-Glo 3/7 reagents were purchased from Promega. Rabbit antibodies for HDAC1, 2 and 3 were from CellSignaling. Mouse monoclonal antibody to tubulin was from Sigma. Secondary horseradish peroxidase-conjugated goat anti-mouse and anti-rabbit antibodies were from Thermo Fisher Scientific. HDAC inhibitors were purchased from Sigma or synthesized in-house.

Measurement of cellular ATP levels. INS-1E cells were seeded at 10,000 cells/well using a Multidrop Combi (Thermo LabSystems) in white optical 384-well plates (Corning Life Sciences). After overnight incubation, medium was removed and 50 μ L RPMI containing the treated compound, 1% FBS and a combination of cytokines (10 ng/mL IL-1 β , 50 ng/mL IFN- γ , 25 ng/mL TNF- α) was added to every well. After incubation for 48 hr, medium was removed and 20 μ L CellTiter-Glo reagent was

added. Luminescence was measured after 10-min incubation using an EnVision plate reader (PerkinElmer).

Measurement of cellular nitrite production. INS-1E cells were seeded at 10,000 cells/well using a Multidrop Combi (Thermo Labsystems) in white optical 384-well plates (Corning Life Sciences). After overnight incubation, medium was removed and 50 μ L RPMI containing the treated compound, 1% FBS and a combination of cytokines (10 ng/mL IL-1 β , 50 ng/mL IFN- γ , 25 ng/mL TNF- α) was added to every well. After treatment with cytokine and compounds for 48 hr, 10 μ L modified Griess reagent (1:1 mixture of 1% sulfanilamide in 30% acetic acid and 0.1% *N*-(1-naphthyl) ethylenediamine dihydrochloride in 60% acetic acid) was added to each well. After 5-min incubation at room temperature, the absorbance at 540 nm was measured using an Envision plate reader (PerkinElmer).

Measurement of mitochondrial membrane potential. INS-1E cells were seeded at 10,000 cells/well using a Multidrop Combi (Thermo Labsystems) in white optical 384-well plates (Corning Life Sciences). After overnight incubation, medium was removed and 50 μ L RPMI containing the treated compound, 1% FBS and a combination of cytokines (10 ng/mL IL-1 β , 50 ng/mL IFN- γ , 25 ng/mL TNF- α) was

added to every well. After treatment with cytokine and compounds for 48 hr, 20 μ L of 3.25 μ M JC-1 was added to each well. After 3hr incubation at 37°C, the cells were gently washed three times with 50 μ L per well of 1X PBS (with Ca²⁺ and Mg²⁺). Fluorescence was measured with an EnVision plate reader (PerkinElmer) at the rhodamine spectra (excitation/emission 530 nm/580 nm) followed by fluorescein (excitation/emission 485 nm/530 nm). The ratio of rhodamine to fluorescein intensity was determined and represents the degree of mitochondrial membrane potential.

Caspase-3 activity assay. INS-1E cells were seeded at 5,000 cells/well using a Multidrop Combi (Thermo Labsystems) in white optical 384-well plates (Corning Life Sciences). After overnight incubation, medium was removed and 50 μ L RPMI containing the treated compound, 1% FBS and a combination of cytokines (10 ng/mL IL-1 β , 50 ng/mL IFN- γ , 25 ng/mL TNF- α) was added to every well. After treatment with cytokines and compounds for 48 hr, medium was removed and 20 μ L Caspase-Glo 3/7 reagent was added. Luminescence was measured after 2-hr incubation using an Envision plate reader (PerkinElmer).

Measurement of cellular apoptosis. INS-1E cells were seeded at 10,000 cells/well using a Multidrop Combi (Thermo Labsystems) in white optical 384-well plates

(Corning Life Sciences). After overnight incubation, medium was removed and 50 μ L RPMI containing the treated compound, 1% FBS and a combination of cytokines (10 ng/mL IL-1 β , 50 ng/mL IFN- γ , 25 ng/mL TNF- α) was added to every well for a 48hr-treatment. The degree of cytokine-induced apoptosis was determined by cell-death detection ELISA (Roche) measuring the amount of DNA-histone complexes present in the cytoplasmic lysates according to manufacturer's description. This assay is based on a sensitive fluorescent nucleic acid stain facilitating the quantification of double-stranded DNA in solution.

RNA interference and Western blotting. Small-interfering RNAs against *Hdac1*, 2 and 3 were obtained from Dharmacon. siRNAs (100 nM) were transfected into INS-1E cells (5,000 cells/well in a 384-well plate) using DharmaFECT reagent. Transfected cells were cultured for 72hr, then collected for Western blot analysis and cell-based assays. For Western blotting, cells were lysed in RIPA buffer. Total protein was separated by 4-12% SDS-PAGE and transferred to a PVDF membrane. Blots were developed using the chemiluminescence detection system SuperSignal (Thermo Fisher Scientific) and light emission was captured using an Imaging Station 4000MM (Carestream).

Glucose-stimulated insulin secretion. INS-1E cells were seeded in 96-well plates at 20,000 cells/well in 100 μ L RPMI and incubated for 48 hr in 100 μ L fresh RPMI containing 1% FBS and the cytokine cocktail in the presence or absence of 5 μ M MS-275. Cells were washed and incubated for 2 hr in KRBH buffer (135 mM NaCl, 3.6 mM KCl, 5 mM NaHCO₃, 0.5 mM NaH₂PO₄, 0.5 mM MgCl₂, 1.5 mM CaCl₂, 10 mM HEPES, pH 7.4, 0.1% BSA) lacking glucose. Cells were subsequently incubated with KRBH buffer containing 2 mM or 16 mM glucose for 1 hr. The supernatant was collected for measurement of secreted insulin. Insulin was measured with a rat insulin ELISA kit (Alpco).

3.7 References

1. Davie, J. R., and Spencer, V. A. (1999) Control of histone modifications, *J Cell Biochem Suppl* 32-33, 141-148.
2. Bhaumik, S. R., Smith, E., and Shilatifard, A. (2007) Covalent modifications of histones during development and disease pathogenesis, *Nat Struct Mol Biol* 14, 1008-1016.
3. Hubbert, C., Guardiola, A., Shao, R., Kawaguchi, Y., Ito, A., Nixon, A., Yoshida, M., Wang, X. F., and Yao, T. P. (2002) HDAC6 is a microtubule-associated deacetylase, *Nature* 417, 455-458.
4. Matsuyama, A., Shimazu, T., Sumida, Y., Saito, A., Yoshimatsu, Y., Seigneurin-Berny, D., Osada, H., Komatsu, Y., Nishino, N., Khochbin, S., Horinouchi, S., and Yoshida, M. (2002) In vivo destabilization of dynamic microtubules by HDAC6-mediated deacetylation, *EMBO J* 21, 6820-6831.
5. Michan, S., and Sinclair, D. (2007) Sirtuins in mammals: insights into their biological function, *Biochem J* 404, 1-13.
6. Kruhlak, M. J., Hendzel, M. J., Fischle, W., Bertos, N. R., Hameed, S., Yang, X. J., Verdin, E., and Bazett-Jones, D. P. (2001) Regulation of global acetylation

- in mitosis through loss of histone acetyltransferases and deacetylases from chromatin, *J Biol Chem* 276, 38307-38319.
7. Neely, K. E., and Workman, J. L. (2002) The complexity of chromatin remodeling and its links to cancer, *Biochim Biophys Acta* 1603, 19-29.
 8. Gregoret, I. V., Lee, Y. M., and Goodson, H. V. (2004) Molecular evolution of the histone deacetylase family: functional implications of phylogenetic analysis, *J Mol Biol* 338, 17-31.
 9. Itazaki, H., Nagashima, K., Sugita, K., Yoshida, H., Kawamura, Y., Yasuda, Y., Matsumoto, K., Ishii, K., Uotani, N., Nakai, H., and et al. (1990) Isolation and structural elucidation of new cyclotrapeptides, trapoxins A and B, having detransformation activities as antitumor agents, *J Antibiot (Tokyo)* 43, 1524-1532.
 10. Kijima, M., Yoshida, M., Sugita, K., Horinouchi, S., and Beppu, T. (1993) Trapoxin, an antitumor cyclic tetrapeptide, is an irreversible inhibitor of mammalian histone deacetylase, *J Biol Chem* 268, 22429-22435.
 11. Yoshida, M., Horinouchi, S., and Beppu, T. (1995) Trichostatin A and trapoxin: novel chemical probes for the role of histone acetylation in chromatin structure and function, *Bioessays* 17, 423-430.
 12. Taunton, J., Hassig, C. A., and Schreiber, S. L. (1996) A mammalian histone deacetylase related to the yeast transcriptional regulator Rpd3p, *Science* 272, 408-411.
 13. Hassig, C. A., Fleischer, T. C., Billin, A. N., Schreiber, S. L., and Ayer, D. E. (1997) Histone deacetylase activity is required for full transcriptional repression by mSin3A, *Cell* 89, 341-347.
 14. Minucci, S., and Pelicci, P. G. (2006) Histone deacetylase inhibitors and the promise of epigenetic (and more) treatments for cancer, *Nat Rev Cancer* 6, 38-51.
 15. Finnin, M. S., Donigian, J. R., Cohen, A., Richon, V. M., Rifkind, R. A., Marks, P. A., Breslow, R., and Pavletich, N. P. (1999) Structures of a histone deacetylase homologue bound to the TSA and SAHA inhibitors, *Nature* 401, 188-193.
 16. Bradner, J. E., West, N., Grachan, M. L., Greenberg, E. F., Haggarty, S. J., Warnow, T., and Mazitschek, R. Chemical phylogenetics of histone deacetylases, *Nat Chem Biol* 6, 238-243.
 17. Marsoni, S., Damia, G., and Camboni, G. (2008) A work in progress: the clinical development of histone deacetylase inhibitors, *Epigenetics* 3, 164-171.
 18. Abel, T., and Zukin, R. S. (2008) Epigenetic targets of HDAC inhibition in neurodegenerative and psychiatric disorders, *Curr Opin Pharmacol* 8, 57-64.

19. Hutt, D. M., Herman, D., Rodrigues, A. P., Noel, S., Pilewski, J. M., Matteson, J., Hoch, B., Kellner, W., Kelly, J. W., Schmidt, A., Thomas, P. J., Matsumura, Y., Skach, W. R., Gentsch, M., Riordan, J. R., Sorscher, E. J., Okiyoneda, T., Yates, J. R., 3rd, Lukacs, G. L., Frizzell, R. A., Manning, G., Gottesfeld, J. M., and Balch, W. E. Reduced histone deacetylase 7 activity restores function to misfolded CFTR in cystic fibrosis, *Nat Chem Biol* 6, 25-33.
20. Christensen, D. P., Dahllof, M., Lundh, M., Rasmussen, D. N., Nielsen, M. D., Billestrup, N., Grunnet, L. G., and Mandrup-Poulsen, T. (2011) HDAC inhibition as a novel treatment for diabetes mellitus, *Mol Med*.
21. Larsen, L., Tonnesen, M., Ronn, S. G., Storling, J., Jorgensen, S., Mascagni, P., Dinarello, C. A., Billestrup, N., and Mandrup-Poulsen, T. (2007) Inhibition of histone deacetylases prevents cytokine-induced toxicity in beta cells, *Diabetologia* 50, 779-789.
22. Lewis, E. C., Blaabjerg, L., Storling, J., Ronn, S. G., Mascagni, P., Dinarello, C. A., and Mandrup-Poulsen, T. (2010) The oral histone deacetylase inhibitor ITF2357 reduces cytokines and protects islet beta-cells in vivo and in vitro, *Mol Med*.
23. Chou, D. H., Bodycombe, N. E., Carrinski, H. A., Lewis, T. A., Clemons, P. A., Schreiber, S. L., and Wagner, B. K. (2010) Small-Molecule Suppressors of Cytokine-Induced beta-Cell Apoptosis, *ACS Chem Biol* 5, 729-734.
24. Merglen, A., Theander, S., Rubi, B., Chaffard, G., Wollheim, C. B., and Maechler, P. (2004) Glucose sensitivity and metabolism-secretion coupling studied during two-year continuous culture in INS-1E insulinoma cells, *Endocrinology* 145, 667-678.
25. Methot, J. L., Chakravarty, P. K., Chenard, M., Close, J., Cruz, J. C., Dahlberg, W. K., Fleming, J., Hamblett, C. L., Hamill, J. E., Harrington, P., Harsch, A., Heidebrecht, R., Hughes, B., Jung, J., Kenific, C. M., Kral, A. M., Meinke, P. T., Middleton, R. E., Ozerova, N., Sloman, D. L., Stanton, M. G., Szewczak, A. A., Tyagarajan, S., Witter, D. J., Secrist, J. P., and Miller, T. A. (2008) Exploration of the internal cavity of histone deacetylase (HDAC) with selective HDAC1/HDAC2 inhibitors (SHI-1:2), *Bioorg Med Chem Lett* 18, 973-978.
26. Miret, S., De Groene, E. M., and Klaffke, W. (2006) Comparison of in vitro assays of cellular toxicity in the human hepatic cell line HepG2, *J Biomol Screen* 11, 184-193.
27. Kiernan, R., Bres, V., Ng, R. W., Coudart, M. P., El Messaoudi, S., Sardet, C., Jin, D. Y., Emiliani, S., and Benkirane, M. (2003) Post-activation turn-off of NF-kappa B-dependent transcription is regulated by acetylation of p65, *J Biol Chem* 278, 2758-2766.

28. Chen, L., Fischle, W., Verdin, E., and Greene, W. C. (2001) Duration of nuclear NF-kappaB action regulated by reversible acetylation, *Science* 293, 1653-1657.

Chapter 4: Identification of BRD0476 as a novel suppressor of cytokine-induced beta-cell apoptosis

4.1 Introduction

Type-1 diabetes is caused by the autoimmune destruction of insulin-producing beta cells in the pancreas. The infiltration of pancreatic islets by macrophages and secretion of inflammatory cytokines such as IL-1 β , IFN- γ , and TNF- α are believed to cause beta-cell death(1). Activation of transcription factors such as NF κ B and STAT1 by these cytokines triggers the intrinsic apoptotic pathway in both rodent and human cell models(2). A small-molecule probe capable of preventing or reversing cytokine-induced beta-cell death could have great potential in developing therapies for early-stage type-1 diabetes.

Previous efforts to suppress beta-cell apoptosis with small molecules involved compounds with antioxidant or antiinflammatory activity(3-4), and more recently with inhibitors of histone deacetylase activity(5-6). In chapter 2, I described a suite of cell-based assays that can be used to identify small-molecule suppressors of beta-cell death, and examined the effects of inhibitors of glycogen synthase kinase 3 β , pyrazole derivatives, and glucocorticoids(7). This pilot-scale screen identified small molecules that increased ATP levels, but the majority of these compounds did not have effects on other aspects of beta-cell biology, such as insulin secretion. Therefore,

I sought to identify more complete suppressors of cytokine-induced beta-cell apoptosis that result in normal beta-cell function.

In this chapter, I will describe a large-scale high-throughput screen (HTS) effort to identify suppressors of cytokine-induced beta-cell apoptosis. I screened 29,760 compounds and identified several hit compounds. Among them, BRD0608, a compound synthesized via diversity-oriented synthesis (DOS)(8-10), was chosen for follow-up studies. I will also describe the development of a stereochemically diverse library of medium-sized rings, which led to the synthesis of BRD0608. Further optimization of the initial hit cluster and follow-up biological studies resulted in a compound, BRD0476, capable of restoring physiological properties to beta cells in the presence of these cytokines.

4.2 Results of a 29,760-compound library screen

As described in Chapter 2, I developed a high-throughput assay using INS-1E cells to screen for suppressors of cytokine-induced beta-cell apoptosis(7). I collaborated with Dr. Patrick Faloon in the Chemical Biology Platform of Broad Institute to screen a 29,760-compound library. Dr. Faloon provided guidance in using screening instruments and analyzing screening data. In the screen, the rat beta cell line INS-1E(11) was treated in 384-well format with this library in the presence of a

cocktail of inflammatory cytokines (IL-1 β , IFN- γ , and TNF- α) for 48 hours. Luciferase-based measurement of cellular ATP levels was used as a surrogate of cell viability. In the primary high-throughput screen (HTS), compounds were called active if they increased cellular ATP levels, indicated by an increase in luminescence. The positive control, the pyrazole SPB07503 (Figure 2-7), increased ATP levels at 10 μ M, and was used to normalize data. For the primary screen and other assays, negative-control (NC) wells and positive-control (PC) wells were included on every plate. Compounds with activities >3 standard deviation of NC were considered hits and chosen for confirmation in dose studies. The raw signals of the plate wells were normalized using the software Genedata Assay Analyzer (v7.0.3). The median raw signal of the intra-plate NC wells was set to a normalized activity value of 0, while the median raw signal of the intra-plate PC wells was set to a normalized activity value of 100. Experimental wells were scaled to this range, resulting in an activity score representing the percent change in signal relative to the intra-plate controls. In total, 29,760 compounds were screened in duplicate and the two replicates correlated well since most of the points were near the diagonal (Figure 4-1).

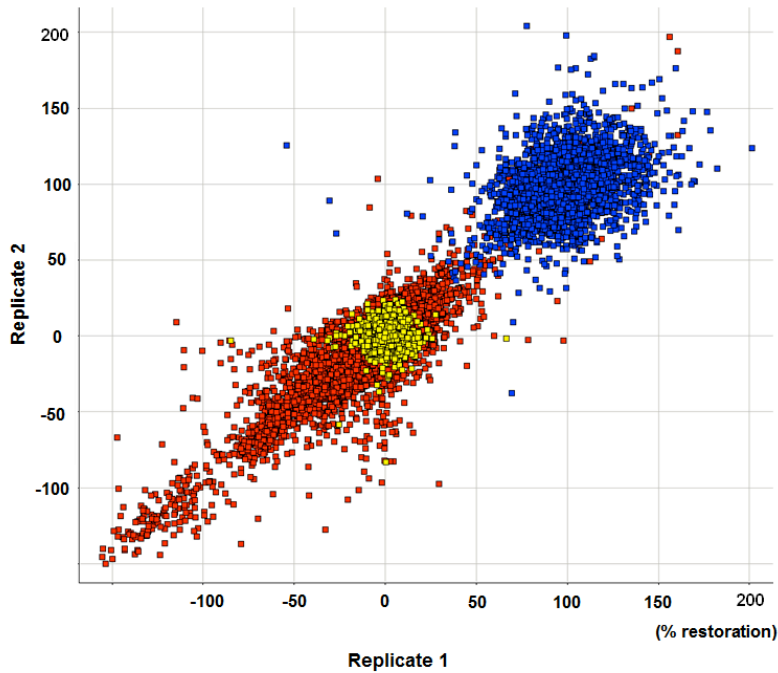


Figure 4-1. Scatter-plot of the HTS result. Each plate was screened twice. Yellow dots are mock controls- wells treated with cytokine cocktails and DMSO. Blue dots are positive controls. Red dots

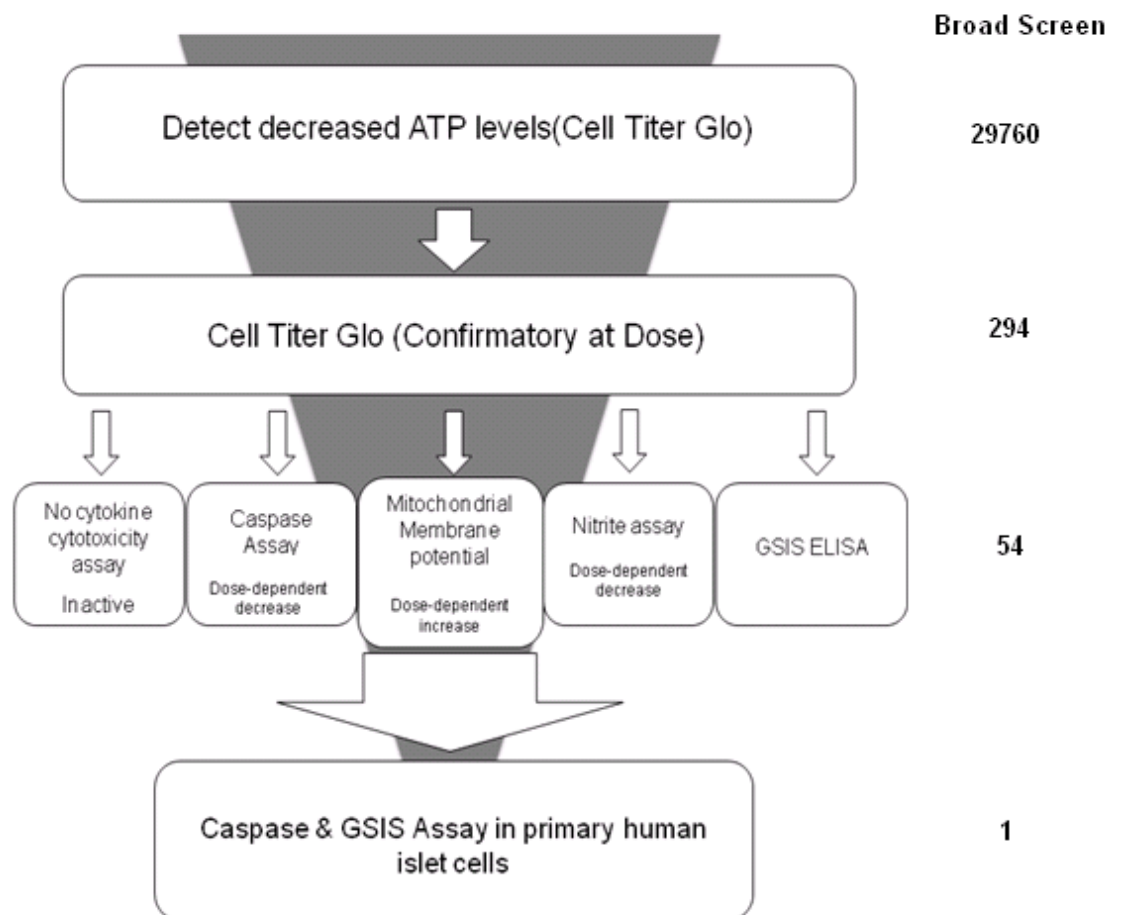


Figure 4-2. Critical path for high-throughput screen. 29,760 compounds were screened in HTS. Among them, 294 were chosen for further 8-dose retest confirmation. 54 out of 294 were

Fig. 4-2 (Continued)

confirmed to increase cellular ATP levels in a dose-dependent manner. These 54 compounds were further tested in secondary assays including caspase-3 activity, mitochondrial membrane potential, nitrite production and glucose-stimulated insulin secretion (GSIS). In the end, one compound was prioritized for human islets studies.

After the primary screen, I chose 294 compounds for further 8-dose retest confirmation (Figure 4-2). The 294 compounds included active compounds selected from the primary screen, and their structurally similar analogs. 42 out of the 294 are compounds with activities >3 standard deviation of NC. Other active compounds were picked using several other analysis methods. The results of the 294 compounds were then used to evaluate different analysis methods. Analogs were only chosen for chemical similarity without the consideration of any cellular activity. 54 out of 294 were confirmed to increase cellular ATP levels in a dose-dependent manner with an EC_{50} value in Genedata Assay Analyzer. These 54 compounds were further tested in secondary assays, including caspase-3 activity, mitochondrial membrane potential, nitrite production, and glucose-stimulated insulin secretion (GSIS). A suppressor of beta-cell apoptosis should be able to reduce caspase-3 activity in the presence of cytokines. However, most compounds fell out of consideration after running the caspase-3 assay. For example, 17-allylamino-17-demethoxygeldanamycin (17-AAG), an analog of geldanamycin, increased cellular ATP levels to 150% of the positive control in the presence of the cytokine cocktail (Figure 4-3 A). However, it not

only could not reduce caspase-3 activity, but further increased its activity by nearly 50% (Figure 4-3 B). 17-AAG, an Hsp90 inhibitor, is a less toxic and more stable analog of geldanamycin(12). 17-AAG induces the degradation of proteins that are mutated in tumor cells such as v-src, bcr-abl and p53 preferentially over their normal cellular counterparts by inhibiting Hsp90(13). Therefore, it is not surprising that 17-AAG can increase caspase-3 activity, an apoptosis marker, since it could also induce apoptosis in cancer cells.

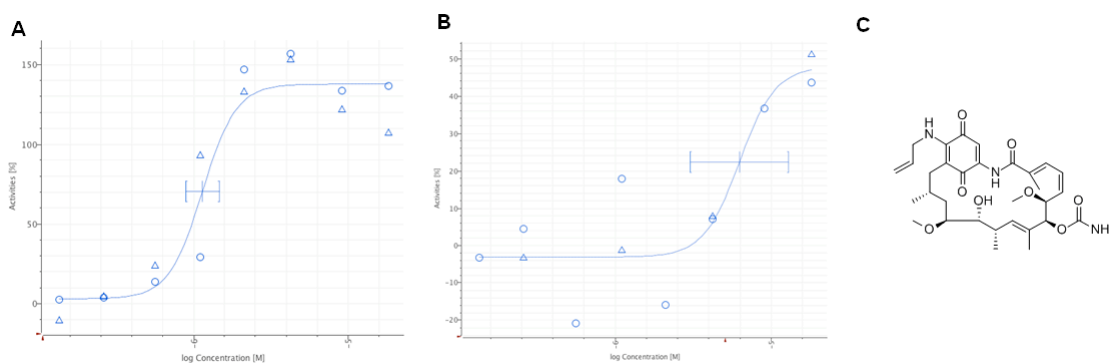


Figure 4-3. Effects of 17-AAG in dose studies. 17-AAG was tested in 8 does in duplicate (circles and triangles are two independent experiments) for **A)** cellular ATP levels and **B)** caspase-3 activity. The median raw signal of the intra-plate NC wells was set to a normalized activity value of 0, while the median raw signal of the intra-plate PC wells was set to a normalized activity value of 100. **C)** Chemical structure of 17-AAG, an analog of geldanamycin.

There were also compounds that had the desired protective effects. Hemanthamine is a crinine-type alkaloid natural product. The crinine-type alkaloids, which have the 5,10b-ethanophenanthridine skeleton as the core structure, represented by hemanthidine, pretazettine, and tazettine, have received considerable

attention, since they have been reported to possess antiviral, anticancer, and other interesting activities(14-16). Hemanthamine restored cellular ATP levels to ~60% of the positive control (Figure 4-4 A) and slightly reduced caspase-3 activity (Figure 4-4 B). However, owing to the lack of commercial availability and to the difficulty of synthesizing this alkaloid, I decided not to pursue hemanthamine in further follow-up studies.

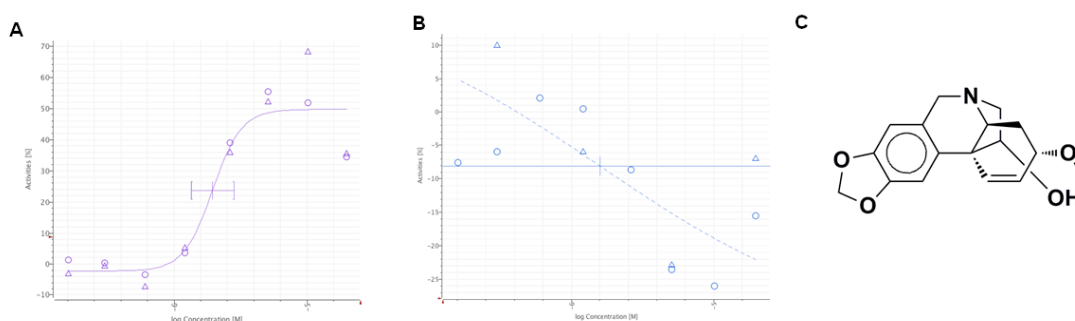


Figure 4-4. Effects of hemanthamine in dose studies. Hemanthamine was tested in 8 doses in duplicate (circles and triangles are two independent experiments) for **A)** cellular ATP levels and **B)** caspase-3 activity. The median raw signal of the intra-plate NC wells was set to a normalized activity value of 0, while the median raw signal of the intra-plate PC wells was set to a normalized activity value of 100. **C)** Chemical structure of hemanthamine.

Another promising compound, 9-methylstreptimidone, was first isolated as an antibiotic(17) but later rediscovered from the culture filtrate of *Streptomyces* species by Umezawa and co-workers in 2006 as an inhibitor of NF κ B pathway(18). 9-methylstreptimidone inhibited NO production and iNOS expression in lipopolysaccharide-stimulated RAW264.7 macrophage cells and induced apoptosis in Jurkat T lymphocytes, similar to other NF κ B pathway inhibitors(18). Therefore,

9-methylstreptimidone had been suggested as a lead for developing new antiinflammatory agents. In this screen, I found that 9-methylstreptimidone restored cellular ATP levels to ~40% of the positive control (Figure 4-5 A) and slightly reduced caspase-3 activity by 20% (Figure 4-5 B). Since 9-methylstreptimidone was annotated as an inhibitor of NF κ B pathway, it is not surprising that this compound could block the apoptotic effect of cytokines. Because of the lack of commercial availability, 9-methylstreptimidone was not further studied.

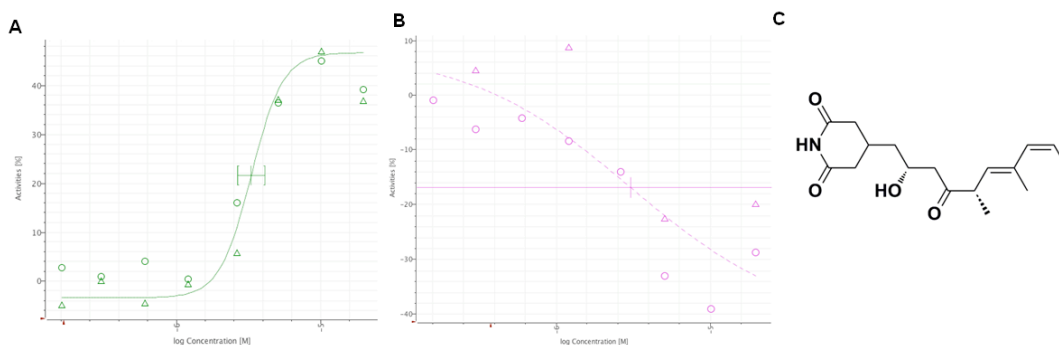


Figure 4-5. Effects of 9-methylstreptimidone in dose studies. 9-methylstreptimidone was tested in 8 does in duplicate (circles and triangles are two independent experiments) for **A**) cellular ATP levels and **B**) caspase-3 activity. The median raw signal of the intra-plate NC wells was set to a normalized activity value of 0, while the median raw signal of the intra-plate PC wells was set to a normalized activity value of 100. **C**) Chemical structure of 9-methylstreptimidone.

I also identified BRD0608, synthesized via diversity-oriented synthesis, as a novel suppressor of beta-cell apoptosis. It restored cellular ATP levels to ~100% of the positive control (Figure 4-6 A) and reduced caspase-3 activity by 70% (Figure 4-6 B). Because of the interesting chemical and biological properties, BRD0608 was

further studied in other secondary assays. Moreover, analogs of BRD0608 were synthesized to improve both potency and maximum effect of the suppressor. In the end, one compound, BRD0476, was selected for studies in human islets. BRD0476 was also used to study the mechanism of action of this series of compounds.

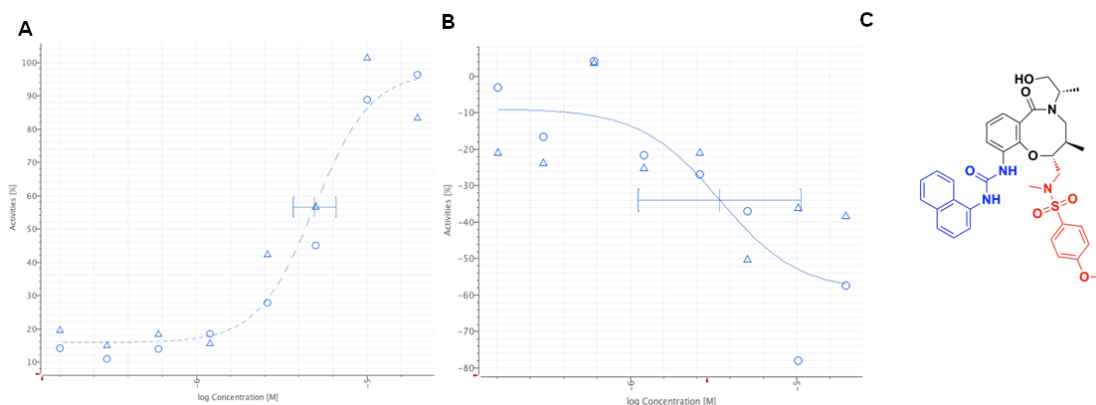
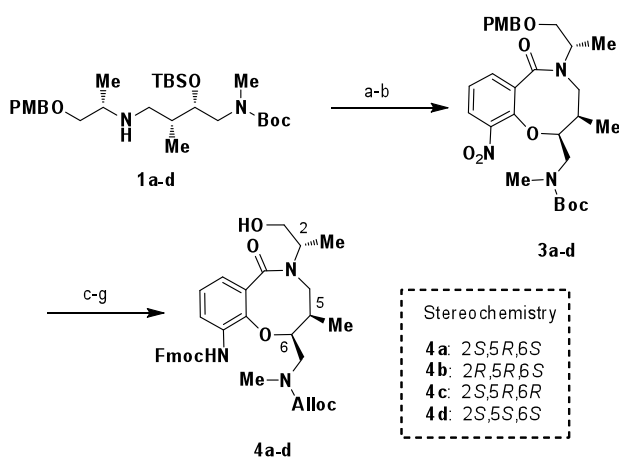


Figure 4-6. Effects of BRD0608 in dose studies. BRD0608 was tested in 8 does in duplicate (circles and triangles are two independent experiments) for **A)** cellular ATP levels and **B)** caspase-3 activity. The median raw signal of the intra-plate NC wells was set to a normalized activity value of 0, while the median raw signal of the intra-plate PC wells was set to a normalized activity value of 100. **C)** Chemical structure of BRD0608.

4.3 Identification of BRD0608 and structure-activity relationships

Diversity-oriented synthesis (DOS) has emerged as a practical strategy to assemble compound libraries with a high degree of stereochemical and skeletal diversity, serving to augment traditional screening collections of commercially available compounds and natural products(19-23). DOS compounds rival natural products in terms of complexity (as measured by sp^3 -content and the presence of stereogenic centers)(24-25) yet are designed to be easily modified in order to facilitate

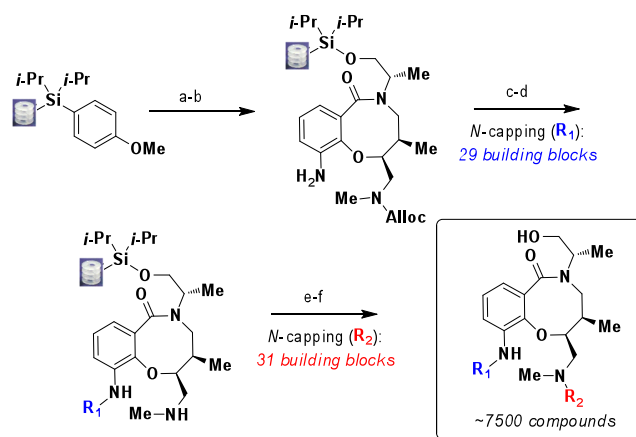
downstream chemistry optimization. These principles were highlighted recently by an aldol-based ‘build/couple/pair’ (B/C/P) strategy, resulting in a collection of various medium- and large-sized rings derived from a common linear intermediate(26). The DOS team at the Broad Institute sought to capitalize on this versatile intermediate to further increase the diversity of our compound collection. Building on the past success with the S_NAr reaction for cycloetherification(26), the team aimed to build a library that would provide both structure-activity relationships (SAR) and stereochemical structure-activity relationships (SSAR) in primary screens for biological activity. Coupling this information with the ability to synthesize analogs rapidly, exploiting short, modular synthetic pathways, provides a quick and efficient process to optimize hits identified in high-throughput screening (HTS).



Scheme 4-1. (a) 2-fluoro-3-nitrobenzoic acid chloride (**2**), NEt₃, DCM, RT, 84-100%. (b) CsF, DMF, 85 °C, 97-99%. (c) 10% Pd/C, H₂, EtOH. (d) FmocCl, aq. NaHCO₃, dioxane, 65-98% over 2 steps. (e) TBSOTf, then HF/pyridine. (f) AllocCl, pyridine. (g) DDQ, pH 7 buffer, 75-89% over 3 steps.

The DOS team within the Chemical Biology Platform at the Broad Institute

originally synthesized the whole library. After the identification of BRD0608, I started to synthesize analogs using the same synthesis route. The synthesis of the library scaffolds leading to the synthesis of BRD0608 commenced with linear intermediate **1**, which was accessed by coupling a suitably protected γ -amino acid with an amino alcohol, followed by reduction of the resulting amide (Scheme 4-1).^{Error! Bookmark not defined.} All stereoisomers of both the γ -amino acid and the amino alcohol were coupled together, resulting in the generation of **1a-d** and *ent*-**1a-d**, allowing for the full stereochemical matrix of scaffolds to be synthesized. Acylation of **1a-d** with 2-fluoro-3-nitrobenzoic acid chloride (**2**) proceeded smoothly to give the precursor to the key step, an intramolecular S_NAr reaction (Scheme 4-1). Regardless of the different stereochemistry in the linear chain, all stereoisomers reacted smoothly with cesium fluoride for de-silylation followed by cyclization to give desired **3a-d** in excellent yield. Functional group manipulation to prepare for solid-phase library production was achieved through a step-wise process involving: 1) nitro reduction and subsequent protection of the aniline as the Fmoc carbamate, 2) protecting group exchange from the incompatible Boc group to an Alloc, and 3) PMB removal to reveal the site for immobilization onto solid support. The sequence was high yielding and could be carried out on a multi-gram scale.



Scheme 4-2. (a) TfOH, DCM; then **4a-d**, 2,6-lutidine. (b) 20% piperidine/DMF. (c) *N*-capping (R₁): RSO₂Cl, RNCO, RCOCl, RCHO or skip (30 building blocks). (d) Pd(PPh₃)₄, barbuturic acid. (e) *N*-capping (R₂): RSO₂Cl, RNCO, RCHO, skip (31 building blocks). (f) 15% HF/pyridine, THF; TMSOMe.

Immobilization of the scaffold first involved activation of SynPhase Lanterns with triflic acid to give the silyl triflate, followed by exposure with the scaffold in the presence of 2,6-lutidine (Scheme 4-2). Typical loading levels for the immobilization step were 15-18 μmol/Lantern. Removal of the Fmoc-protecting group under standard conditions followed by capping with sulfonyl chlorides, isocyanates, acid chlorides, or formaldehyde (29 building blocks) introduced the first appendage diversity (R₁) at the aniline. Palladium mediated Alloc deprotection in the presence of barbuturic acid revealed the second appendage diversity site (R₂) at the amine, which was capped with sulfonyl chlorides, isocyanates, acids, or aldehydes (31 building blocks). Release from solid support was achieved with HF/pyridine, yielding an average of 14.1 μmol of each final compound per Lantern. All possible combinations of building blocks were

used for each stereoisomers to afford a 7384-membered library. All compounds were analyzed by ultraperformance liquid chromatography (UPLC) and those samples with purity >75% at 210 nm (6408 compounds, 87% pass rate) were submitted for HTS.

The S_NAr-based library was included with other DOS and commercial libraries in a HTS campaign designed to identify suppressors of cytokine-induced beta-cell apoptosis. Several DOS compounds partially restored beta-cell viability in the presence of these cytokines, and I was able to determine some SSAR features from the primary assay (Figure 4-7). Lactams **4c** and *ent-4d* were the preferred stereoisomers demonstrating the importance of the stereochemistry within the 8-membered ring. The 5*R*,6*R* stereochemistry was required for activity while the configuration of the exocyclic stereocenter was less critical. Urea substituents appeared to be favored at the aniline position, compared to sulfonamides and amides. At the amine position, sulfonamides resulted in greater ATP levels compared to ureas and amines. (2*S*,5*R*,6*R*)-**5**, BRD0608, was the most potent member of the library, with an EC₅₀ of 4.9 μM in restoring beta-cell viability.

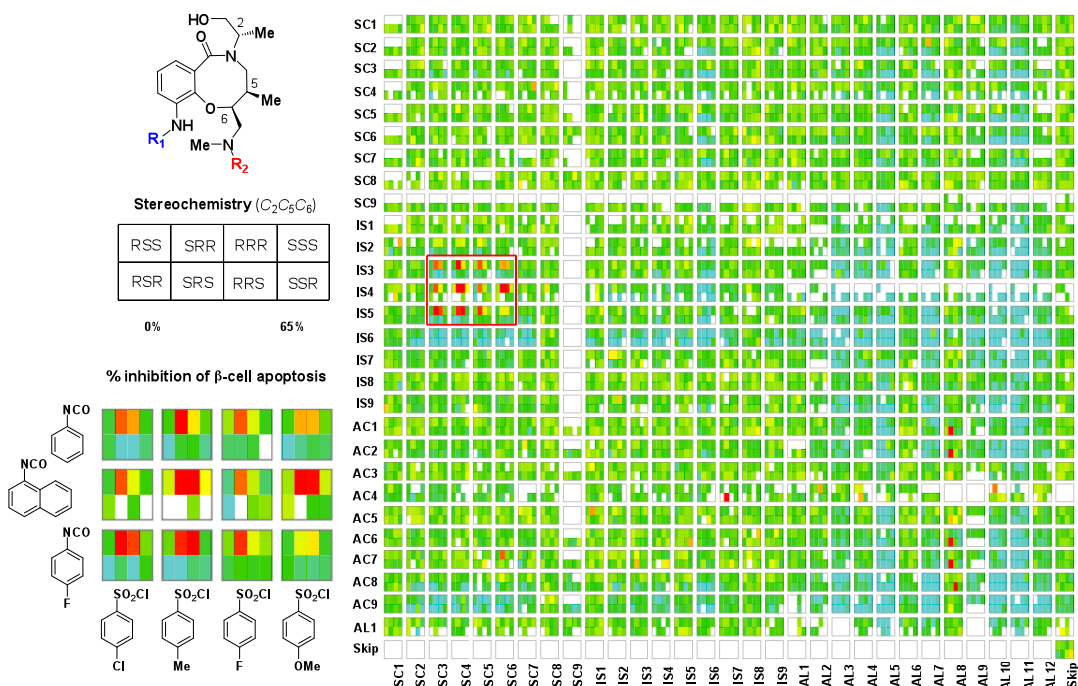
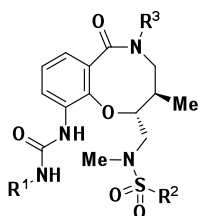


Figure 4-7. Performance of the SNAr library in the primary screen. The highlighted blocks represented the top-scored compounds identified in the primary screen.

4.4 Synthesis of analogs and discovery of BRD0476

Using BRD0608, **5**, as a starting point, additional SAR was explored via the preparation of a variety of analogs and subsequent testing for the restoration of cellular ATP levels in INS-1E cells as a readout. We first explored the nature of the urea substituent at R_1 . Based on primary screening results, the bulky naphthyl substituent appeared to be preferred over simple phenyl groups, thus we focused on subtle modifications to the naphthyl ring. Biological activities of all synthesized analogs are in Appendix 1. As shown in Table 4-1, saturation of the naphthyl ring was not tolerated (compounds **6** and **7**), nor was replacement with a benzofuran ring

(compound **8**). We next explored modifications to the sulfonamide at R₂. When the *para*-methoxyl group was moved to either the *ortho*- or *meta*-position (compound **9** and **10**), the activity was abolished. Replacement with a more bulky phenoxy group



compound	R ¹	R ²	R ³	EC ₅₀ (μM)	maximum activity (%)
5				4.89	62
6		"	"	>20	0
7		"	"	>20	0
8		"	"	>20	0
<hr/>					
9				>20	0
10	"		"	>20	0
11	"		"	>20	0
12	"		"	3.5	76
13	"		"	0.78	99
<hr/>					
14				>20	0
15				2.79	89
16				3.06	76

Table 4-1. EC₅₀ (μM) and maximum activity of synthesized analogs in restoring cytokine-induced β-cell death.

(compound **11**) also resulted in a loss of activity. Potency was retained and even

increased with the introduction of a *m,p*-disubstituted analogs (compound **12** and **13**).

Compound **13** (**BRD0476**) in particular was a potent suppressor of beta-cell death, resulting in the best performance among all analogs, with an EC₅₀ of 0.78 μM and 99% maximum activity. The 2,3-dichlorophenyl urea was also synthesized and tested (compound **14**) to explore further the replacement of the naphthyl ring, however this compound was inactive. Removal of the primary alcohol did not affect activity (compound **15** and **16**).

The most potent analog, compound **13** (**BRD0476**), was chosen for further characterization of its effects on different aspects of beta-cell biology. Caspase-3 activity is normally highly elevated in apoptotic beta cells. Inflammatory cytokines induced a 6.5-fold increase in caspase-3 activity (Figure 4-8 A). Treatment with **13** in the presence of cytokines reduced caspase-3 activity in a dose-dependent manner. IL-1β is known to induce gene expression of nitric oxide synthase (iNOS), an effect that is potentiated by IFN-γ.(27) The subsequent formation of NO drives cell death by both necrosis and apoptosis. Nitrite production is a surrogate measurement of nitric oxide generated by cytokine-treated INS-1E cells, and is measured colorimetrically using the Griess reagent (a commercially available mixture of naphthylenediamine dihydrochloride and sulfanilamide). Compound **13** induced a dose-dependent decrease in the production of nitrite (Figure 4-8 B), although the effect was more

modest than caspase-3 activity. Cytokine-mediated beta-cell apoptosis has been reported to cause a loss of the mitochondrial membrane potential ($\Delta\Psi_m$). JC-1 is a dye commonly used to measure $\Delta\Psi_m$. Mitochondrial membrane potential was reduced 2.5-fold in the presence of cytokines, and is restored to normal levels by treatment with compound **13** (Figure 4-8 C). Finally, glucose-stimulated insulin secretion (GSIS) is one of the most important physiological functions of beta cells. After brief starvation

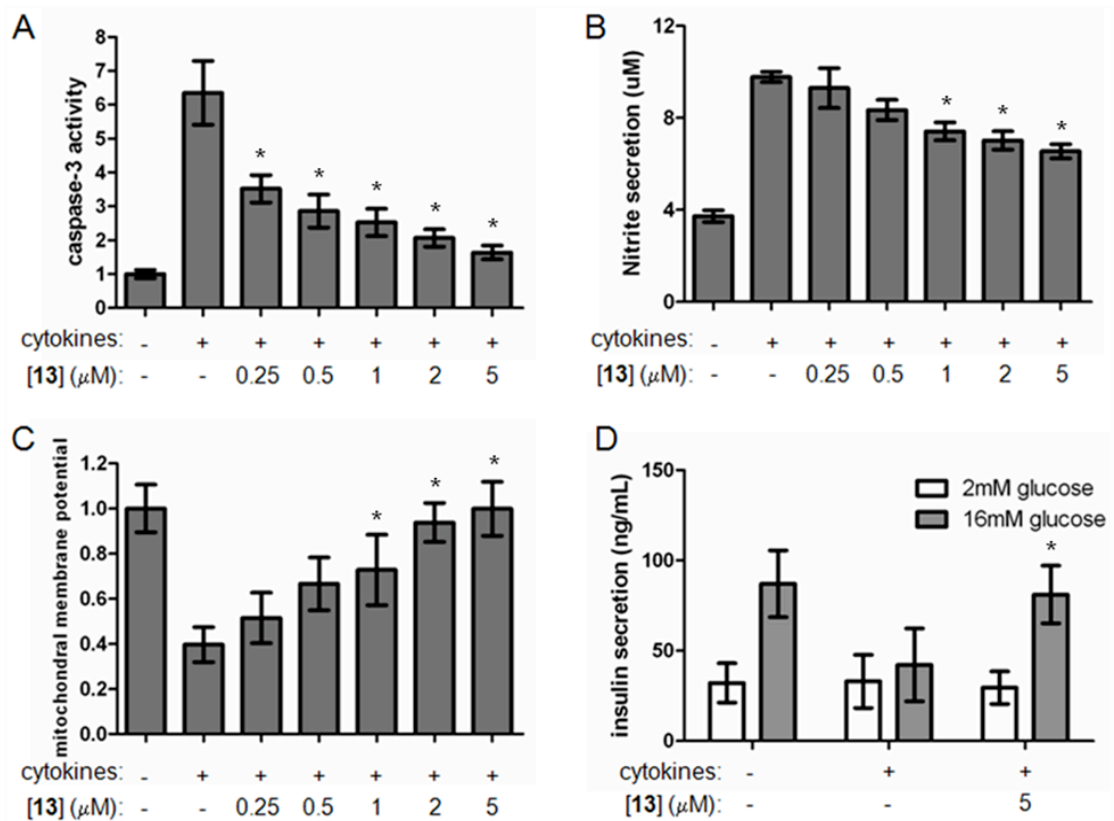


Figure 4-8. Cellular effects of **13** in cytokine-induced β -cell death. A) Effects of **13** on caspase-3 activity after 48-h treatment. B) Effects of **13** on the cellular production of nitrite after 48-h treatment. C) Effects of **13** on mitochondrial membrane potential after 48-h treatment. D) Effects of **13** on glucose-stimulated insulin secretion after 48-h treatment. Data represents the mean \pm standard deviation of 8 independent wells for insulin secretion and 24 independent wells for A-C. * indicates $p < 0.01$ as compared to the cytokine treatment alone.

followed by challenge with high (16 mM) glucose levels, beta cells secrete insulin into the cell-culture media. GSIS was abolished after two-day treatment with inflammatory cytokines; however, simultaneous treatment with 5 μ M of compound **13** restored GSIS to nearly normal levels (Figure 4-8 D).

4.5 Conclusion

In summary, I identified novel small-molecule suppressors of cytokine-induced beta-cell apoptosis. I chose BRD0608 for further chemistry studies because of its interesting SSAR property. These results show that the improved DOS analog **13** (**BRD0476**) protected rat beta cells from inflammatory cytokines, and may represent a viable strategy to protecting pancreatic beta cells in the context of type-1 diabetes. In chapter 5, I will focus on the identification of the lead compound's mechanism of action.

4.6 Methods and Materials

Cell culture and reagents. INS-1E cells (generously provided by Claes Wollheim and Pierre Maechler, University of Geneva, Switzerland) were maintained in culture medium (RPMI 1640 containing 11 mM glucose, 10% fetal bovine serum, 10 mM HEPES, 50 μ M 2-mercaptoethanol, 1 mM sodium pyruvate) and cultivated at 37C

with 5% CO₂ in a humidified atmosphere. Recombinant rat IL-1 β and recombinant mouse TNF- α were purchased from R&D Systems. Recombinant mouse IFN- γ and Griess reagent were purchased from Sigma. CellTiter-Glo and Caspase-Glo 3/7 reagents were purchased from Promega. JC-1 was obtained from Invitrogen.

High-Throughput Screening for Compounds Affecting Cellular ATP Levels

INS-1E cells were seeded at 10,000 cells per well using a Multidrop Combi (Thermo Labsystems) in white optical 384-well plates (Corning Life Sciences). After overnight incubation, medium was removed and 50 μ L of RPMI containing 1% FBS and a combination of cytokines (10 ng mL⁻¹ IL-1 β , 50 ng mL⁻¹ IFN- γ , 25 ng mL⁻¹ TNF- α) was added to every well. Using libraries of compounds dissolved in DMSO and a CyBi-Well pin-transfer robot (CyBio Corp.), 0.1 μ L of each compound was added. After 48 h, medium was removed and 20 μ L of CellTiter-Glo reagent was added. Luminescence was measured after 10 min of incubation using an EnVision plate reader (PerkinElmer).

Solid-phase synthesis of analogs:

General Methods: Solid-phase synthesis was conducted on silicon-functionalized polystyrene SynPhaseTM Lanterns (L-series). Quality-control Lanterns were included

at each synthesis step for reaction monitoring by UPLC (UV 210 nm) after HF-cleavage. All reactions were conducted in heavy wall pressure vessels from ChemGlass with agitation in New Brunswick Scientific incubator shakers.

Scaffold loading: The starting material was provided by Dr. Jeremy R. Duvall from Broad Institute. To a flame-dried flask containing silicon-functionalized Lanterns was added a freshly prepared solution of TfOH in anhydrous DCM (9.0 equiv, 5 g of TfOH/100 mL of DCM) was added. Each flask was shaken at RT for 10 min at which time the Lanterns had turned bright orange. The deep red TfOH solution was removed via cannula and anhydrous 2,6-lutidine (12.0 equiv relative to Si) was added. Once the Lantern color had changed from orange to white, the scaffold (1.2 equiv. relative to Si) was added as a solution in anhydrous DCM (0.4 mL/Lantern) and the reaction mixture was shaken for 48h overnight. The loading mixture was removed and set aside (to recover any unreacted alcohol) and the Lanterns were washed with the following solvents for 30 min intervals: DCM, THF, 3:1 THF/IPA, 3:1 THF/H₂O, DMF, 3:1 THF/H₂O, 3:1 THF/IPA, THF, DCM. The Lanterns were then dried on a lyophilizer overnight prior to sorting.

Fmoc removal: To a flask containing Lanterns was added a solution of 20% piperidine in DMF (0.8mL/Lantern). After shaking at rt for 30 min, the piperidine solution was removed and the Lanterns were washed with the following solvents for

30 min intervals: DMF, 3:1 THF/H₂O, 3:1 THF/IPA, THF, DCM. The Lanterns were then dried on a lyophilizer overnight prior to sorting.

N-Capping/Isocyanates: To each flask containing Lanterns was added DCM (0.8 mL/Lantern) followed by the desired isocyanate (15 equiv). The Lanterns were shaken at rt overnight and then washed with following solvents for 30 min intervals: DCM, DMF, 3:1 THF/ H₂O, 3:1 THF/IPA, THF, DCM. The Lanterns were then dried on a lyophilizer overnight prior to sorting.

Alloc removal: To the reaction vessel containing Lanterns, THF (0.8 mL/Lantern) was added, followed by Pd(PPh₃)₄ (1 equiv) and 1,3-dimethylbarbituric acid (30 equiv). The flask was sealed and shaken at rt for 1 day. The reaction mixture was removed and the Lanterns were washed with DMF until the washings were clear (without any yellow color). Subsequently the Lanterns were washed with the following solvents for 30 min intervals: 3:1 THF/H₂O, 3:1 THF/IPA, THF, DCM. The Lanterns were then dried on a lyophilizer overnight prior to sorting.

N-Capping/Sulfonyl Chlorides: To each flask containing Lanterns was added DCM (0.8 mL/Lantern) followed by 2,6-lutidine (20 equiv) and the desired sulfonyl chloride (35 equiv). The Lanterns were shaken at rt overnight and then washed with following solvents for 30 min intervals: DCM, DMF, 3:1 THF/H₂O, 3:1 THF/IPA, THF, DCM. The

Lanterns were then dried on a lyophilizer overnight prior to sorting.

Cleavage Protocol: To a 96-well plate containing Lanterns was added a 15% solution of HF/pyridine in stabilized THF (350 μ L/Lantern). After 2 h the cleavage solution was quenched with TMSOMe (700 μ L/Lantern) and the contents of each well were transferred to a pre-weighed 2-mL vial. The Lanterns were washed with an additional 200 μ L of stabilized THF (or THF/MeOH) and the solution was transferred to the 2-mL vial. The samples were concentrated on a Genevac® solvent evaporation system overnight without heating.

Characterization of active analogs: Chemical characterization of active analogs are in Appendix 2.

Measurement of cellular ATP levels. INS-1E cells were seeded at 10,000 cells/well using a Multidrop Combi (Thermo LabSystems) in white optical 384-well plates (Corning Life Sciences). After overnight incubation, medium was removed and 50 μ L RPMI containing the treated compound, 1% FBS and a combination of cytokines (10 ng/mL IL-1 β , 50 ng/mL IFN- γ , 25 ng/mL TNF- α) was added to every well. After incubation for 48 hr, medium was removed and 20 μ L CellTiter-Glo reagent was

added. Luminescence was measured after 10-min incubation using an EnVision plate reader (PerkinElmer).

Measurement of cellular nitrite production. INS-1E cells were seeded at 10,000 cells/well using a Multidrop Combi (Thermo LabSystems) in white optical 384-well plates (Corning Life Sciences). After overnight incubation, medium was removed and 50 μ L RPMI containing the treated compound, 1% FBS and a combination of cytokines (10 ng/mL IL-1 β , 50 ng/mL IFN- γ , 25 ng/mL TNF- α) was added to every well. After treatment with cytokine and compounds for 48 hr, 10 μ L modified Griess reagent (1:1 mixture of 1% sulfanilamide in 30% acetic acid and 0.1% *N*-(1-naphthyl) ethylenediamine dihydrochloride in 60% acetic acid) was added to each well. After 5-min incubation at room temperature, the absorbance at 540 nm was measured using an Envision plate reader (PerkinElmer).

Measurement of mitochondrial membrane potential. INS-1E cells were seeded at 10,000 cells/well using a Multidrop Combi (Thermo LabSystems) in white optical 384-well plates (Corning Life Sciences). After overnight incubation, medium was removed and 50 μ L RPMI containing the treated compound, 1% FBS and a combination of cytokines (10 ng/mL IL-1 β , 50 ng/mL IFN- γ , 25 ng/mL TNF- α) was

added to every well. After treatment with cytokine and compounds for 48 hr, 20 μ L of 3.25 μ M JC-1 was added to each well. After 3hr incubation at 37°C, the cells were gently washed three times with 50 μ L per well of 1X PBS (with Ca²⁺ and Mg²⁺). Fluorescence was measured with an EnVision plate reader (PerkinElmer) at the rhodamine spectra (excitation/emission 530 nm/580 nm) followed by fluorescein (excitation/emission 485 nm/530 nm). The ratio of rhodamine to fluorescein intensity was determined and represents the degree of mitochondrial membrane potential.

Caspase-3 activity assay. INS-1E cells were seeded at 5,000 cells/well using a Multidrop Combi (Thermo LabSystems) in white optical 384-well plates (Corning Life Sciences). After overnight incubation, medium was removed and 50 μ L RPMI containing the treated compound, 1% FBS and a combination of cytokines (10 ng/mL IL-1 β , 50 ng/mL IFN- γ , 25 ng/mL TNF- α) was added to every well. After treatment with cytokines and compounds for 48 hr, medium was removed and 20 μ L Caspase-Glo 3/7 reagent was added. Luminescence was measured after 2-hr incubation using an Envision plate reader (PerkinElmer).

Glucose-stimulated insulin secretion. INS-1E cells were seeded in 96-well plates at 20,000 cells/well in 100 μ L RPMI and incubated for 48 hr in 100 μ L fresh RPMI

containing 1% FBS and the cytokine cocktail in the presence or absence of 5 μ M MS-275. Cells were washed and incubated for 2 hr in KRBH buffer (135 mM NaCl, 3.6 mM KCl, 5 mM NaHCO₃, 0.5 mM NaH₂PO₄, 0.5 mM MgCl₂, 1.5 mM CaCl₂, 10 mM HEPES, pH 7.4, 0.1% BSA) lacking glucose. Cells were subsequently incubated with KRBH buffer containing 2 mM or 16 mM glucose for 1 hr. The supernatant was collected for measurement of secreted insulin. Insulin was measured with a rat insulin ELISA kit (Alpco).

4.7 References

1. Cnop, M., Welsh, N., Jonas, J. C., Jorns, A., Lenzen, S., and Eizirik, D. L. (2005) Mechanisms of pancreatic beta-cell death in type 1 and type 2 diabetes: many differences, few similarities, *Diabetes 54 Suppl 2*, S97-107.
2. Grunnet, L. G., Aikin, R., Tonnesen, M. F., Paraskevas, S., Blaabjerg, L., Stirling, J., Rosenberg, L., Billestrup, N., Maysinger, D., and Mandrup-Poulsen, T. (2009) Proinflammatory cytokines activate the intrinsic apoptotic pathway in beta-cells, *Diabetes 58*, 1807-1815.
3. Kim, E. K., Kwon, K. B., Song, M. Y., Han, M. J., Lee, J. H., Lee, Y. R., Ryu, D. G., Park, B. H., and Park, J. W. (2007) Flavonoids protect against cytokine-induced pancreatic beta-cell damage through suppression of nuclear factor kappaB activation, *Pancreas 35*, e1-9.
4. Matsuda, T., Ferreri, K., Todorov, I., Kuroda, Y., Smith, C. V., Kandeel, F., and Mullen, Y. (2005) Silymarin protects pancreatic beta-cells against cytokine-mediated toxicity: implication of c-Jun NH2-terminal kinase and janus kinase/signal transducer and activator of transcription pathways, *Endocrinology 146*, 175-185.
5. Larsen, L., Tonnesen, M., Ronn, S. G., Stirling, J., Jorgensen, S., Mascagni, P., Dinarello, C. A., Billestrup, N., and Mandrup-Poulsen, T. (2007) Inhibition of histone deacetylases prevents cytokine-induced toxicity in beta cells, *Diabetologia 50*, 779-789.

6. Lewis, E. C., Blaabjerg, L., Storling, J., Ronn, S. G., Mascagni, P., Dinarello, C. A., and Mandrup-Poulsen, T. (2011) The oral histone deacetylase inhibitor ITF2357 reduces cytokines and protects islet beta cells in vivo and in vitro, *Mol Med* 17, 369-377.
7. Chou, D. H., Bodycombe, N. E., Carrinski, H. A., Lewis, T. A., Clemons, P. A., Schreiber, S. L., and Wagner, B. K. Small-Molecule Suppressors of Cytokine-Induced beta-Cell Apoptosis, *ACS Chem Biol* 5, 729-734.
8. Burke, M. D., and Schreiber, S. L. (2004) A planning strategy for diversity-oriented synthesis, *Angew Chem Int Ed Engl* 43, 46-58.
9. Schreiber, S. L. (2000) Target-oriented and diversity-oriented organic synthesis in drug discovery, *Science* 287, 1964-1969.
10. Nielsen, T. E., and Schreiber, S. L. (2008) Towards the optimal screening collection: a synthesis strategy, *Angew Chem Int Ed Engl* 47, 48-56.
11. Merglen, A., Theander, S., Rubi, B., Chaffard, G., Wollheim, C. B., and Maechler, P. (2004) Glucose sensitivity and metabolism-secretion coupling studied during two-year continuous culture in INS-1E insulinoma cells, *Endocrinology* 145, 667-678.
12. Kamal, A., Thao, L., Sensintaffar, J., Zhang, L., Boehm, M. F., Fritz, L. C., and Burrows, F. J. (2003) A high-affinity conformation of Hsp90 confers tumour selectivity on Hsp90 inhibitors, *Nature* 425, 407-410.
13. Whitesell, L., Bagatell, R., and Falsey, R. (2003) The stress response: implications for the clinical development of hsp90 inhibitors, *Curr Cancer Drug Targets* 3, 349-358.
14. Jin, Z. (2005) Amaryllidaceae and Scelletium alkaloids, *Nat Prod Rep* 22, 111-126.
15. Abdel-Halim, O. B., Morikawa, T., Ando, S., Matsuda, H., and Yoshikawa, M. (2004) New crinine-type alkaloids with inhibitory effect on induction of inducible nitric oxide synthase from *Crinum yemense*, *J Nat Prod* 67, 1119-1124.
16. Szlavik, L., Gyuris, A., Minarovits, J., Forgo, P., Molnar, J., and Hohmann, J. (2004) Alkaloids from *Leucojum vernum* and antiretroviral activity of Amaryllidaceae alkaloids, *Planta Med* 70, 871-873.
17. Saito, N., Kitame, F., Kikuchi, M., and Ishida, N. (1974) Studies on a new antiviral antibiotic, 9-methylstreptimidone. I. Physicochemical and biological properties, *J Antibiot (Tokyo)* 27, 206-214.
18. Wang, Z. I., M.; Ikeda, Y.; Horie, R.; Umezawa, K. (2006) Inhibition of NF-Kappa B Activation by 9-Methylstreptimidone Isolated from *Streptomyces*, *Heterocycles*.

19. Bauer, R. A., Wurst, J. M., and Tan, D. S. Expanding the range of 'druggable' targets with natural product-based libraries: an academic perspective, *Curr Opin Chem Biol* 14, 308-314.
20. Goess, B. C., Hannoush, R. N., Chan, L. K., Kirchhausen, T., and Shair, M. D. (2006) Synthesis of a 10,000-membered library of molecules resembling carpanone and discovery of vesicular traffic inhibitors, *J Am Chem Soc* 128, 5391-5403.
21. Koch, M. A., Schuffenhauer, A., Scheck, M., Wetzel, S., Casaulta, M., Odermatt, A., Ertl, P., and Waldmann, H. (2005) Charting biologically relevant chemical space: a structural classification of natural products (SCONP), *Proc Natl Acad Sci U S A* 102, 17272-17277.
22. Marcaurelle, L. A., Johannes, C., Yohannes, D., Tillotson, B. P., and Mann, D. (2009) Diversity-oriented synthesis of a cytosine-inspired pyridone library leading to the discovery of novel inhibitors of Bcl-2, *Bioorg Med Chem Lett* 19, 2500-2503.
23. Pelish, H. E., Westwood, N. J., Feng, Y., Kirchhausen, T., and Shair, M. D. (2001) Use of biomimetic diversity-oriented synthesis to discover galanthamine-like molecules with biological properties beyond those of the natural product, *J Am Chem Soc* 123, 6740-6741.
24. Dandapani, S., and Marcaurelle, L. A. Grand challenge commentary: Accessing new chemical space for 'undruggable' targets, *Nat Chem Biol* 6, 861-863.
25. Comer, E., Liu, H., Joliton, A., Clabaut, A., Johnson, C., Akella, L. B., and Marcaurelle, L. A. Fragment-based domain shuffling approach for the synthesis of pyran-based macrocycles, *Proc Natl Acad Sci U S A* 108, 6751-6756.
26. Marcaurelle, L. A., Comer, E., Dandapani, S., Duvall, J. R., Gerard, B., Kesavan, S., Lee, M. D. t., Liu, H., Lowe, J. T., Marie, J. C., Mulrooney, C. A., Pandya, B. A., Rowley, A., Ryba, T. D., Suh, B. C., Wei, J., Young, D. W., Akella, L. B., Ross, N. T., Zhang, Y. L., Fass, D. M., Reis, S. A., Zhao, W. N., Haggarty, S. J., Palmer, M., and Foley, M. A. An aldol-based build/couple/pair strategy for the synthesis of medium- and large-sized rings: discovery of macrocyclic histone deacetylase inhibitors, *J Am Chem Soc* 132, 16962-16976.
27. Darville, M. I., and Eizirik, D. L. (1998) Regulation by cytokines of the inducible nitric oxide synthase promoter in insulin-producing cells, *Diabetologia* 41, 1101-1108.

Page intentionally left blank

Chapter 5: Mechanistic studies of BRD0476 in suppressing of cytokine-induced beta-cell apoptosis

5.1 Introduction

In Chapter 4, I discussed the efforts using high-throughput screening to discover novel suppressors of cytokine-induced beta-cell apoptosis. Several different classes of compounds were identified for their ability to preserve cell viability in the presence of the cytokine cocktail. Specifically, BRD0608, a compound synthesized via diversity-oriented synthesis, was prioritized due to its interesting biological and chemical properties. Follow-up medicinal chemistry efforts led to the synthesis of BRD0476, a more potent analog of BRD0608. BRD0476 has an EC_{50} of 0.78 μ M in preserving cellular ATP levels of INS-1E cells in the presence of cytokines. Moreover, BRD0476 could reduce cytokine-induced caspase-3 activity, increase the mitochondrial membrane potential, and decrease nitrite production in a dose-dependent manner. Insulin secretion, the most important physiological function for beta cells, was also restored by addition of BRD0476. These results show that the BRD0476 protects a rat beta-cell line from inflammatory cytokines, and may represent a viable strategy to protect pancreatic beta cells in the context of type-1 diabetes.

Because of the previously promising results of BRD0476 on rat beta cells, I wanted to study the effects of BRD0476 on primary human pancreatic islets.

Furthermore, since BRD0476 is a novel suppressor of beta-cell apoptosis, I sought to determine the mechanism of action in protecting beta cells from cytokine-induced apoptosis. I will describe my efforts in these two directions in the following sections.

5.2 Effects of BRD0476 on primary dissociated human islets

BRD0476 suppresses cytokine-induced apoptosis in INS-1E cells. I wanted to know whether its protective effect could be phenocopied in primary human islets. If so, the value of BRD0476 as a probe for beta-cell apoptosis would be enhanced. Before experimenting on human islets, I wanted to make sure that BRD0476 is selective toward cytokine-induced apoptosis, and is not a generic inhibitor of apoptosis. For this purpose, I used thapsigargin, tunicamycin, and high glucose as apoptosis inducers in INS-1E cells. As described in Chapter 1, these agents can induce ER stress or glucotoxicity in pancreatic beta cells. In this experiment, INS-1E cells were treated with a series of concentrations of these compounds, as well as either DMSO vehicle or 10 μ M BRD0476. As measured by cellular ATP levels, INS-1E started to die at 16nM thapsigargin, 16 μ g/mL tunicamycin, or 125mM glucose (Figure 5-1). Unlike its ability to restore cell viability in the presence of cytokines, BRD0476 could not restore INS-1E viability in the presence of each of the three apoptosis inducers (Figure 5-1). This result suggests that BRD0476 is not a generic apoptosis blocker that can restore

cell viability in response of various apoptosis inducers; instead, BRD0476 shows selectivity toward cytokine-induced apoptosis in INS-1E beta cells.

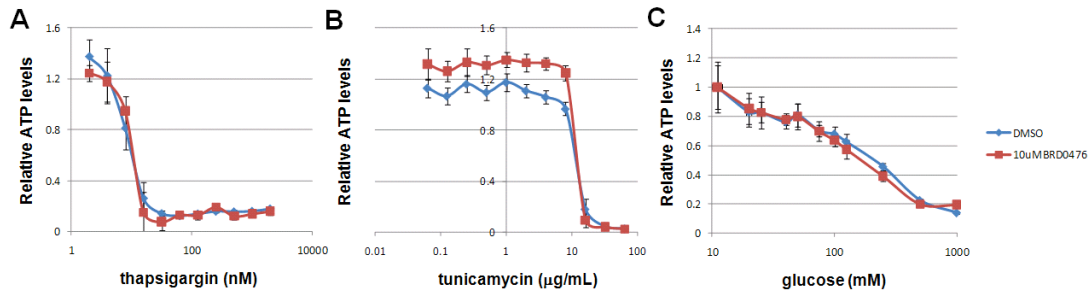


Figure 5-1. Effects of BRD0476 on beta-cell apoptosis induced by different apoptosis inducers. INS-1E cells were treated with 11 different concentrations of A) thapsigargin; B) tunicamycin; and C) glucose. ATP measurements were normalized to the no-treatment condition. Data represent the mean \pm standard deviation of 24 independent wells.

Next, I wanted to study whether the protective effect of BRD0476 in INS-1E cells can be translated to primary human islets. It has been reported that primary human islets treated with pro-inflammatory cytokines were undergoing apoptosis after 6-9 days (1-2). In our lab, Deepika Walpita had developed a system for culturing primary dissociated human islet cells (Walpita *et al.*, manuscript submitted). Briefly, the human bladder cell line HTB9 was cultured in 384-well plates. HTB9 cells secrete extracellular matrix (ECM) on the bottom of the wells. After several days of culture, HTB9 cells were washed away while leaving ECM on the plates. Human pancreatic islets were then cultured on top of the ECM. I used this system to measure the apoptotic effect of cytokines in primary human islets. The quality and quantity of

human islets have donor-to-donor variability. Therefore, the data generated from human islets is not as consistent as in cell-line models. Moreover, since human islets contain a mixed population of cells, including insulin-releasing beta cells, glucagon-releasing alpha cells, and somatostatin-releasing delta cells, a simple cell viability assay may not represent the viability of beta cells alone. In the literature, beta cells were found to be more sensitive to cytokines compared to other cell types in the islets (3). A cell viability assay would only observe a small decrease in signal in this case. For this reason, I decided to use caspase-3 activity as the measurement. The addition of cytokines should lead to an increased signal of caspase-3 activity, which is easier to detect. Moreover, since beta cells are the only cells that can secrete insulin in a glucose-responsive manner, an insulin secretion assay would be another suitable assay to measure the viability of beta cells.

When primary dissociated human islets were treated with the cytokine cocktail for six days, caspase-3 activity was elevated nearly 2-fold (Figure 5-2). The same trend was observed in islets from two different donors. Addition of BRD0476 reduced caspase-3 activity dose-dependently to normal levels (Figure 5-2). Normally, primary dissociated human islets secreted 2-3-fold amounts of insulin when challenged with a high glucose concentration (Figure 5-3). This fold change is less than that of intact islets, but it is still very detectable by ELISA. When islets were treated with the

cytokine cocktail for 6 days, insulin secretion was impaired (Figure 5-3). I observed this effect in islet samples from two different donors. Addition of BRD0476 fully restored the insulin secretion in donor 3 and partially, but significantly, restored the insulin secretion in donor 4 (Figure 5-3). BRD0476 seemed to have a better protective effect in donor 3 than in donor 4. Nevertheless, BRD0476 appears to have protective effects in primary dissociated human islets from several donors.

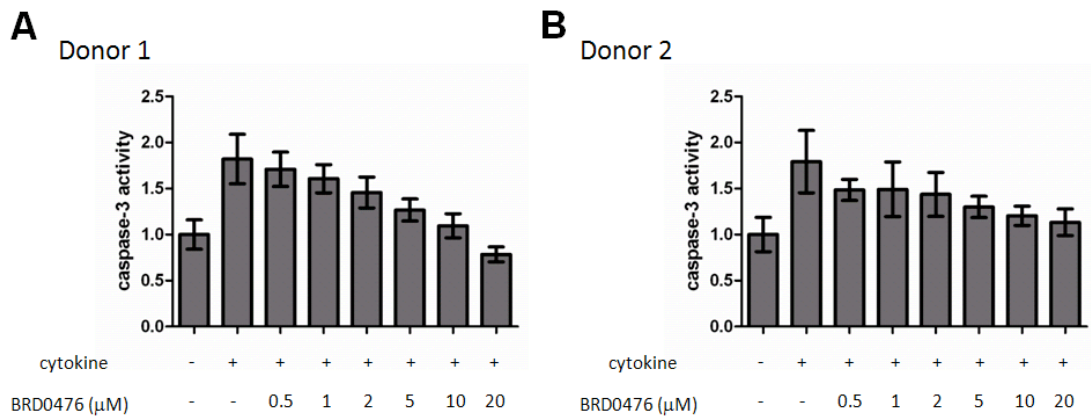


Figure 5-2. Effects of BRD0476 on caspase-3 activity in dissociated human islet cells undergoing cytokine-induced apoptosis. Cells were treated with cytokines and different doses of BRD0476 for six days. Data represent the mean \pm standard deviation of 12 independent wells.

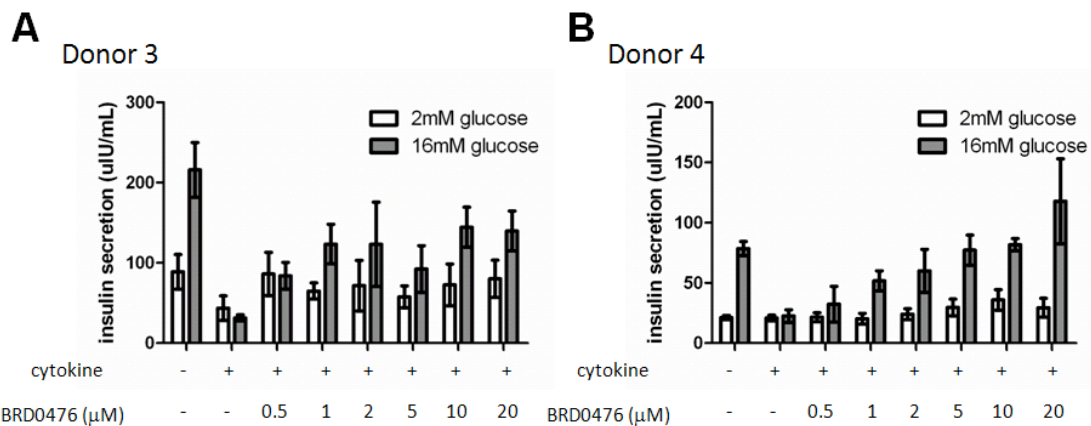


Figure 5-3.

Figure 5-3. (Continued) Effects of BRD0476 on glucose-stimulated insulin secretion in dissociated human islet cells undergoing cytokine-induced apoptosis. Cells were treated with cytokines and different doses of BRD0476 for six days. Data represent the mean \pm standard deviation of 4 independent wells.

5.3 Genome-wide gene expression profile revealed the JAK-STAT pathway as a target for the effects of BRD0476

Recognition of some of the limitations of target-based drug and probe discovery has led to the phenotype-based approach, in which complex biological systems are investigated for phenotypic changes upon exposure to small molecules(4-7). The subsequent identification of the molecular targets that underlie an observed phenotype is not only important for elucidating the mechanisms of action, but will also greatly allow efficient structure-activity relationship studies to be carried out in follow-up chemistry by use of target-specific assays. Therefore, target identification is an important aspect of a phenotypic screen(8-9).

BRD0476 has shown a great potential in protecting beta cells from cytokine-induced apoptosis in both rat INS-1E cells and primary dissociated human islets. Since BRD0476 was identified in a phenotypic screen and had no biological annotation, I wanted to study the mechanisms of actions for BRD0476. One approach to investigate the genes and pathways that BRD0476 interacts with is to use genome-wide gene-expression microarrays to look for genes or gene sets that are regulated by BRD0476. The underlying principle is to compare the gene-expression

profiles of samples between cytokines alone and cytokines plus BRD0476. The difference in mRNA levels may point to genes that are regulated by BRD0476 in the presence of cytokines. For this purpose, I treated rat INS-1E cells with 10 μ M BRD0476 for 6, 12, and 48 hours in the presence of cytokines. The detailed conditions are shown in Table 5-1 and each condition consisted of three biological replicates.

Time	Cytokine	BRD0476
48hr	-	-
	+	-
	+	+
12hr	-	-
	-	+
	+	+
6hr	-	-
	-	+
	+	+

Table 5-1. Time doses and treatments for all microarray samples

After the indicated treatments, I isolated the RNA from all the samples and submitted them to the Genetic Analysis Platform (GAP) at the Broad Institute. The GAP team used the Affymetrix rat 230 2.0 array for acquiring gene-expression data. The information about each probe on the chip is extracted from the image data by image analysis software. The information is stored in the CEL file. The CEL file, provided by the GAP team, includes an intensity value, standard deviation of the intensity, the number of pixels used to calculate the intensity value, a flag to indicate an outlier as calculated by the algorithm, and a user defined flag indicating the feature

should be excluded from future analysis. After I processed the CEL files and converted the expression of each probe to fold changes over the mean signal of the no cytokine control, I first looked at the number of genes that are regulated significantly by BRD0476 alone. Very few genes were regulated by BRD0476 in the absence of cytokines (Scheme 5-1). Among 20,494 genes tested, only 15 genes were up-regulated and 2 genes were down-regulated greater than 2-fold after 6-hour treatment. At 12 hours, only 7 genes were up-regulated and 5 genes were down-regulated more than 2-fold. As a comparison, 147 genes were up-regulated and 417 genes were down-regulated more than 2-fold in the presence of cytokines after 6 hours, and at 12 hours, 381 genes were up-regulated and 739 genes were down-regulated more than 2-fold by cytokines. This result indicates that BRD0476 has little effect on regulating gene expression in normal conditions. However, in the presence of pro-inflammatory cytokines, BRD0476 regulates more genes.

	> 2-fold changes
6hr_no cytokine	15/2
12hr_no cytokine	7/5
6hr_cytokine	147/417
12hr_cytokine	381/739

of up-regulated genes/ # of down-regulated genes
Total # of genes = 20494

Scheme 5-1. Numbers of genes up- and down-regulated by BRD0476 in the absence and presence of cytokines.

I then decided to use Gene-Set Enrichment Analysis (GSEA) to look for gene sets that are regulated by the addition of BRD0476. GSEA is a computational method

that determines whether an existing defined set of genes shows statistically significant, concordant differences between two biological states (10). The method derives its power by focusing on gene sets, groups of genes that share common biological function, chromosomal location, or regulation. Since single-gene analysis may find little similarity between two independent samples or may miss other important effects on pathways, GSEA reveals many biological pathways in common. I used GSEA to compare cytokine treatment with cytokines plus BRD0476 at the three different time points. mRNA levels are thought to be regulated in a relatively short time frame compared to protein levels. Therefore, I expected to see more gene expression changes in both 6- and 12-hour treatments. At 48 hours, cells would achieve a new homeostasis and some acute changes would probably not been discovered in this case.

The analysis revealed that the top gene sets regulated by BRD0476 in the presence of cytokines are gene sets that are related to interferon pathways (Table 5-2). The same gene sets were observed at all three time points. In the gene set “Browne_interferon_responsive_genes” (the set names are annotated by the name of the researcher who submits the set), most of the genes are increased by cytokines and expressed at lower levels when BRD0476 was added (Figure 5-4 A). These genes are all related to the JAK-STAT pathway, which is activated by IFN- γ , one of

the three cytokines in the cocktail (Figure 5-4 B). This result shows that BRD0476 downregulates genes that are activated by IFN- γ , leading to the hypothesis that BRD0476 may protect beta cells from cytokine-induced apoptosis by blocking the JAK-STAT pathway.

NAME	NES	FDR q-value
BROWNE_INTERFERON_RESPONSIVE_GENES	2.4686	0
RADAEVA_RESPONSE_TO_IFNA1_UP	2.4326	0
KRIGE_AMINO_ACID_DEPRIVATION	2.3738	0
REACTOME_UNFOLDED_PROTEIN_RESPONSE	2.3553	0
HELLER_HDAC_TARGETS_DN	2.3505	0
REACTOME_TRANSLATION	2.3404	5.83E-05
BERTUCCI_MEDULLARY_VS_DUCTAL_BREAST_CANCER_UP	2.3251	1.49E-04
ZHANG_ANTIVIRAL_RESPONSE_TO_RIBAVIRIN_UP	2.2559	0.00147254
REACTOME_REGULATION_OF_ORNITHINE_DECARBOXYLASE	2.2358	0.00142011
HELLER_HDAC_TARGETS_SILENCED_BY_METHYLATION_DN	2.2351	0.0012781
REACTOME_HOST_INTERACTIONS_OF_HIV_FACTORS	2.2136	0.00169521
REACTOME_P53_INDEPENDENT_DNA_DAMAGE_RESPONSE	2.1899	0.00213049

Table 5-2. Microarray data analyzed by GSEA. Gene sets were ranked by NES (normalized enrichment score). NES accounts for differences in gene set size and in correlations between gene sets and the expression dataset; therefore, NES can be used to compare analysis results across gene sets. The highlighted gene sets are related to interferon pathways.

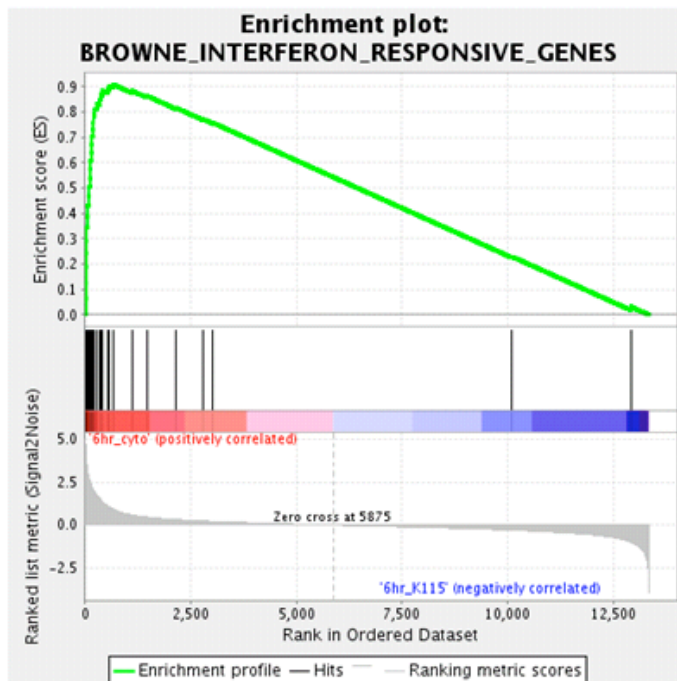
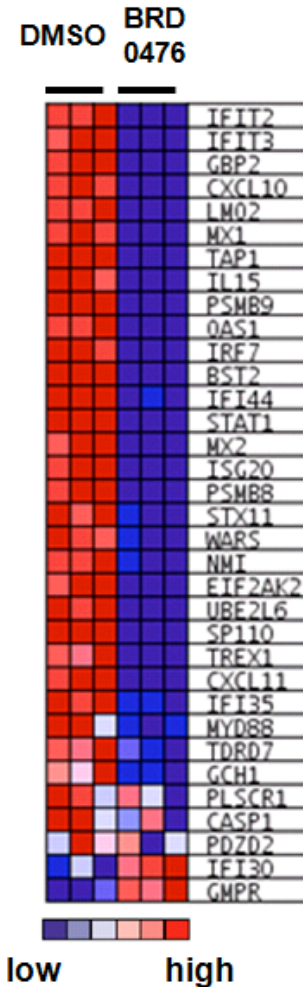
A**B**

Figure 5-4. Detailed information on a gene set regulated by BRD0476. A) Genes in the “Browne_interferon_responsive_genes” gene set are mostly correlated in one direction. B) Most of the genes are highly expressed in the cytokine alone treatment and expressed at lower levels when BRD0476 was added. The highest and lowest fold changes are 12- and 1-fold relative to the no cytokine control.

As mentioned in Chapter 1, IFN- γ binding to its receptor, IFN-R, induces the recruitment of the kinases JAK1 and JAK2. Once activated by phosphorylation, JAK1 and 2 recruit STAT1 and trigger its activation by phosphorylation. STAT1 then homodimerizes and translocates to the nucleus, where it regulates the expression of genes containing gamma-activated sequence (GAS) elements in their promoter

(Figure 5-5 A). The microarray data suggests that BRD0476 may block the activation of the JAK-STAT pathway. To see whether that is the case, I transfected a plasmid containing a firefly luciferase gene with six GAS in the promoter region, and a *Renilla* luciferase gene for control (Figure 5-5 B). The *Renilla* luciferase is driven by a CMV promoter; therefore, the signal of *Renilla* luciferase is proportional to the total number of cells. The ratio of luciferase activity from firefly and *Renilla* luciferases thus reflects the transcriptional activity of STAT1. After a 12-hour treatment with cytokines, the transcriptional activity of STAT1 was elevated 12-fold compared to the no-cytokine control (Figure 5-5 C). In the absence of cytokines, BRD0476 did not change the low basal transcriptional activity of STAT1. However, in the presence of cytokines, the transcriptional activity of STAT1 was reduced by 60% when 10 μ M BRD0476 was added (Figure 5-5 C). These results are consistent with the microarray data: BRD0476 alone has little effect under normal conditions, but it appears to block the JAK-STAT pathway in the presence of cytokines.

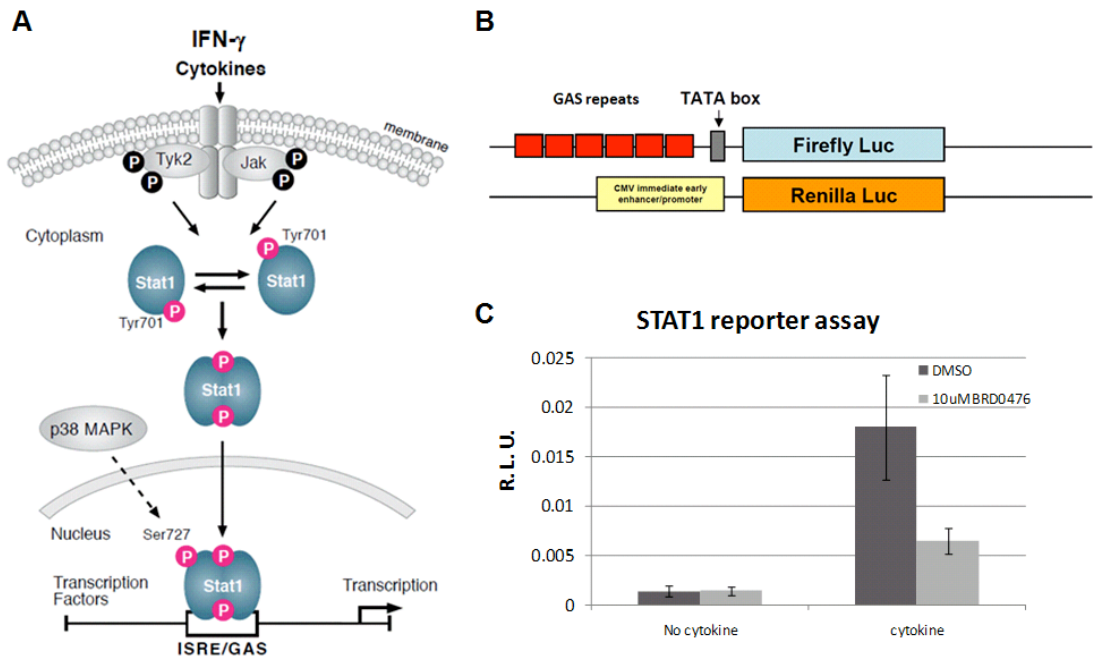


Figure 5-5. The JAK-STAT pathway and measurement of STAT1 transcriptional activity. A) The JAK-STAT pathway is activated by IFN- γ , one of the cytokines added to induce apoptosis in this model. (This part of the figure is modified from a figure taken from Cell Signaling website.) B) Two plasmids were transfected into INS-1E cells for the measurement of STAT1 transcriptional activity. C) Measurement of STAT1 transcriptional activity after 12-hour treatment with cytokines.

Next, I studied the protein levels of STAT1 by Western blot. The mRNA levels of STAT1 were increased by cytokines, and reduced by BRD0476 (Figure 5-4B). By protein level, the same trend was observed. STAT1 protein was elevated and reached its peak at 12 hours of cytokine treatment (Figure 5-6). When BRD0476 was added, the level of STAT1 was moderately reduced (Figure 5-6). There are two main phosphorylation sites for STAT1: tyrosine 701 (Y701) and serine 727 (S727). The Y701 site is the predominant one for phosphorylation by JAK2. The level of p-STAT1 at Y701 was elevated as soon as the first hour, and reached its peak at 4 hours

(Figure 5-6). The level then reduced back to normal after 4 additional hours. Addition of BRD0476 nearly completely blocked the phosphorylation of STAT1 at Y701, with only a weak signal observed at 4 hours (Figure 5-6). At the S727 site, the level of p-STAT1 was slightly elevated within 4 hours, but the level sustained after 4 more hours. Addition of BRD0476 reduced the level after 4 hours. Taken together, BRD0476 moderately reduced the protein levels of STAT1 and also blocked the phosphorylation of STAT1 at both Y701 and S727. This is consistent with my previous results, since STAT1 should not homodimerize and migrate into nucleus in a non-phosphorylated form. To show this, I used a nuclear extraction kit to isolate nucleus from cytoplasm, using histone H3 as a control for nuclear proteins. Addition of cytokines increased STAT1 protein levels in the nucleus (Figure 5-7). STAT1 levels were then reduced when BRD0476 was added, although the level did not completely return to normal levels (Figure 5-7). In the cytoplasm, addition of cytokines only slightly reduced STAT1 protein level (Figure 5-7). This could be explained by a higher total STAT1 level in cytokine-treated cells. Therefore, the decrease in the cytoplasm is not striking. Addition of BRD0476 also slightly increased STAT1 level in the cytoplasm (Figure 5-7). Taken together, these results suggest that BRD0476 inhibits STAT1 phosphorylation and its migration into the nucleus.

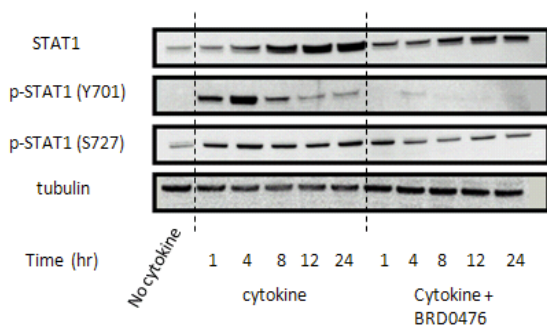


Figure 5-6. Western blots of STAT1 and phosphorylated STAT1 after 10 μ M BRD0476 treatments.

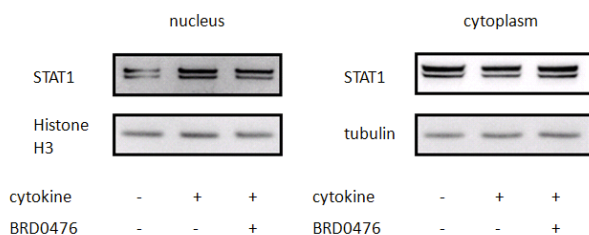


Figure 5-7. Western blots of STAT1 in nucleus and cytoplasm. The concentration of BRD0476 is 10 μ M.

5.4 SILAC studies suggested USP9X as a possible primary target for BRD0476

In the last section, I used genome-wide gene-expression microarray data to identify the genes and gene sets that BRD0476 regulates. This led to the hypothesis that BRD0476 blocks the JAK-STAT pathway. However, I still did not know the direct cellular binding target(s). Uncovering direct targets would not only help to understand the mechanisms of action for BRD0476, but would also significantly aid follow-up medicinal chemistry studies. For this purpose, I collaborated with the Proteomics Platform at the Broad Institute to take a quantitative proteomics approach to identify potential cellular binding proteins.

The Proteomics Platform has adapted a robust and unbiased method for probing the proteins that bind to the small molecule of interest in a biologically

relevant setting. This method, Stable Isotope Labeling by Amino acids in Cell culture (SILAC), is a powerful approach in mass spectrometry (MS)-based quantitative proteomics (Figure 5-8) (11-13). SILAC labels cellular proteomes through normal metabolic processes, incorporating non-radioactive, stable isotope containing amino acids in newly synthesized proteins. Growth medium is prepared where natural ('light') arginines are replaced by 'heavy' C¹³ and N¹⁵ arginines. INS-1E cells grown in this medium incorporate the heavy amino acids after seven to eight cell passages and the heavy amino acids have no effect on cell morphology or growth rates. When light and heavy cell populations are mixed, they remain distinguishable by MS, and protein abundances are determined from the relative MS signal intensities.

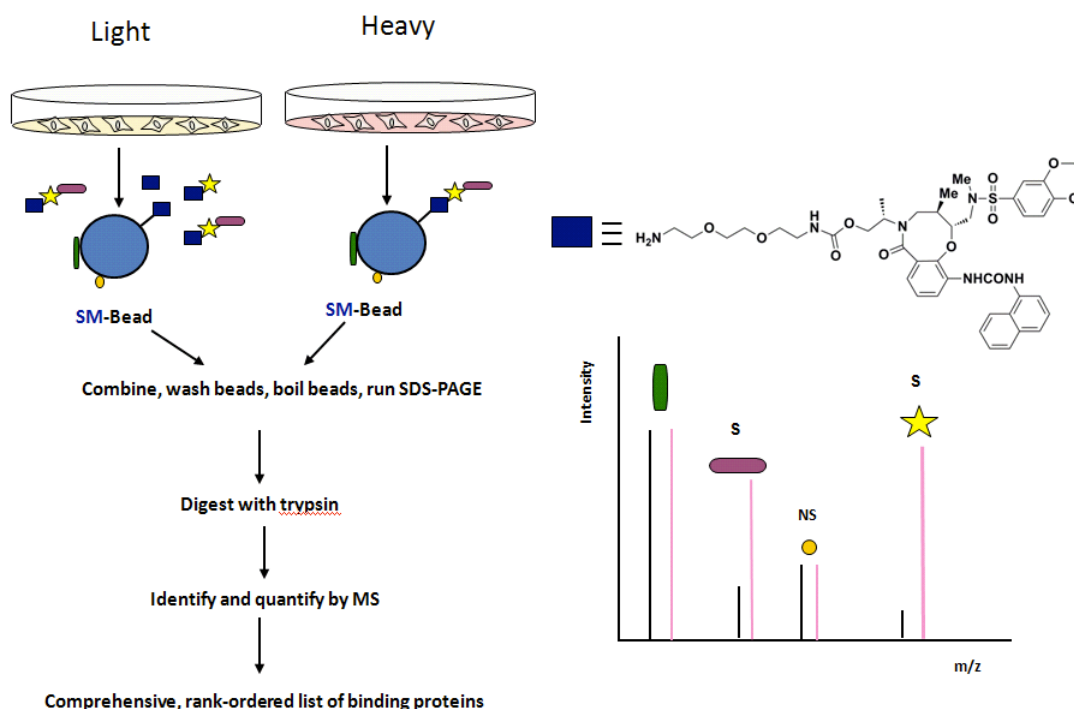


Figure 5-8. Steps for target identification using Stable Isotope Labeling by Amino acids in Cell culture (SILAC) and quantitative proteomics. After the incorporation of special amino acids, both lysates were incubated with the bait, but

(Figure 5-8. continued) excess free CR-6 was added to one lysate, to competitively displace target proteins. The beads from both lysates were then washed, combined, and proteins that remained bound to the immobilized small molecule were eluted off. Eluted proteins were separated using gel electrophoresis. Proteins were trypsin digested and analyzed on a mass spectrometer. This figure was modified from a figure made by Dr. Shao-En Ong at the Broad Institute.

In order to “pull down” binding proteins, generation of the affinity reagent (bait) is a critical first step, which involves tethering the BRD0476 to solid support. The synthesis of this bait was performed by Dr. Eamon Comer and Ms. Claire Reddy in the Chemical Biology Platform. In Chapter 4, I described the structure-activity relationship (SAR), which suggested that the alcohol group in the side chain of BRD0476 is not crucial for the protective effect of BRD0476. Therefore, a PEG linker was placed at this position, and CR-6 was synthesized in two steps from BRD0476 (Figure 5-9). I then tested CR-6 in the cellular ATP and caspase-3 assays to ensure that the protective activity was retained. In the presence of cytokines, CR-6 restored cellular ATP levels and reduced caspase-3 activity in a dose-dependent fashion, similar to BRD0476 (Figure 5-10). After the activity of CR-6 was confirmed, the compound was attached to solid support and the resulting bait could be used for pull-down studies.

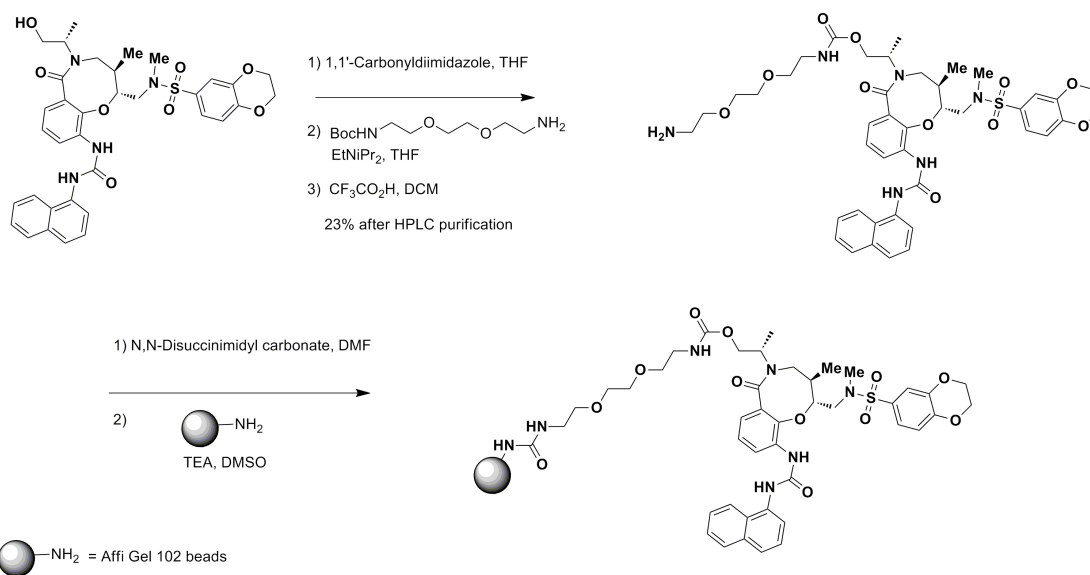


Figure 5-9. Synthetic route to the synthesis of CR-6. The side-chain hydroxyl group was first activated by 1,1'-carbonyldiimidazole and followed by nucleophilic attack of the Boc-protected amine. Acid-catalyzed removal of the Boc group gave CR-6.

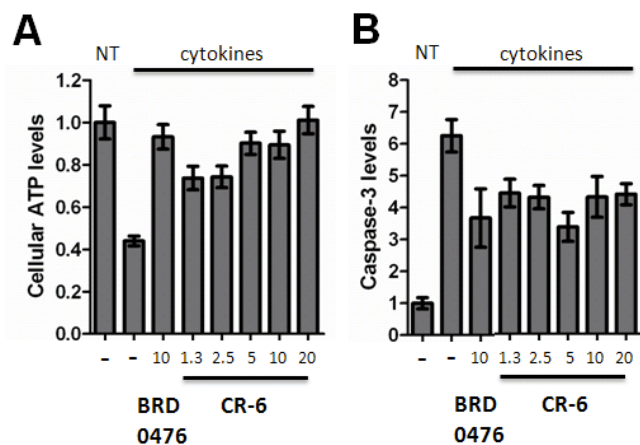


Figure 5-10. Effects of CR-6 on cytokine-induced beta-cell apoptosis. Cells were treated for two days and tested for A) cellular ATP levels and B) caspase-3 activity.

The proteomics team then used SILAC-labeled INS-1E lysates in pull-down experiments. Both lysates were incubated with the bait, but 30-fold excess free CR-6 was added to one lysate, to competitively displace target proteins. The beads from both lysates were then washed, combined, and proteins that remained bound to the

immobilized small molecule were reduced by DTT and alkylated by iodoacetamide.

Proteins were then eluted by LDS buffer and separated by molecular weight using gel electrophoresis. The entire gel lane was then cut into several bands to simplify the process, and proteins were trypsin digested and analyzed on a mass spectrometer.

The proteomics team then identified and compared the relative enrichment of target proteins, generating differential SILAC ratios between the two states (Table 5-3).

Each protein's rank is based on the fold enrichment, which is then converted to a *p*-value. The list here includes all the proteins that have a *p*-value less than 0.05.

There were two importins and one exportin in the list, which are involved in nuclear transport.

<u>Symbol</u>	<u>Folds</u>	<u>p-value</u>	<u>Description</u>
Mcm6	3.10	2.3 * 10 ⁻²⁶	DNA replication licensing factor MCM6
Blvrb	2.87	7.2 * 10 ⁻²³	biliverdin reductase B
Usp9x	1.97	2.1 * 10 ⁻⁹	ubiquitin specific peptidase 9, X-linked isoform
Ap3b2	1.79	1.0 * 10 ⁻⁶	adaptor-related protein complex 3, beta 2
Cand1	1.72	7.5 * 10 ⁻⁶	cullin-associated and neddylation-dissociated 1
Gapdh	1.67	3.3 * 10 ⁻⁵	similar to glyceraldehyde-3-phosphate dehydrogenase
	1.65	7.0 * 10 ⁻⁵	similar to TBC1 domain family member 15
Gapdh	1.65	7.8 * 10 ⁻⁵	glyceraldehyde-3-phosphate dehydrogenase
Ahcy	1.65	8.7 * 10 ⁻⁵	adenosylhomocysteinase
Kpna4	1.62	1.6 * 10 ⁻⁴	importin 4
	1.59	4.2 * 10 ⁻⁴	similar to CG5937-PA
Lrpprc	1.56	1.0 * 10 ⁻³	leucine-rich PPR motif-containing protein
Ipo9	1.49	5.1 * 10 ⁻³	importin 9
Retsat	1.49	5.4 * 10 ⁻³	all-trans-retinol 13,14-reductase
Xpo1	1.47	1.1 * 10 ⁻²	exportin 1
Timm44	1.43	2.7 * 10 ⁻²	translocase of inner mitochondrial membrane 44
Cand2	1.41	5.1 * 10 ⁻²	cullin-associated and neddylation-dissociated 2

Table 5-3. A list of proteins pull down by CR-6. Proteins are ranked by fold changes. The fold change is calculated between the signals of the protein in the absence and presence of soluble competitor, CR-6.

I decided to use siRNAs to knock down individual genes from the protein list, to test whether the knock-down can phenocopy the protective effect of BRD0476. The rationale is based on the hypothesis that BRD0476 is a direct inhibitor of a particular target. On the other hand, I also wanted to test whether the protective effect of BRD0476 would be impaired if a protein was knocked down. Therefore, if BRD0476 is an *activator* of a given protein, I would expect to see no protective effect for BRD0476 if the protein was knocked down. Based on these ideas, I tested a number of proteins from the list (Table 5-4). Here, I would like to focus on two of the proteins, Mcm6 and Usp9x.

target	knock-down	restore ATP after knock-down	blocking BRD0476 after knock-down
Mcm6	yes (qPCR)	no	no
Blvrb	yes (qPCR)	no	no
Usp9x	yes (WB)	yes	no
Gapdh	yes (WB)	no	no
Kpna4	yes (WB)	no	no
Ipo9	yes (WB)	no	no
Xpo1	yes (WB)	no	no

Table 5-4. Summary of knock-down studies. The effect of knock-down was confirmed by either qPCR or western blots.

MCM6, a DNA replication licensing factor, was the top-ranked protein on the list. MCM6 acts as component of the MCM2-7 complex, which is the replicative helicase essential for DNA replication initiation and elongation in eukaryotic cells (14). Therefore, MCM6 is an important protein for DNA replication, but had no reported relationship with cytokine signaling pathways. When I knocked down MCM6 (Figure

5-11 A) and treated INS-1E cells with cytokines, I did not see a restoration of cellular ATP levels (Figure 5-11 B). Furthermore, knock-down of MCM6 had no influence on the protective effect of BRD0476 (Figure 5-11 C). This result suggested that MCM6 is not a direct target that leads to the protective effect of BRD0476. Similar results were observed for IPO4, IPO9, XPO1, BLVRA, GAPDH, and CAND1.

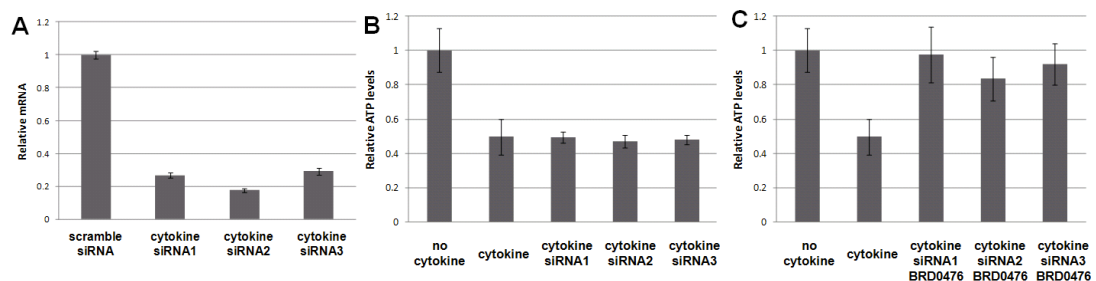


Figure 5-11. Effects of knocking down MCM6 in cytokine-induced beta-cell apoptosis. A) Validation of siRNAs using quantitative PCR . B) Effects of MCM6 knock-down on ATP levels in the presence of cytokines. C) Effects of MCM6 knock-down on ATP levels in the presence of cytokines and 10µM BRO0476.

USP9X is a member of the peptidase C19 family and is a deubiquitinase.

Though this gene is located on the X chromosome, it is one of the 15% of genes that escape X-inactivation. It is involved in the processing of both ubiquitin precursors and of ubiquitinated proteins (15-17). Therefore, it may play an important role at the level of protein turnover, by preventing degradation of proteins through the removal of conjugated ubiquitin. When I knocked down USP9X (Figure 5-12 A) and treated INS-1E cells with cytokines, I observed a full restoration of cellular ATP levels (Figure

5-12 B) and reduction of caspase-3 activity (Figure 5-12 C). Knocking down USP9X also restored mitochondrial membrane potential in the presence of cytokines (Figure 5-12 D). These effects were observed in three different siRNA constructs. The effect of knocking down USP9X is similar to that of BRD0476, suggesting that USP9X may be a binding target of BRD0476.

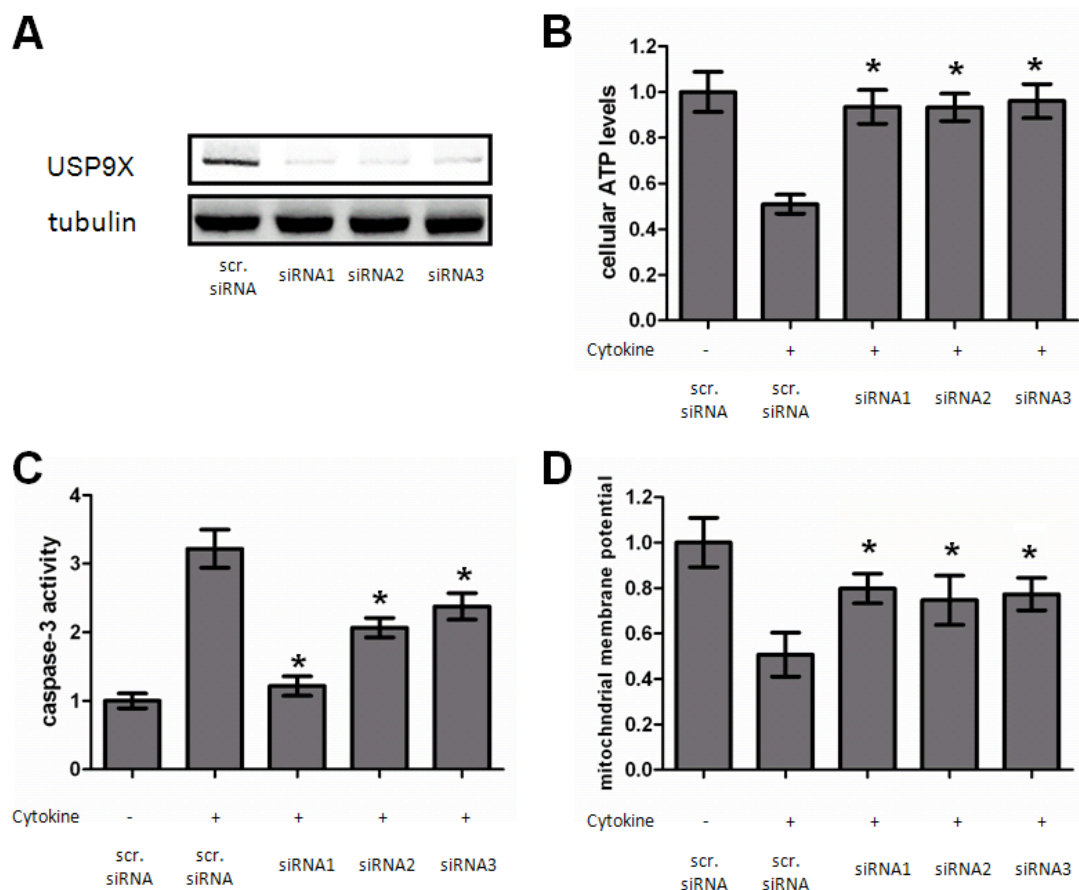


Figure 5-12. Effects of knocking down USP9X in cytokine-induced beta-cell apoptosis. A) Validation of siRNAs using Western blot. B) Effects of knocking down USP9X on ATP levels after 48-h treatment. C) Effects of knocking down USP9X on caspase-3 activity after 48-h treatment. D) Effects of knocking down USP9X on mitochondrial membrane potential after 48-h treatment. Data represents the mean \pm standard deviation of 24 independent wells for B-D. * indicates $p < 0.01$ as compared to the cytokine treatment alone.

Next, I wanted to see whether there is direct binding between USP9X and BRD0476. One way to do that is to use the normal lysate and bait to do a low-throughput pull-down assay. I used CR-6-beads as the bait and unloaded beads as a negative control. After washing, I boiled the sample and ran a Western blot using a USP9X antibody. USP9X was pulled down by the bait but not the control beads (Figure 5-13). However, when I added 5 to 40 μ M BRD0476 as a soluble competitor, I saw only a small decrease in the band intensity. This result may be due to the poor solubility of BRD0476 in aqueous solution, and the fact that Western blotting is not as sensitive as MS methods. Nonetheless, this served as an independent experiment to show that USP9X binds BRD0476. However, this result is not strong enough to definitively conclude that USP9X is a direct binder of BRD0476.

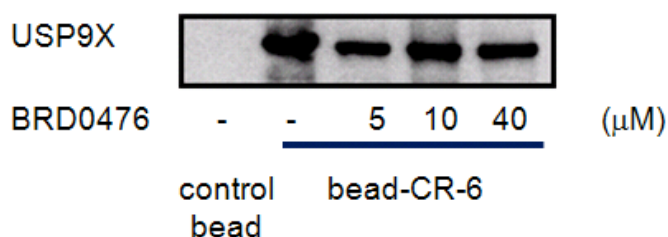


Figure 5-13. USP9X was pulled down by CR-6.

Cell lysate was preincubated with BRD0476 for 1 hour before shaken with beads overnight. BRD0476 cannot be added more due to poor solubility in aqueous solution.

In order to further show direct binding, I tried to make recombinant USP9X protein, which turned out to be extremely difficult. USP9X is a 295-kD protein. Therefore, simple organisms such as bacteria could not be used as the host for

expression. I was fortunate to obtain a HEK293 cell line containing a tetracycline-inducible USP9X-expression plasmid from Dr. Dario Alessi at University of Dundee, Scotland (18). I cultured this cell line, used blasticidin and hygromycin B for selection, added tetracycline to induce expression, and lysed cells for protein purification. The purification process was challenging because both the induction efficiency and the protein yield were quite low. I finally arrived at a fraction that was “relatively pure”. This fraction still had several bands, one of which was USP9X (Figure 5-14 A).

Using this fraction, I tested the binding between USP9X and BRD0476 using a thermal shift assay. Ligand binding to a target protein can either stabilize or destabilize a protein's native state, as shown by the increase in the bound protein's melting temperature (19). The midpoint of the melting curve of a protein will either increase or decrease in the presence of ligands (Figure 5-14 B). The temperature where the midpoint of the melting curve of a protein happens is the melting temperature, T_m . Using this assay, I found that BRD0476 decreased the melting temperature of the protein fraction by 1.4 degrees compared to the control (Figure 5-14 C). Normally, a shift larger than 1 degree will be considered significant. Therefore, 1.4 degrees of shift is considered a significant shift for thermal shift assays. WP1130, a reported nonselective deubiquitinase inhibitor (20), also decreased the

melting temperature by 2.1 degrees (Figure 5-14 C). However, I cannot test the protective effect of WP1130 on cytokine-induced beta-cell apoptosis because WP1130 alone is toxic to INS-1E cells as low as 1 μ M. This result suggests that at least one component of the protein mixture binds BRD0476. Based on the positive control from WP1130, it strongly suggests that USP9X is a direct binder of BRD0476.

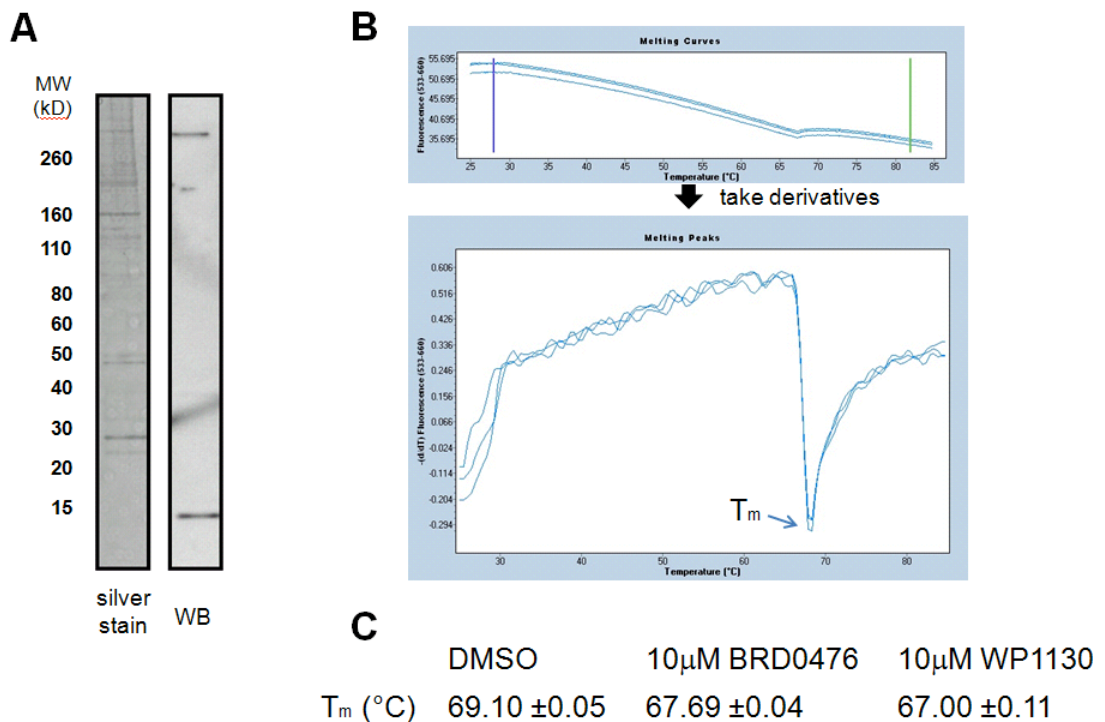


Figure 5-14. Thermal-shift assay to detect protein bindings. A) Silver stain of the protein fraction and a Western blot using a USP9X antibody. B) A representative melting curve. X-axis is the temperature; Y-axis is the fluorescence from the dye, Nile red. C) Summary of the melting temperature. Data represents the mean \pm standard deviation of 3 independent wells.

Recently, USP9X was found to stabilize MCL1 and thereby promote cell survival in colon cancer cells (21). USP9X binds MCL1 and removes the Lys 48-linked polyubiquitin chains that normally mark MCL1 for proteasomal degradation.

Knockdown of USP9X increased MCL1 polyubiquitination, which enhanced MCL1 turnover and sensitized cells to the BH3 mimetic ABT-737. If BRD0476 is an inhibitor of USP9X, I would expect to see that addition of BRD0476 can also enhance the effect of ABT-737 on cancer cell death. Therefore, I treated the colon cancer cell line DLD-1 with different doses of ABT-737 in the presence and absence of 10 μ M BRD0476. Addition of BRD0476 to ABT-737 shifted the curve to the left (Figure 5-15) in a very similar way as USP9X knock-down. This result strengthens the hypothesis that BRD0476 is an inhibitor of USP9X.

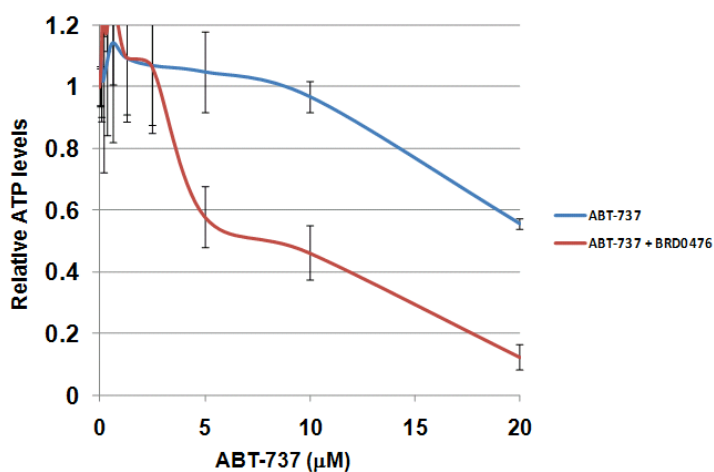


Figure 5-15. Killing curves of DLD-1 cells
DLD-1 cells were treated with ABT-737 in the absence or presence of 10 μ M BRD0476 for 2 days.

5.5 Relationship between the JAK-STAT pathway and USP9X

By using gene-expression microarrays, I discovered that BRD0476 is likely to be involved in perturbing the JAK-STAT pathway. From a quantitative proteomics approach, USP9X appears to be a direct binding target for BRD0476. In the literature,

there is no obvious connection between USP9X and the JAK-STAT pathway. Since BRD0476 blocks the phosphorylation of STAT1, I hypothesized that BRD0476 might be a JAK inhibitor. I submitted BRD0476 to Millipore to test the effects of BRD0476 on 100 different kinases, including JAK2 and JAK3. However, BRD0476 did not show significant inhibition towards any of the kinases tested (Appendix 3). Moreover, I tested the effects of two selective JAK2 inhibitors, SD-1029 and Z3, on cytokine-induced beta-cell apoptosis (Figure 5-16). However, they are either too toxic or have no protective effects. These results suggest that BRD0476 is not a kinase inhibitor and likely blocks the phosphorylation of STAT1 in a more indirect manner.

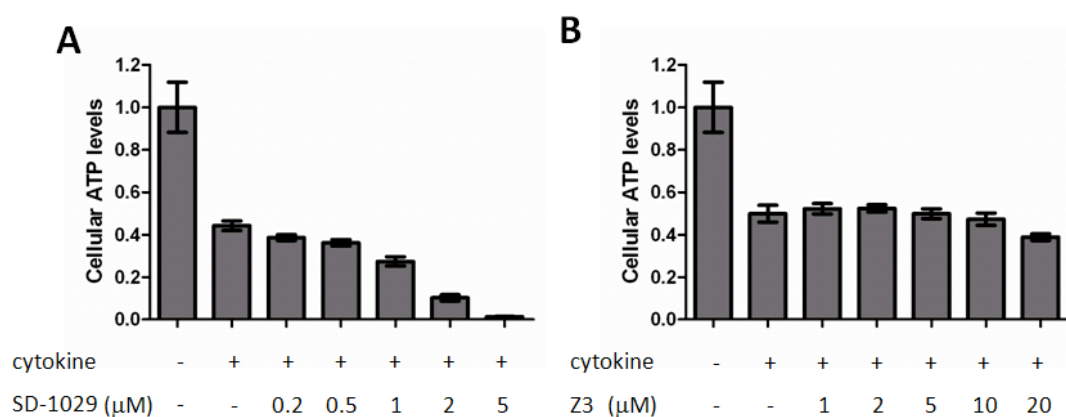


Figure 5-16. Effects of selective JAK2 inhibitors in cytokine-induced beta-cell apoptosis. Effects of JAK2 inhibitors on ATP levels after 48-h cytokine treatment for A) SD-1029 and B) Z3. Data represents the mean \pm standard deviation of 24 independent wells.

I also tried to knock down USP9X in INS-1E cells to study the phosphorylation of STAT1. Protein levels of STAT1 did not decrease in USP9X-knockdown cells (Figure

5-16). More importantly, knock-down of USP9X did not block the phosphorylation of STAT1, at either the Y701 or S727 sites (Figure 5-17). These results seemed to be confusing in light of my original results. If USP9X is the primary target for BRD0476, knock-down of USP9x should also inhibit STAT1 phosphorylation. Thus, the situation appears to be more complicated. A possible explanation is that the two events are independent of each other, and BRD0476 happens to have effects on both USP9x and STAT1. Blocking the JAK-STAT pathway is a known approach to suppress cytokine-induced beta-cell apoptosis, as demonstrated by Eizirik and coworkers (22). However, knock-down of USP9X would represent a novel approach. Another explanation is that USP9X deubiquitinates a protein downstream of the JAK-STAT pathway. Therefore, the phosphorylation of STAT1 is too upstream to be influenced by knock-down of USP9X. Taken together, although the JAK-STAT pathway and USP9X were confirmed to related to the protective effects of BRD0476, further studies are still required to completely understand the mechanism of action.

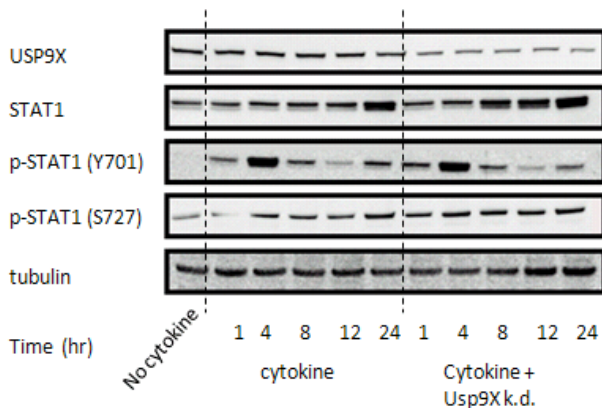


Figure 5-17. Western blots of STAT1 and phosphoSTAT1 after knocking down USP9X. INS-1E cells were treated with Usp9x siRNA overnight and cultured for two days before treated with cytokines for the indicated times.

5.5 Conclusion

The process of target identification is a challenging but required part of the probe discovery process. BRD0476 is a novel compound synthesized via diversity-oriented synthesis capable of suppressing cytokine-induced apoptosis in both rat INS-1E cells and primary human dissociated islets. However, the mechanism of action was still unknown. By using gene-expression microarrays, I discovered that BRD0476 appears to inhibit activation of the STAT1 pathway. I further demonstrated that BRD0476 could reduce the protein level of STAT1 and block STAT1 phosphorylation. Moreover, BRD0476 also blocks the migration of STAT1 into nucleus and, therefore, reduces the transcriptional activity of STAT1. From a quantitative proteomics “SILAC” approach, USP9X appears to be a direct binding target for BRD0476. I demonstrated that knock-down of USP9X could phenocopy the effect of BRD0476. Moreover, BRD0476 could shift the melting temperature of a protein fraction containing USP9X. The same effect was also seen by using a known USP9X inhibitor, WP1130. However, I could

not make a connection between JAK-STAT pathway and USP9X. In the future, a gene-expression profile data of USP9X knock-down cells would help to understand the underlying mechanism behind the protective effect. Moreover, a better quality and quantity of recombinant USP9X protein could help to develop a biochemical assay to prove whether BRD0476 is an inhibitor of the enzymatic activity of USP9X. Also, global analysis of ubiquitinated proteins would also be helpful to look for substrates of USP9X that are related to the protective effects of BRD0476. In conclusion, BRD0476 suppresses cytokine-induced beta-cell apoptosis by blocking interferon-induced STAT1 activation. Moreover, USP9X is a putative direct binding target for BRD0476. Knock-down of USP9X phenocopies the effects of BRD0476. However, detail connections between the two targets are still unknown. The discovery of USP9X as a target to suppress cytokine-induced beta-cell apoptosis could help future screening using USP-9X in a target-based screening approach.

5.6 Methods and Materials

Cell culture and reagents. INS-1E cells (generously provided by Claes Wollheim and Pierre Maechler, University of Geneva, Switzerland) were maintained in culture medium (RPMI 1640 containing 11 mM glucose, 10% fetal bovine serum, 10 mM HEPES, 50 μ M 2-mercaptoethanol, 1 mM sodium pyruvate) and cultivated at 37C

with 5% CO₂ in a humidified atmosphere. Recombinant human IL-1 β , recombinant human IFN- γ and recombinant human TNF- α were purchased from R&D Systems. CellTiter-Glo, Dual-Glo and Caspase-Glo 3/7 reagents were purchased from Promega. Antibodies for USP9X, IPO9, IPO4 and XPO1 were from Abcam. Thapsigargin, tunicamycin, blasticidin, hygromycin B, nucleus isolation kit and mouse monoclonal antibody to tubulin were from Sigma. Secondary horseradish peroxidase-conjugated goat anti-mouse and anti-rabbit antibodies were from Thermo Fisher Scientific. Antibodies for STAT1 and p-STAT1 were purchased from Cell Signaling. GAS reporter assay kit and rat primers for Mcm6 and Blvrb were from SABiosciences. All siRNA constructs were from Dharmacon. WP-1130 was synthesized in house by Dr. Mingji Dai. ABT-737 was purchase from Selleck Chem. JAK2 inhibitors were from EMD4Biosciences.

Human islet culture. Human islets were obtained through variable sources. The purity and viability of human islets are reported to be 80–85% and 86–95%, respectively, and the average age of donors was 46 y (range 36–58 y; $n = 4$). Specific data on individual donors is reported below. Islets were washed with PBS and incubated in CMRL medium supplemented with 10% FBS, 2 mM glutamine, 100 U/mL penicillin, and 100 μ g/mL streptomycin. Islets were gently dissociated into a cell

suspension by incubating in Accutase (37 °C, 10 min), and seeded in 96-well plates containing extracellular matrix secreted by the HTB9 human bladder carcinoma cell line (23).

Donor	Source	Islet Purity	Islet Viability	Age	Gender	Height (cm)	Weight (kg)	BMI	Ethnicity
1	U Pitt	85%	95%	36	M	190.5	104	28.7	W
2	Prodo lab	80%	90%	43	N/A	N/A	N/A	27.0	N/A
3	Prodo lab	85%	95%	58	N/A	N/A	N/A	30.4	N/A
4	U Penn	85%	86%	47	M	177.0	89.5	28.6	B

Treatment of human pancreatic islets. Human pancreatic islets were treated at with 0.5ng/mL human IL-1 β , 50ng/mL human IFN- γ and 25ng/mL human TNF- α for 6 days in white optical 384-well plates or black 96-well plates (Corning Life Sciences).

Measurement of cellular ATP levels. INS-1E cells were seeded at 10,000 cells/well using a Multidrop Combi (Thermo LabSystems) in white optical 384-well plates (Corning Life Sciences). After overnight incubation, medium was removed and 50 μ L RPMI containing the treated compound, 1% FBS and a combination of cytokines (10 ng/mL IL-1 β , 50 ng/mL IFN- γ , 25 ng/mL TNF- α) was added to every well. After

incubation for 48 hr, medium was removed and 20 μ L CellTiter-Glo reagent was added. Luminescence was measured after 10-min incubation using an EnVision plate reader (PerkinElmer).

Measurement of cellular nitrite production. INS-1E cells were seeded at 10,000 cells/well using a Multidrop Combi (Thermo Labsystems) in white optical 384-well plates (Corning Life Sciences). After overnight incubation, medium was removed and 50 μ L RPMI containing the treated compound, 1% FBS and a combination of cytokines (10 ng/mL IL-1 β , 50 ng/mL IFN- γ , 25 ng/mL TNF- α) was added to every well. After treatment with cytokine and compounds for 48 hr, 10 μ L modified Griess reagent (1:1 mixture of 1% sulfanilamide in 30% acetic acid and 0.1% *N*-(1-naphthyl) ethylenediamine dihydrochloride in 60% acetic acid) was added to each well. After 5-min incubation at room temperature, the absorbance at 540 nm was measured using an Envision plate reader (PerkinElmer).

Measurement of mitochondrial membrane potential. INS-1E cells were seeded at 10,000 cells/well using a Multidrop Combi (Thermo Labsystems) in white optical 384-well plates (Corning Life Sciences). After overnight incubation, medium was removed and 50 μ L RPMI containing the treated compound, 1% FBS and a

combination of cytokines (10 ng/mL IL-1 β , 50 ng/mL IFN- γ , 25 ng/mL TNF- α) was added to every well. After treatment with cytokine and compounds for 48 hr, 20 μ L of 3.25 μ M JC-1 was added to each well. After 3hr incubation at 37°C, the cells were gently washed three times with 50 μ L per well of 1X PBS (with Ca²⁺ and Mg²⁺). Fluorescence was measured with an EnVision plate reader (PerkinElmer) at the rhodamine spectra (excitation/emission 530 nm/580 nm) followed by fluorescein (excitation/emission 485 nm/530 nm). The ratio of rhodamine to fluorescein intensity was determined and represents the degree of mitochondrial membrane potential.

Caspase-3 activity assay. INS-1E cells were seeded at 5,000 cells/well using a Multidrop Combi (Thermo LabSystems) in white optical 384-well plates (Corning Life Sciences). After overnight incubation, medium was removed and 50 μ L RPMI containing the treated compound, 1% FBS and a combination of cytokines (10 ng/mL IL-1 β , 50 ng/mL IFN- γ , 25 ng/mL TNF- α) was added to every well. After treatment with cytokines and compounds for 48 hr, medium was removed and 20 μ L Caspase-Glo 3/7 reagent was added. Luminescence was measured after 2-hr incubation using an Envision plate reader (PerkinElmer). The same protocol was used for human pancreatic islets.

RNA interference and Western blotting. siRNAs (100 nM) were transfected into INS-1E cells (5,000 cells/well in a 384-well plate) using DharmaFECT reagent. Transfected cells were cultured for 72hr, then collected for Western blot analysis and cell-based assays. For Western blotting, cells were lysed in RIPA buffer. Total protein was separated by 4-12% SDS-PAGE and transferred to a PVDF membrane. Blots were developed using the chemiluminescence detection system SuperSignal (Thermo Fisher Scientific) and light emission was captured using an Imaging Station 4000MM (Carestream).

Quantitative PCR for mRNA levels. Following knock-down by siRNA, cells were lysed and RNA was isolated using the RNeasy Mini Kit (Qiagen) according to the manufacturer's protocol. RNA was reverse transcribed with random primers using the High Capacity cDNA Reverse Transcription Kit with RNase inhibitor (Applied Biosystems). Quantitative PCR was performed with Power SYBR Green PCR Master Mix (Applied Biosystems) on an Applied Biosystems 7900HT real-time PCR machine using primers for rat Mcm6 and Blvrbl from SABiosciences.

Glucose-stimulated insulin secretion. INS-1E cells were seeded in 96-well plates at 20,000 cells/well in 100 μ L RPMI and incubated for 48 hr in 100 μ L fresh RPMI

containing 1% FBS and the cytokine cocktail in the presence or absence of 5 μ M MS-275. Cells were washed and incubated for 2 hr in KRBH buffer (135 mM NaCl, 3.6 mM KCl, 5 mM NaHCO₃, 0.5 mM NaH₂PO₄, 0.5 mM MgCl₂, 1.5 mM CaCl₂, 10 mM HEPES, pH 7.4, 0.1% BSA) lacking glucose. Cells were subsequently incubated with KRBH buffer containing 2 mM or 16 mM glucose for 1 hr. The supernatant was collected for measurement of secreted insulin. Insulin was measured with a rat insulin ELISA kit (Alpco). The same protocol was used for human pancreatic islets.

GAS reporter assay. INS-1E cells were transfected with plasmids (GAS reporter assay kit) using DharmaFECT reagent according to the manufacturer's protocol (SABiosciences) in white optical 384-well plates (Corning Life Sciences). After overnight incubation, medium was removed and 50 μ L RPMI containing the treated compound, 1% FBS and a combination of cytokines (10 ng/mL IL-1 β , 50 ng/mL IFN- γ , 25 ng/mL TNF- α) was added to every well. After treatment with cytokines and compounds for 18 hr, luminescence was measured using Dual-Glo according to the manufacturer's protocol (Promega).

Purification of recombinant USP9X. For each purification, fifty 25-cm dishes of confluent HEK-293 cell lines stably expressing wild-type USP-9X (generously

provided by Dr. Dario Alessi, University of Dundee, Scotland) were employed. Cells were washed twice with ice-cold PBS and lysed in 1 ml of ice-cold lysis buffer. The combined lysates were centrifuged at 26000 **g** for 30 min at 4 °C and the supernatant incubated with 0.2 ml of rabbit IgG–agarose beads (Sigma) for 1 h at 4 °C. The IgG–agarose was washed extensively with lysis buffer containing 0.15 M NaCl, then with several washes in buffer B prior to incubation with 0.250 ml of buffer B containing 0.1 mg of TEV protease (Invitrogen). After 3 h at 4 °C ~70–90% of the TAP-tagged protein had been cleaved from the IgG–agarose and the eluted protein was incubated with 0.1 ml of rabbit calmodulin–Sepharose (Roche) equilibrated in buffer C. After 1 h at 4 °C, the calmodulin–Sepharose was washed with buffer C. To elute the protein, the calmodulin–Sepharose was then incubated with 0.1 ml of buffer D for 10 min at 4 °C. The eluate was removed from the beads and the elution repeated two or three times. To remove the NaCl present in the buffer containing the eluate protein, the eluates were centrifuged at 1500 **g** for 1 min at 4 °C in protein desalting spin columns. Lysis buffer contained 50 mM Tris/HCl (pH 7.5), 1 mM EGTA, 1 mM EDTA, 1% (w/v) Nonidet P40, 1 mM sodium orthovanadate, 10 mM sodium b-glycerophosphate, 50 mM sodium fluoride, 5 mM sodium pyrophosphate, 0.27 M sucrose, 1 mM DTT (dithiothreitol) and complete proteinase inhibitor cocktail (one tablet/50 ml). Buffer B contained 50 mM Tris/HCl (pH 7.5), 0.15 M NaCl, 0.27 M sucrose, 1% (w/v) Nonidet

P40 and 1 mM DTT. Buffer C contained 50mM Tris/HCl (pH 7.5), 0.15 M NaCl, 1 mM MgCl₂, 1 mM imidazole, 2 mM CaCl₂, 0.27 M sucrose and 1 mM DTT. Buffer D contained 50 mM Tris/HCl (pH 7.5), 20 mM EGTA, 150 mM NaCl and 5 mM DTT. TBS-Tween buffer contained 50 mM Tris/HCl (pH 7.5), 0.15 M NaCl and 0.2% (v/v) Tween 20.

5.7 References

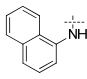
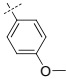
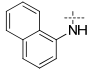
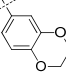
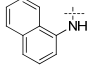
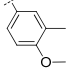
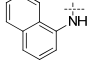
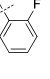
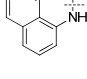
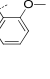
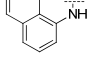
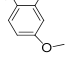
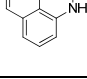
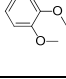
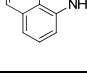
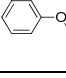
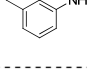
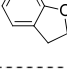
1. Delaney, C. A., Pavlovic, D., Hoorens, A., Pipeleers, D. G., and Eizirik, D. L. (1997) Cytokines induce deoxyribonucleic acid strand breaks and apoptosis in human pancreatic islet cells, *Endocrinology* 138, 2610-2614.
2. Riachy, R., Vandewalle, B., Kerr Conte, J., Moerman, E., Sacchetti, P., Lukowiak, B., Gmyr, V., Bouckenoghe, T., Dubois, M., and Pattou, F. (2002) 1,25-dihydroxyvitamin D3 protects RINm5F and human islet cells against cytokine-induced apoptosis: implication of the antiapoptotic protein A20, *Endocrinology* 143, 4809-4819.
3. Feroni, A., Pileggi, A., Molano, R. D., Sanabria, N. Y., Tejada, T., Gonzalez-Quintana, J., Ichii, H., Inverardi, L., Ricordi, C., and Pastori, R. L. (2008) Inhibition of c-jun N terminal kinase (JNK) improves functional beta cell mass in human islets and leads to AKT and glycogen synthase kinase-3 (GSK-3) phosphorylation, *Diabetologia* 51, 298-308.
4. Dush, M. K., McIver, A. L., Parr, M. A., Young, D. D., Fisher, J., Newman, D. R., Sannes, P. L., Hauck, M. L., Deiters, A., and Nascone-Yoder, N. Heterotaxin: a TGF-beta signaling inhibitor identified in a multi-phenotype profiling screen in *Xenopus* embryos, *Chem Biol* 18, 252-263.
5. Saxe, J. P., Wu, H., Kelly, T. K., Phelps, M. E., Sun, Y. E., Kornblum, H. I., and Huang, J. (2007) A phenotypic small-molecule screen identifies an orphan ligand-receptor pair that regulates neural stem cell differentiation, *Chem Biol* 14, 1019-1030.
6. Won, J., Kim, M., Kim, N., Ahn, J. H., Lee, W. G., Kim, S. S., Chang, K. Y., Yi, Y. W., and Kim, T. K. (2006) Small molecule-based reversible reprogramming of cellular lifespan, *Nat Chem Biol* 2, 369-374.

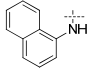
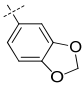
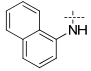
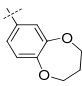
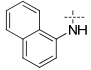
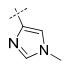
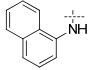
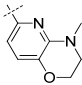
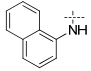
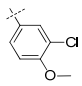
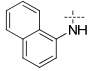
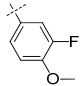
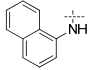
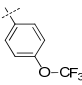
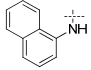
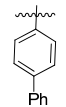
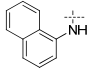
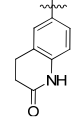
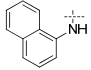
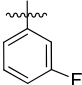
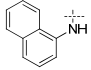
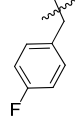
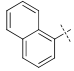
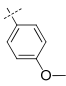
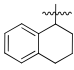
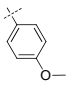
7. Hung, D. T., Shakhnovich, E. A., Pierson, E., and Mekalanos, J. J. (2005) Small-molecule inhibitor of *Vibrio cholerae* virulence and intestinal colonization, *Science* *310*, 670-674.
8. Cong, F., Cheung, A. K., and Huang, S. M. Chemical Genetics-Based Target Identification in Drug Discovery, *Annu Rev Pharmacol Toxicol*.
9. Raida, M. Drug target deconvolution by chemical proteomics, *Curr Opin Chem Biol* *15*, 570-575.
10. Subramanian, A., Tamayo, P., Mootha, V. K., Mukherjee, S., Ebert, B. L., Gillette, M. A., Paulovich, A., Pomeroy, S. L., Golub, T. R., Lander, E. S., and Mesirov, J. P. (2005) Gene set enrichment analysis: a knowledge-based approach for interpreting genome-wide expression profiles, *Proc Natl Acad Sci U S A* *102*, 15545-15550.
11. Ong, S. E., and Mann, M. (2006) A practical recipe for stable isotope labeling by amino acids in cell culture (SILAC), *Nat Protoc* *1*, 2650-2660.
12. Ong, S. E., and Mann, M. (2005) Mass spectrometry-based proteomics turns quantitative, *Nat Chem Biol* *1*, 252-262.
13. Ong, S. E., Schenone, M., Margolin, A. A., Li, X., Do, K., Doud, M. K., Mani, D. R., Kuai, L., Wang, X., Wood, J. L., Tolliday, N. J., Koehler, A. N., Marcaurelle, L. A., Golub, T. R., Gould, R. J., Schreiber, S. L., and Carr, S. A. (2009) Identifying the proteins to which small-molecule probes and drugs bind in cells, *Proc Natl Acad Sci U S A* *106*, 4617-4622.
14. Wei, Z., Liu, C., Wu, X., Xu, N., Zhou, B., Liang, C., and Zhu, G. Characterization and structure determination of the Cdt1 binding domain of human minichromosome maintenance (Mcm) 6, *J Biol Chem* *285*, 12469-12473.
15. Vucic, D., Dixit, V. M., and Wertz, I. E. Ubiquitylation in apoptosis: a post-translational modification at the edge of life and death, *Nat Rev Mol Cell Biol* *12*, 439-452.
16. Xu, J., Burgoyne, P. S., and Arnold, A. P. (2002) Sex differences in sex chromosome gene expression in mouse brain, *Hum Mol Genet* *11*, 1409-1419.
17. Sacco, J. J., Coulson, J. M., Clague, M. J., and Urbe, S. Emerging roles of deubiquitinases in cancer-associated pathways, *IUBMB Life* *62*, 140-157.
18. Al-Hakim, A. K., Zagorska, A., Chapman, L., Deak, M., Pegg, M., and Alessi, D. R. (2008) Control of AMPK-related kinases by USP9X and atypical Lys(29)/Lys(33)-linked polyubiquitin chains, *Biochem J* *411*, 249-260.
19. Niesen, F. H., Berglund, H., and Vedadi, M. (2007) The use of differential scanning fluorimetry to detect ligand interactions that promote protein stability,

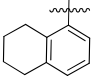
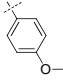
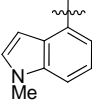
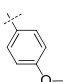
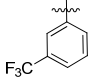
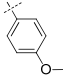
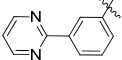
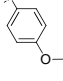
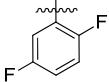
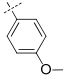
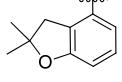
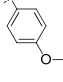
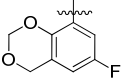
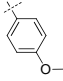
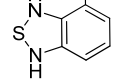
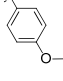
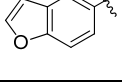
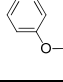
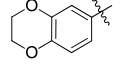
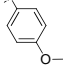
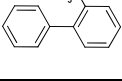
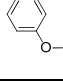
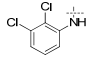
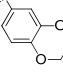
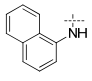
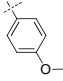
Nat Protoc 2, 2212-2221.

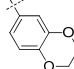
20. Bartholomeusz, G. A., Talpaz, M., Kapuria, V., Kong, L. Y., Wang, S., Estrov, Z., Priebe, W., Wu, J., and Donato, N. J. (2007) Activation of a novel Bcr/Abl destruction pathway by WP1130 induces apoptosis of chronic myelogenous leukemia cells, *Blood* 109, 3470-3478.
21. Schwickart, M., Huang, X., Lill, J. R., Liu, J., Ferrando, R., French, D. M., Maecker, H., O'Rourke, K., Bazan, F., Eastham-Anderson, J., Yue, P., Dornan, D., Huang, D. C., and Dixit, V. M. Deubiquitinase USP9X stabilizes MCL1 and promotes tumour cell survival, *Nature* 463, 103-107.
22. Moore, F., Naamane, N., Colli, M. L., Bouckennooghe, T., Ortis, F., Gurzov, E. N., Igoillo-Esteve, M., Mathieu, C., Bontempi, G., Thykjaer, T., Orntoft, T. F., and Eizirik, D. L. (2011) STAT1 is a master regulator of pancreatic {beta}-cell apoptosis and islet inflammation, *J Biol Chem* 286, 929-941.
23. Beattie, G. M., Cirulli, V., Lopez, A. D., and Hayek, A. (1997) Ex vivo expansion of human pancreatic endocrine cells, *J Clin Endocrinol Metab* 82, 1852-1856.

Appendix 1. Complete EC₅₀ values and maximum activity for all synthesized analogs.

Entry	Structure			Cellular activity	
	R1	R2	R3	EC ₅₀ (μM)	Maximum Activity (%)
1	OH			4.89±2.41	62
2	OH			0.78±0.45	99
3	OH			3.48±1.40	76
4	OH			>20	0
5	OH			>20	0
6	OH			>20	0
7	OH			>20	0
8	OH			>20	0
9	OH			>20	0

10	OH			>20	0
11	OH			>20	0
12	OH			>20	0
13	OH			>20	0
14	OH			>20	0
15	OH			>20	0
16	OH			>20	0
17	OH			>20	0
18	OH			>20	0
19	OH			>20	0
20	OH			>20	0
21	OH			>20	0
22	OH			>20	0

23	OH			>20	0
24	OH			>20	0
25	OH			>20	0
26	OH			>20	0
27	OH			>20	0
28	OH			>20	0
29	OH			>20	0
30	OH			>20	0
31	OH			>20	0
32	OH			>20	0
33	OH			>20	0
34	OH			>20	0
35	H			3.06±1.41	76

36	H			2.79±1.73	89
----	---	---	--	-----------	----

Appendix 2. Characterization of Active Compounds

For all the analogs synthesized through solid-phase synthesis, the final amount of each analog after purification by HPLC (with >95% purity) is around 1mg, which is not enough for detailed chemical characterizations. However, biologically active analogs were resynthesized in a larger scale. ¹H NMR, ¹³C NMR and high-resolution mass spec data were obtained for these compounds.

***N*-(((2*R*,3*R*)-5-((*S*)-1-Hydroxypropan-2-yl)-3-methyl-10-(3-(naphthalen-1-yl)ureido)-6-oxo-3,4,5,6-tetrahydro-2H-benzo[*b*][1,5]oxazocin-2-yl)methyl)-4-methoxy-Nmethylbenzenesulfonamide, compound 5 in Table 4-1.**

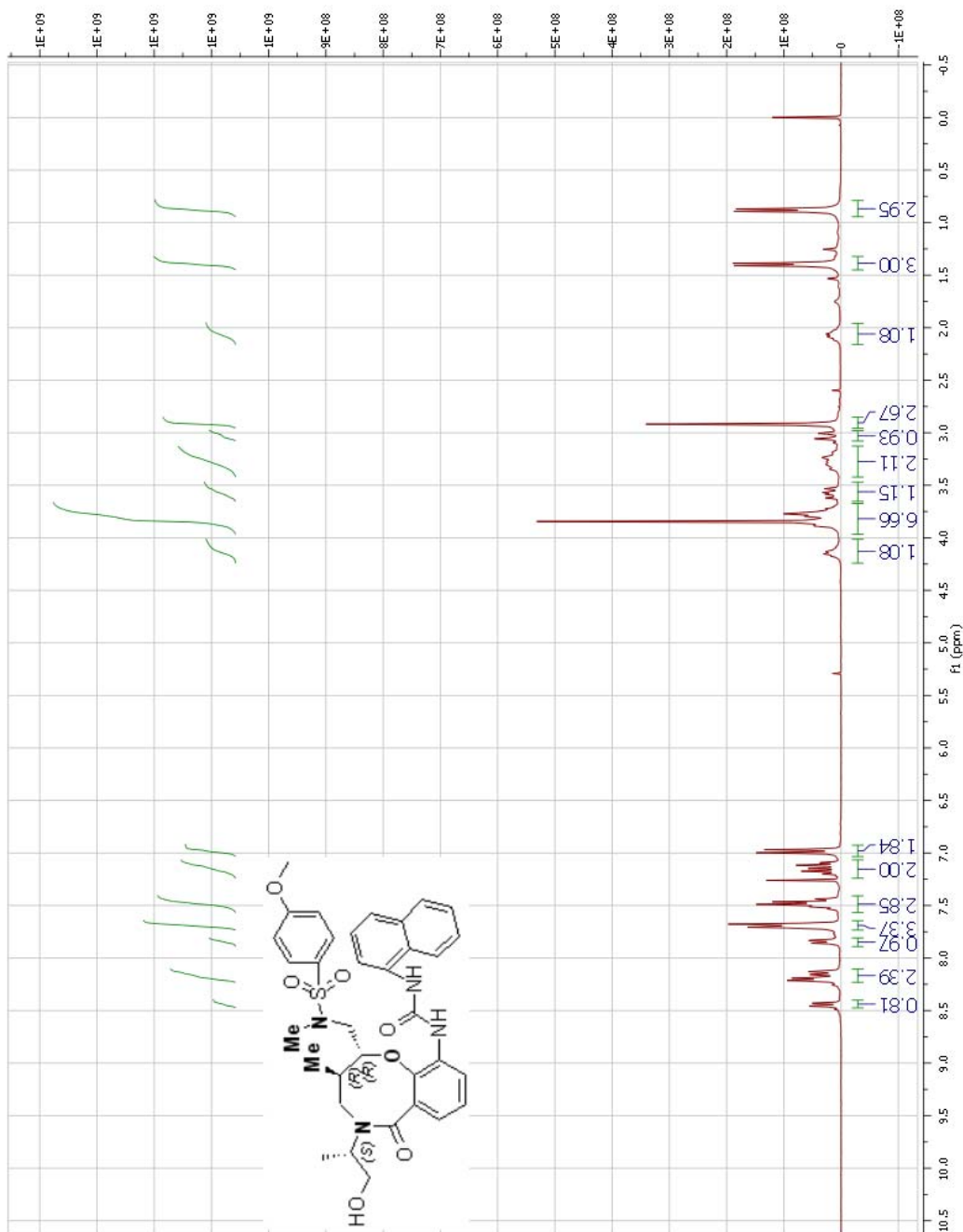
¹H NMR (300 MHz, CDCl₃) δ 8.44 (d, *J* = 8.0 Hz, 1H), 8.17 (dd, *J* = 7.5, 18.1 Hz, 2H), 7.85 (d, *J* = 7.0 Hz, 1H), 7.69 (d, *J* = 9.0 Hz, 3H), 7.57-7.41 (m, 3H), 7.13 (dd, *J* = 7.2, 16.3 Hz, 2H), 6.98 (d, *J* = 8.8 Hz, 2H), 4.15 (s, 1H), 3.81 (d, *J* = 21.9 Hz, 7H), 3.55 (d, *J* = 10.7 Hz, 1H), 3.24 (s, 2H), 3.03 (d, *J* = 15.3 Hz, 1H), 2.92 (s, 3H), 2.06 (s, 1H), 1.40 (d, *J* = 6.9 Hz, 3H), 0.88 (d, *J* = 6.7 Hz, 3H). ¹³C NMR (75 MHz, CDCl₃) δ 169.7, 163.8, 153.9, 142.8, 134.4, 133.3, 132.5, 131.1, 130.1, 129.2, 128.3, 126.2, 126.0, 125.9, 125.6, 123.0, 122.7, 122.5, 121.9, 114.7, 85.2, 65.2, 56.1, 55.9, 55.7, 51.9, 38.7, 35.2, 16.8, 14.4. HRMS (ESI) calcd for C₃₄H₃₈N₄O₇S [M + H]⁺: 647.2534, found: 647.2532.

***N*-(((2*R*,3*R*)-5-((*S*)-1-Hydroxypropan-2-yl)-3-methyl-10-(3-(naphthalen-1-yl)ureido)-6-oxo-3,4,5,6-tetrahydro-2H-benzo[*b*][1,5]oxazocin-2-yl)methyl)-*N*-methyl-2,3-dihydrobenzo-*b*[1,4]dioxine-6-sulfonamide, compound 13 in Table 4-1.**

[α]_D²⁰ -14.0 (c 1.0, CHCl₃). ¹H NMR (CDCl₃, 500 MHz) δ 8.45 (d, *J* = 8.3 Hz, 1H), 8.23-8.07 (m, 3H), 7.84 (d, *J* = 7.7 Hz, 1H), 7.69 (dd, *J* = 7.8, 14.5 Hz, 2H), 7.57-7.41 (m, 3H), 7.26 (t, *J* = 10.1 Hz, 2H), 7.18 (t, *J* = 7.9 Hz, 1H), 7.11 (d, *J* = 6.6 Hz, 1H), 6.97 (d, *J* = 8.5 Hz, 1H), 4.28 (dd, *J* = 4.6, 16.9 Hz, 4H), 4.15 (s, 1H), 3.88 (d, *J* = 8.7 Hz, 1H), 3.83-3.68 (m, 2H), 3.58 (dd, *J* = 10.9, 15.6 Hz, 1H), 3.25 (s, 2H), 3.03 (d, *J* = 15.4 Hz, 1H), 2.94 (s, 3H), 2.07 (d, *J* = 7.1 Hz, 1H), 1.41 (d, *J* = 6.9 Hz, 3H), 0.89 (d, *J* = 6.7 Hz, 3H). ¹³C NMR (CDCl₃, 125 MHz) δ 169.7, 153.8, 148.3, 143.9, 142.7, 134.3, 133.2, 132.4, 130.9, 129.1, 128.2, 126.9, 126.0, 125.9, 125.9, 125.5, 122.9, 122.6, 121.8, 121.7, 118.1, 117.4, 85.1, 77.2, 76.9, 76.7, 65.2, 64.5, 64.1, 56.1, 55.9, 51.8, 38.8, 35.1, 16.8, 14.4. HRMS (ESI) calcd for C₃₅H₃₈N₄O₈S [M + H]⁺: 675.2483, found: 675.2491.

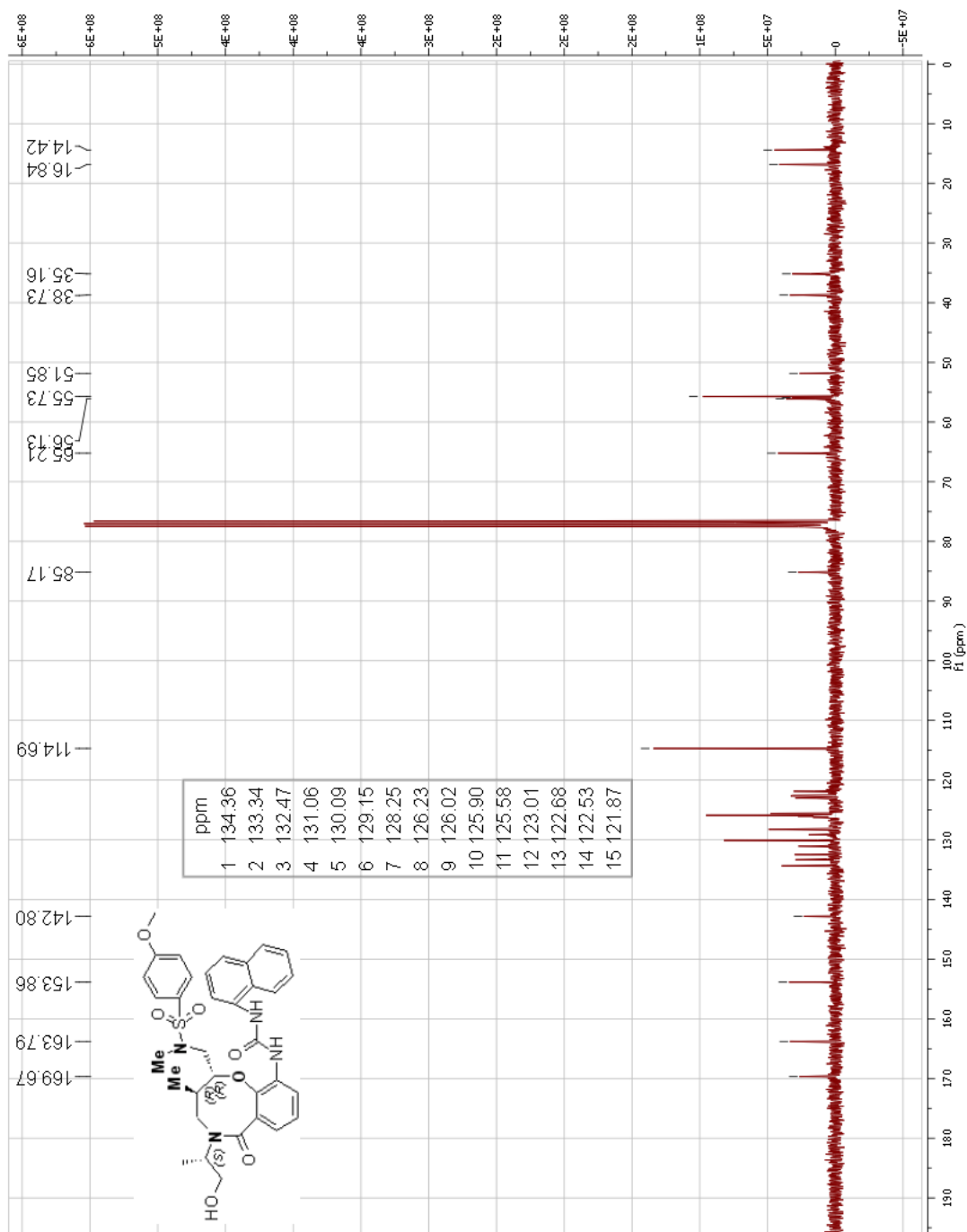
***N*-(((2*R*,3*R*)-5-(((*S*)-1-Hydroxypropan-2-yl)-3-methyl-10-(3-(naphthalen-1-yl)ureido)-6-oxo-3,4,5,6-tetrahydro-2*H*-benzo[*b*][1,5]oxazocin-2-yl)methyl)-4-methoxy-Nmethylbenzenesulfonamide, compound 5 in Table 4-1.**

¹H spectrum



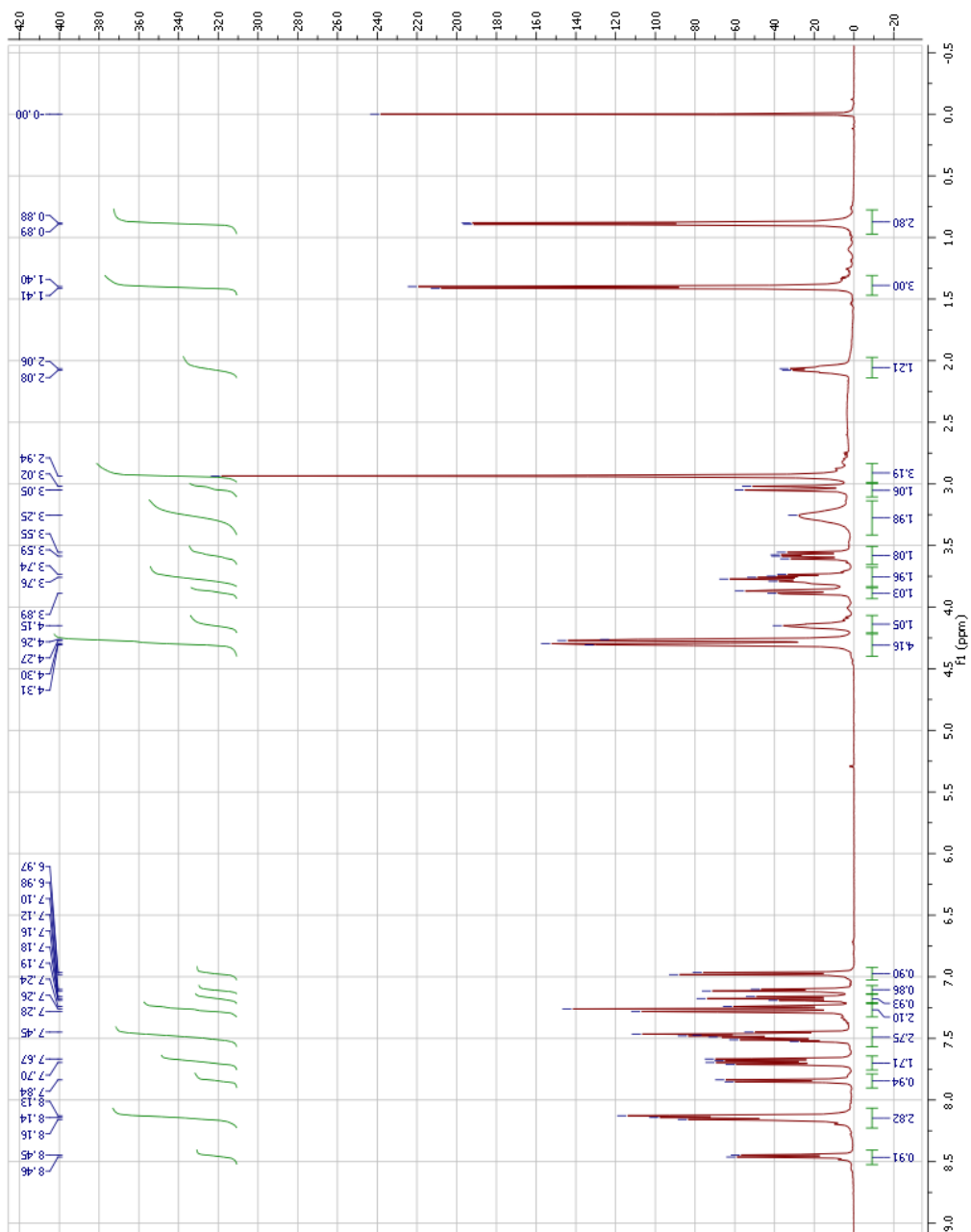
***N*(*((2R,3R)*-5-*((S)*-1-Hydroxypropan-2-yl)-3-methyl-10-(3-(naphthalen-1-yl)ureido)-6-oxo-3,4,5,6-tetrahydro-2H-benzo[*b*][1,5]oxazocin-2-yl)methyl)-4-methoxy-Nmethylbenzenesulfonamide, compound 5 in Table 4-1.**

¹³C spectrum



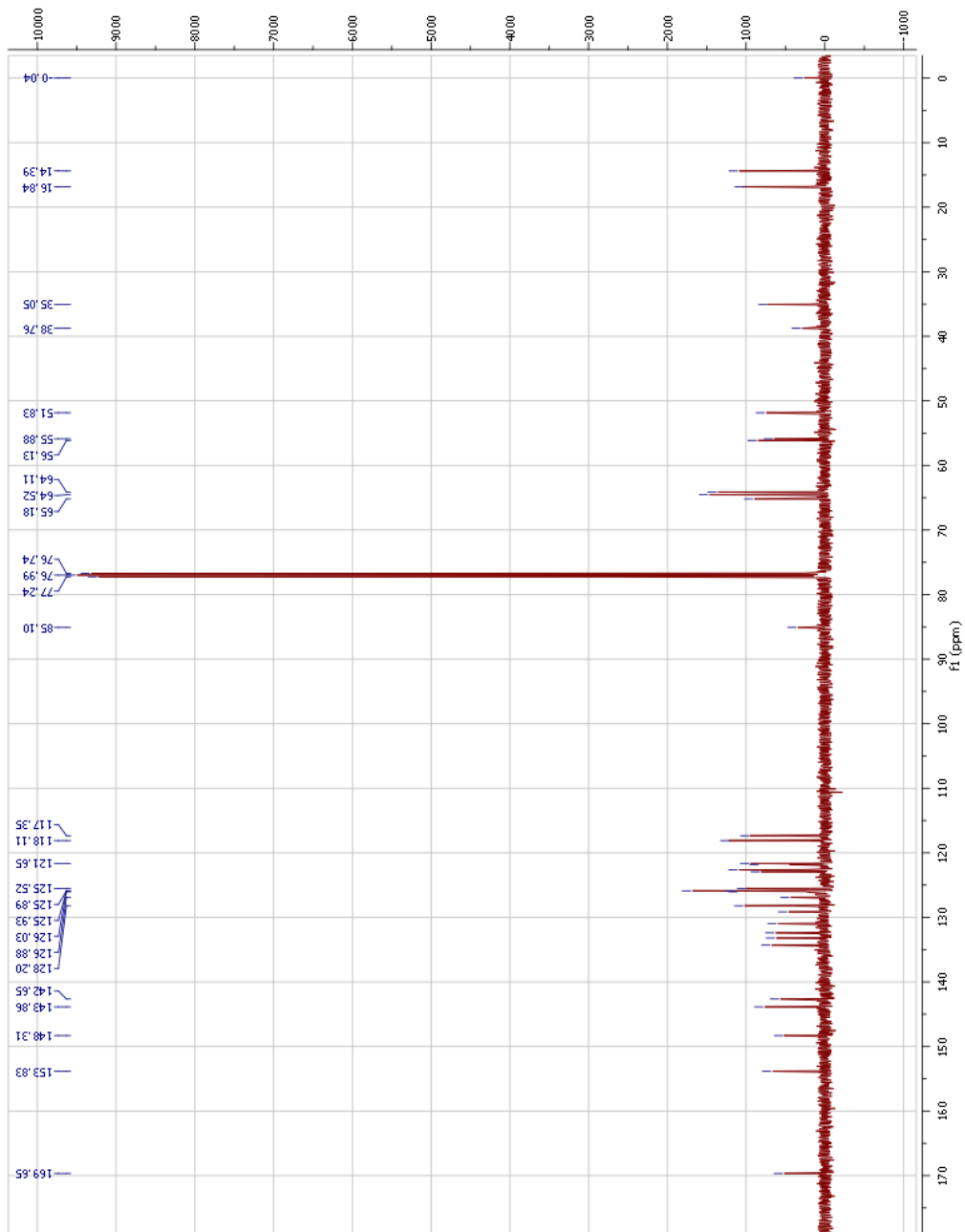
***N*-(((2*R*,3*R*)-5-((*S*)-1-Hydroxypropan-2-yl)-3-methyl-10-(3-(naphthalen-1-yl)ureido)-6-oxo-3,4,5,6-tetrahydro-2*H*-benzo[*b*][1,5]oxazocin-2-yl)methyl)-*N*-methyl-2,3-dihydrobenzo-*b*[1,4]dioxine-6-sulfonamide, compound 13 in Table 4-1.**

¹H spectrum



***N*-(((2*R*,3*R*)-5-((*S*)-1-Hydroxypropan-2-yl)-3-methyl-10-(3-(naphthalen-1-yl)ureido)-6-oxo-3,4,5,6-tetrahydro-2*H*-benzo[*b*][1,5]oxazocin-2-yl)methyl)-*N*-methyl-2,3-dihydrobenzo-*b*[1,4]dioxine-6-sulfonamide, compound 13 in Table 4-1.**

¹³C spectrum



Appendix 3 Kinase profiling result of BRD0476

10 μ M of BRD0476 was tested for duplicates in 100 different kinases which were chosen to be representatives for different classes of kinases. The values below are % activity of each kinase after incubation of 10 μ M BRD0476.

Kinases	BRD0476 @ 10 μ M	Kinases	BRD0476 @ 10 μ M
Abl(h)	99	MAPK2(h)	111
ALK(h)	65	MAPKAP-K2(h)	93
AMPK α 1(h)	83	MAPKAP-K3(h)	92
ASK1(h)	99	MEK1(h)	110
Aurora-A(h)	104	MKK4(m)	112
Aurora-B(h)	77	MKK6(h)	103
Axl(h)	89	MKK7 β (h)	103
BTK(h)	109	MLK1(h)	96
CaMKI(h)	97	Mnk2(h)	97
CDK1/cyclinB(h)	104	MSK1(h)	89
CDK2/cyclinA(h)	105	MSK2(h)	86
CDK5/p25(h)	101	MST1(h)	100
CDK6/cyclinD3(h)	106	mTOR(h)	94
CDK7/cyclinH/MAT1(h)	104	NEK2(h)	102
CDK9/cyclin T1(h)	112	p70S6K(h)	123
CHK1(h)	104	PAK2(h)	97
CK1 γ 1(h)	92	PDGFR β (h)	102
CK1(y)	101	PDK1(h)	102
CK2 α 2(h)	113	Pim-1(h)	98
c-RAF(h)	101	PKA(h)	139
DRAK1(h)	107	PKB α (h)	98
eEF-2K(h)	128	PKB β (h)	92
EGFR(h)	103	PKB γ (h)	99
EphA5(h)	108	PKC α (h)	94
EphB4(h)	101	PKC β II(h)	101
Flt3(h)	109	PKC γ (h)	99
Fyn(h)	90	PKC δ (h)	111
GCK(h)	100	PKC ϵ (h)	110
GSK3 α (h)	137	PKC η (h)	112
GSK3 β (h)	111	PKC ι (h)	108
IGF-1R(h)	86	PKC μ (h)	98
IKK α (h)	130	PKC θ (h)	115
IKK β (h)	97	PKC ζ (h)	108
IR(h)	99	PKG1 α (h)	73
IRR(h)	100	Plk3(h)	103
IRAK1(h)	96	PRAK(h)	60
IRAK4(h)	103	ROCK-I(h)	107
JAK2(h)	108	ROCK-II(h)	97
JAK3(h)	88	Ros(h)	103

JNK1 α 1(h)	107	Rse(h)	100
JNK2 α 2(h)	102	Rsk1(h)	102
JNK3(h)	109	SAPK2a(h)	96
KDR(h)	101	SAPK2b(h)	94
Lck(h)	70	SAPK3(h)	115
LKB1(h)	85	SAPK4(h)	107
LOK(h)	103	Src(1-530)(h)	107
Lyn(h)	102	SRPK1(h)	94
MAPK1(h)	109	TAK1(h)	101